Spring 2012

Behavior of staged externally bonded carbon fiber reinforced polymer sheets for improved ductility

Laura Marie Rathe

Department:

BEHAVIOR OF STAGED EXTERNALLY BONDED CARBON FIBER REINFORCED POLYMER SHEETS FOR IMPROVED DUCTILITY

by

LAURA MARIE RATHE

A THESIS

Presented to the Faculty of the Graduate School of the

MISSOURI UNIVERSITY OF SCIENCE AND TECHNOLOGY

In Partial Fulfillment of the Requirements for the Degree

MASTER OF SCIENCE IN CIVIL ENGINEERING

2012

Approved by

Dr. Genda Chen, Advisor
Dr. Lesley Sneed
Dr. Jeffery Volz

ABSTRACT

Fiber reinforced polymers (FRP) has become increasingly used for the retrofit of aging structures for increased lifespans and for the rapid repair of damaged structures. It has many advantageous such as ease in rapid installation, high strength-to-weight ratio, and corrosion resistance. The main disadvantage of the material is brittle behavior with little warning of impending failures. The main objective of this study is to develop a new system of FRP that exhibits a more ductile behavior. To achieve this objective, separate sheets of FRP were applied at various staged levels and thus engaged at different loads. Ductile behavior was evaluated based on the ability of the FRP sheets to fail the conventional layers before the staged layers. To realize the staged installation of FRP sheets, two methods were explored in this thesis. The first method is to apply FRP sheets under various preloads up to the design load. Such staged FRP sheets theoretically have uniformly distributed debonding points but practically result in irregular spacing between adjacent debonding points. The second method is to intentionally create intermittent debonding areas in arch shape so that regular spacing between debonding areas can be achieved as FRP sheets are applied. In order to evaluate the effectiveness of the new FRP system, a total of 25 thin steel sheets were tension tested to determine their stress-strain curves with various implementations of FRP sheets under preloading. Additionally, 14, 11 ft × 6 in × 18 in reinforced concrete beams were tested to evaluate the effectiveness of FRP sheets directly applied in stage. Test results indicate that the new FRP system is a promising approach to improve the behavior of FRP applications in civil engineering from brittle to pseudo ductile due to nonlinear geometry effects.

ACKNOWLEDGMENTS

First, I would like to thank my advisor Dr. Genda Chen. Without his guidance and funding, I would not have been able to complete this thesis.

I would also like to thank the members of my committee, Drs. Lesley Sneed and Jeffery Volz, for their time and effort reviewing my thesis. I truly appreciate their suggestions for improving this thesis.

Several people contributed to the construction of test specimens. First, I would thank Jason Cox for his extensive knowledge of FRP installations and John Bullock for his assistance from construction thru testing of reinforced concrete beams. I would also like to thank Gary Abbott for his help in testing my specimens. Two of my fellow graduate students in particular helped with specimen construction, Chenglin Wu and Wesley Bevans.

I would like to also thank my fellow graduate students in the Department of Civil, Architectural, and Environmental Engineering. Without the friendship and encouragement I received, this thesis would have never been possible.

Finally, I would like to thank my parents, Chris and Diane, as well as my brother, Daniel, and sister, Michelle. They taught me to always strive for success no matter what obstacles encountered. Their support and prayers were momentous through this and all of my educational achievements. I truly could not have finished this thesis without them.

TABLE OF CONTENTS

LIST OF ILLUSTRATIONS

LIST OF TABLES

1. INTRODUCTION

1.1. GENERAL

Fiber reinforced polymers (FRP) were exclusively used in aerospace industry until the 1980's. Today, FRP has many applications in civil engineering structures for the retrofit of aging structures and the rapid repair of damaged structures.

There are many advantages to using FRP over a conventional method. These can include: speed from installation to completion, high tensile strength, high strength to weight ratio, and corrosion resistance. FRP can also be a cost saving material for some applications, particularly in corrosive environments. While the material costs are higher, FRP can be installed with less cost in labor. These factors indicate that FRP is an excellent material for strengthening reinforced concrete structures.

The main disadvantage of FRP is the brittle behavior of the material. An FRP system often fails with little warning. Part of this is due to the delamination that can occur. Delamination is where the FRP peels away from the concrete surface to which it was attached. This leads to premature failure of the FRP system without reaching the full strength potential of the material.

Hybrid FRP has been used to demonstrate a more ductile behavior in a FRP system. It consists of two or more materials that have different mechanical properties and fail over a larger range of strain than individual materials can achieve. Hybrid FRP is not necessarily more complex in manufacturing or application. Materials can simply be sandwiched together and still receive increased ductility.

FRP can also be prestressed to gain additional benefits over conventional FRP. The first benefit is the ability of the prestressed FRP to carry both dead and live loads. Conventional FRP is only able to hold additional live loads. Prestressed FRP also uses the material more efficiently by increasing the ultimate strength that is achieved. Other benefits to prestressing FRP include: increased serviceability, decreased deflections, and reduced crack widths greater than what is seen with non-prestressed FRP.

With these added benefits of prestressing, additional labor and specialized equipment are often required. Prestressing FRP is more complicated and demanding than applying the same amount of conventional FRP. These factors will add to the overall

cost of a repair project. The cost must be weighted with the benefits to determine if prestressed FRP is the right choice for the project.

1.2. RESEARCH SIGNIFICANCE

Brittle failure is a safety issue in structural design. It provides tenants in a building with no warning for escape in the event of catastrophes. This thesis deals with the brittle behavior of FRP and attempts to develop a staged FRP system for an overall more ductile behavior. The advantage of this system is that it will potentially create a warning impending failure. Therefore, the end results of this study can be significant in engineering design and applications. It can not only provide better serviceability of a retrofitted or repaired building but also address the safety concern associated with brittle failure modes.

Technically, Section 1.1 has already shown that hybrid FRP with various materials can increase ductility. This thesis uses the different nonlinear changes in geometry of FRP sheets to achieve a similar result. As such, it will advance the state of the art of FRP applications in civil engineering.

1.3. RESEARCH OBJECTIVES

The overall goal of this study is to achieve a more ductile behavior with a system of staged sheets over a single conventionally installed sheet. The system has a series of FRP sheets applied side by side with delay mechanisms or mechanically engaged at different time instances. The first stage is the same as conventionally installed FRP sheets. The properly designed staged sheets fail in succession, the conventional strips followed by the staged strips. The failure of the conventional and/or lower staged FRP sheets would be the warning before the entire system fails. When the lower stage level fails, the system must be reevaluated for strength and durability. The sheets are applied next to each other, not layered on top of one another. The system as a whole expects to show a more ductile behavior than the traditional brittle behavior of conventional FRP.

The specific objectives of this study are (a) to develop staged FRP systems with two application procedures, preloading and intermittently debonding method, and (b) to study the behavior of various levels of staged FRP and the ability of the system to

indicate ductile behavior instead of brittle behavior. The scope of work includes but is not limited to:

- Coupon tests to determine the effectiveness of the preloading FRP application method,
- Calculations to determine the optimal configuration of FRP parameters in order to achieve a desirable ductile behavior,
- Large scale beam tests to determine the accuracy of theoretical calculations and their practicality in real world applications, and
- Analysis of FRP behavior both when staged and conventionally installed to RC beams.

2. LITERATURE REVIEW

2.1. BACKROUND

Originally, fiber reinforced polymers were designed for use in the aerospace industry. Today, FRP is used in everything from boats to golf clubs and has even made its way into the field of civil engineering. Professor H. Isler was the first to employ FRP materials in structures during the end of the 1950's (Kachlakev 2000). America did not truly embrace FRP in structures until the 1980's when it was first used in bridges (Kachlakev 2000). The main uses for FRP in the civil industry include the retrofitting of concrete structures, increased strength capacity in existing structures, and rapid repair of damaged structures.

Over the years, structures experienced aging effects and deteriorated for various reasons, therefore needing retrofit and/or repair to remain functional and safe. Bridges, in particular, have had to take increased populations and thus increased traffic flow that the structures were not initially designed for. Another cause of deterioration in bridges is the use of deicing salts. The salt enters through cracks and causes the steel rebar in the reinforced concrete to become corroded. This leads to a weakened bridge that is not able to carry the capacity it was designed to withstand. Natural and man-made disasters can also lead to the need for repair. Earthquakes, normal environmental deteriorations, and vehicle collisions can cause significant damage to bridges making them unsafe. Especially after an earthquake event, time is important in order to get supplies and medical attention to those who are in need. These bridges need to be repaired quickly and efficiently so that they are once again functional and most importantly, safe.

2.2. CONVENTIONAL FRP

Conventional, non-prestressed application is the most common technique used for FRP materials. Including FRP in a beam can raise the strength from 1.5 to 5 times the capacity of the original member (Kachlakev 2000.) The increase in capacity depends on factors such as FRP style, thickness of material, fiber alignment, and condition of the original beam (Kachlakev 2000).

There are three types of fibers used in civil engineering. These are carbon, glass, and aramid. A crude comparison of the types of fibers is given in Table 2.1 (Meier 1995).

Table 2.1. FRP Fiber Comparison

Criteria	Carbon	Aramid	Glass
Tensile Strength	Very Good	Very Good	Very Good
Compressive Strength	Very Good	Inadequate	Good
Modulus of Elasticity	Very Good	Good	Adequate
Long Term Behavior	Very Good	Good	Adequate
Fatigue Behavior	Excellent	Good	Adequate
Alkaline Resistance	Very Good	Good	Inadequate

Over the years increased use of FRP has led to the regulations set forth by ACI 440 to provide guidelines for FRP use in structures. In general, a carbon FRP sheet should fail when the steel rebar is yielding but before a failure in the compression zone of the concrete occurs (Meier 1995). This is important so that in the event of failure of the FRP system, an immediate and catastrophic failure of the entire structure does not occur. Designs must account for the absence of ductility associated with FRP materials (Nanni 2003).

Durability of the FRP material is an important characteristic in the use of FRP. Hydrothermal properties likely govern the decay of FRP materials (Cromwell et al. 2011). Hydrothermal effects result from a combination of heat and moisture that can lead to damage of the FRP. Exposure situations considered by Cromwell et al. (2011) included: water, salt water, alkaline, dry heat, diesel fuel, and freeze-heat. Overall, the tensile strength and modulus of elasticity were not diminished past 90% from the starting point for any of the conditions measured (Cromwell et al. 2011). This shows that the FRP continues to be durable under many exposures. The most common declination was seen in the bond, which is significant to the performance of the FRP-concrete system (Cromwell 2011). This could have been due to absorption, which affects the bond more than the FRP fibers itself (Cromwell et al. 2011).

2.2.1. Advantages. Speed is a major contributing factor for the use of FRP. FRP can go from installation to completion in a matter of days opposed to weeks with other methods of repair. This allows for a faster turn around and less interruption of traffic flow. FRP is also corrosion resistant so that it will not deteriorate from corrosion, like a steel plate would.

FRP also has a high tensile strength and high strength to weight ratio. Because of the lightweight properties, FRP requires less labor for installation. While the cost of labor is reduced, the cost for materials is increased. The primer, saturant, and fiber cost more than conventional materials needed to repair the same area. A balance between the higher material cost and lower labor cost can be struck to make FRP as cost efficient as other repair methods.

2.2.2. Disadvantages. The main disadvantage of FRP is the brittle behavior of the material. Unlike steel, FRP is anisotropic and therefore does not yield before failure (Nanni 2003). This means that the FRP system breaks with little warning. Structures with FRP strengthening are designed that even if the FRP system breaks it will still withstand the loading without catastrophic failure. With this said, it would be beneficial to know when the FRP is about to fail so that a determination can be made on the next action. This brittle failure is often the result of delamination that leads to premature failure of the FRP system.

Delamination can occur in one of two ways. An FRP sheet can debond from its attached substrate around its edge or from the opening of a flexural/shear crack (Pan 2007). Delamination from the end of the sheet is due to the large shear and normal stress concentrations that are present after load is added (Pan 2007). Similar stresses are present at the mouth of a concrete crack as the crack continues to widen since the FRP works together with the concrete. Delamination of the FRP means that the full strength capacity of the material was not reached (Ceroni 2010). A number of techniques can be used to decelerate the onset of FRP debonding, such as U-jacket, L-wrapping, X-wrapping, and fiber anchoring (Wu 2011).

2.3. HYBRID FRP

Hybrid composites combine several materials together to create a single compound material that increases a feature of individual materials used while decreasing a specific disadvantage. The use of hybridization can tailor an FRP system to the particular requirements of a specific building (Kretsis 1987). Hybrid composites are a combination of different FRP materials using glass, carbon, or aramid. These materials can be combined in several ways including: sandwiching one material between two sheets of a different material, layering of materials in a pattern, mixed fibers in an unsystematic or predetermined fashion, and other methods that use ribs or wires throughout the fibers (Kretsis 1987).

Ductility is one of the characteristics that hybrid FRP accentuates. Bakis et al. stated that one of the main restrictions to be improved upon is the use of increased ductile reinforcements that are able to sense imminent tensile failure (Bakis 2001). Bunsell and Harris used the sandwiching method to determine that an effective bond between the sheets of FRP produced a smoother transfer of load (Bunsell 1974). This leads to a much less brittle behavior than either material individually.

A braiding technique has also been successful in improving ductility. Grace et al. developed a fabric with carbon and glass fibers braided in three directions (2004). FRP has the most strength if loaded in the direction of the fibers. Since this braided fabric has fibers in 3 separate directions, it can be used for flexural as well as shear strengthening (Grace 2004).

A comparison of carbon, glass, and a glass/carbon hybrid FRP load strain curves is shown in Figure 2.1 (Kretsis 1987). This curve shows the ductile behavior of the hybrid compared to the brittle individual material behavior.

According to Hosny et al. (2006), the use of a glass and carbon hybrid produced positive ductility results. Their study used both types of fibers on concrete beams without intermixing or sandwiching the materials. The use of both the glass and carbon was successful in increasing the ductility compared to using either material individually (Hosny 2006). It was also determined that the discharge of energy due to the fracture of the CFRP material undesirably affects the bond boundary between the concrete and glass fibers (Hosny 2006). This is not favorable for the ultimate strength of the system.

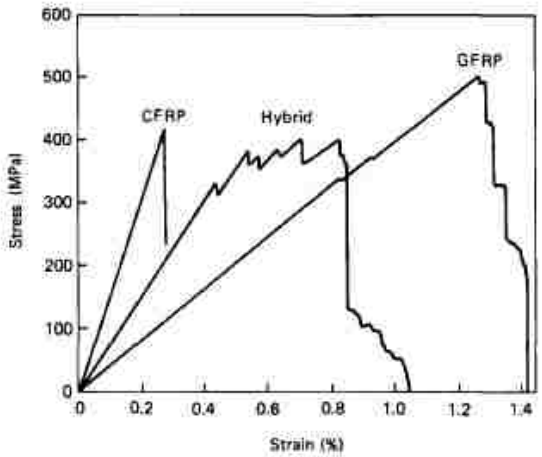

Figure 2.1. Typical Load Strain Curves for Carbon, Glass, and Glass/Carbon Hybrid

2.4. PRESTRESSED FRP

Studies on the durability of prestressed FRP sheets were done by El-Hacha et al. The conditions considered were beams at room and low temperatures. Prestressed FRP bond strength and flexural behavior was not unfavorably affected by the drop in temperature of 92°F (El-Hacha 2004). This study shows that FRP may be used in extreme weather conditions without adverse effects to the bond strength or flexural behavior, although the long term effects still require further research. Diab et al. (2009) found that creep in the epoxy was the key cause of damage to the prestressed force. This creep also leads to the premature failure of the system due to debonding and inability to reach the materials ultimate strength.

2.4.1. Advantages. Pre-stressed FRP has many benefits over conventional FRP installations. The first is the ability of prestressed FRP to carry both dead and live loads (Diab 2009). Non-prestressed FRP is designed to carry additional live loads only. Another benefit of prestressed FRP is a more efficient use of the materials, both in FRP and steel rebar. Prestressed FRP is able to reach a higher ultimate strength than non-prestressed FRP. Along with this, the reinforcing steel is able to achieve a greater percentage of the ultimate capacity before yielding (El-Hacha 2001).

Prestressed FRP is also capable of increasing serviceability, reducing deflections, and decreasing crack widths significantly better than non-prestressed FRP (El-Hacha 2001). Decreasing crack widths is important to reduce the amount of water that is able to penetrate the surface of the concrete. With this comes the decreased possibility of

deicing salts entering and causing corrosion of the steel rebar which would further weaken the structure.

2.4.2. Disadvantages. The main drawback to prestressed FRP is the increase in labor, which leads to an increase in overall cost. Conventional FRP takes very minimal labor to install, one of the main reasons for using FRP in the first place. Prestressed FRP takes far more equipment and labor for installation. In order to use prestressed FRP, the higher cost of installation must be weighed against the multiple benefits of prestressed FRP to determine if it is the best technique for repair.

2.4.3. Methods for Prestressed FRP Installation. There are three main methods for prestressing FRP. According to El-Hacha, these include: cambered beam, tensioned FRP against an independent external frame, and tensioned FRP against the strengthened beam itself (El-Hacha 2001). Each method has its own set of benefits and drawbacks depending on the structure that needs to be strengthened.

The cambered beam system consists of a system of hydraulic jacks that hold the beam in a deflected position so that the FRP can be bonded to the bottom tension face. The epoxy is given time to fully cure before the jacks are slowly released. This method of prestressing is the least effective of the three methods. It provides minor prestressing strength, little control over the prestressing force, and is an ineffective use of the FRP (El-Hacha 2001). In addition, there is also the potential to overstress the beam with the jacks and cause further damage. This procedure is not optimal for applying a prestressing force to FRP. The cambered beam method is shown in Figure 2.2 (El-Hacha 2001).

The tensioned FRP against an independent external frame method achieves prestressing by pulling the FRP at the ends with jacks on an external frame. The FRP is then brought into contact with the bottom face of the beam and bonded with epoxy. The epoxy is allowed to fully cure before the jacks are released slowly and the ends of the FRP are cut. This method provides a higher prestressing force, so that the FRP can be used more efficiently (El-Hacha 2001). Even with the improved control over the prestressing force, this method is not easily achieved in the field. Laboratory use is more realistic for this method due to the specific equipment that is essential for full scale application. The tensioned against an external frame method is shown in Figure 2.3 (El-Hacha 2001).

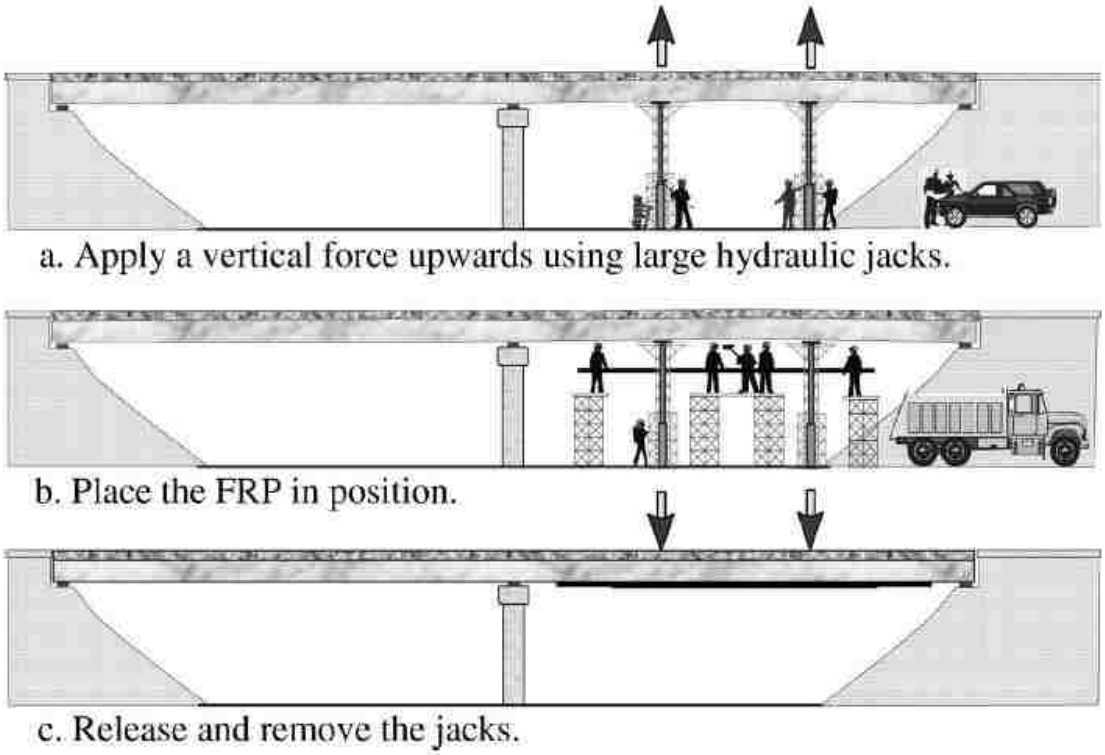

Figure 2.2. Cambered Beam Installation Method

The final method of prestressing is to tension the FRP against the strengthened beam itself. This method is similar to tensioning against an external frame, except that the FRP ends are applied to anchors attached to the beam. The anchors are then moved to provide the prestressing force. This method also provides a high level of prestressing but without the specialized equipment required for tensioning against an external frame (El-Hacha 2001). By using anchors fixed to the beam, a wider variety of structures can be strengthened with this method. The tensioned against the beam method is shown in Figure 2.4 (El-Hacha 2001).

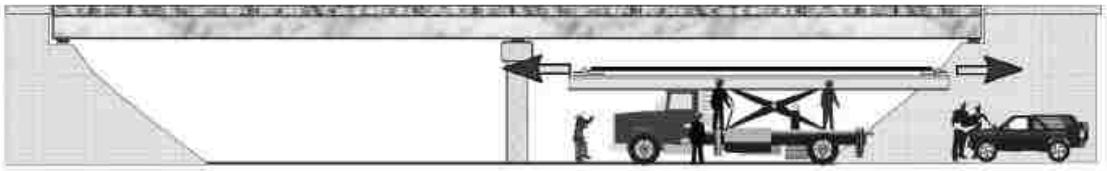

a. Bond the FRP to flat anchors. Tension the FRP on the prestressing rig.

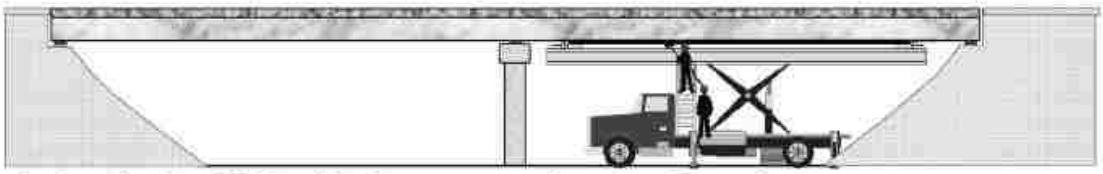

b. Apply the FRP with the prestressing rig. Cure the epoxy.

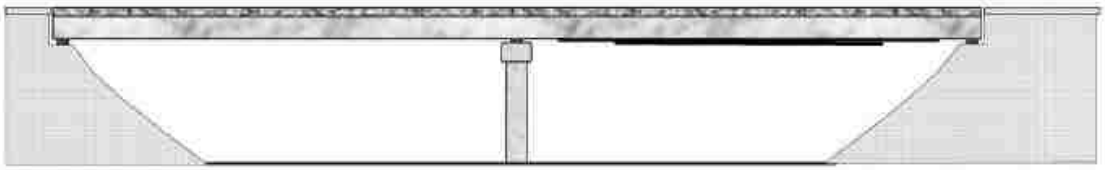

c. Cut the FRP from the anchors and transfer the prestress to the girder.

Figure 2.3. Tensioned Against an External Frame Installation Method

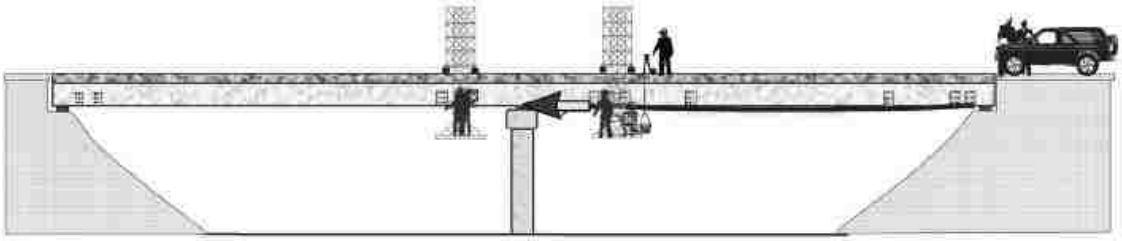

a. Anchorage placement. b. FRP sheet application.

Figure 2.4. Tensioned Against Beam Installation Method

2.5. CONCLUDING REMARKS

FRP has significant advantages for strengthening structures over other methods. The main disadvantage is the lack of ductility shown in failure. Hybrid FRP can decrease the brittle behavior through the use of various fibers in a single FRP system. This thesis attempts to use geometry, instead of materials, to achieve a similar ductile result.

3. PRELOADING FRP SYSTEM WITH COUPON TESTS

3.1. COUPON CONSTRUCTION

One way to develop a more ductile FRP system is to apply several FRP sheets on a substrate side by side under various loads so that, once unload and reload, various FRP sheets will rupture at different times and they together provide pseudo ductile behavior of the strengthened substrate. Such a technique can be viewed as the reverse process of the prestressing method with cambers as discussed in Section 2.4.3.

3.1.1. Steel Coupon. In order to test the carbon FRP under various preloaded conditions, steel coupons were produced to facilitate the application process. The coupons were cut from a sheet of cold formed steel, with a thickness of 0.0598 in. The dog bone shaped coupons measured 18 in long and 2 in wide at the ends with 1.5 in width in the center section. The dimensions for the coupon were taken from ASTM A370. Detailed dimensions for the coupons are shown in Figure 3.1. Coupons with FRP application were sandblasted to aid the adhesion of FRP to the steel.

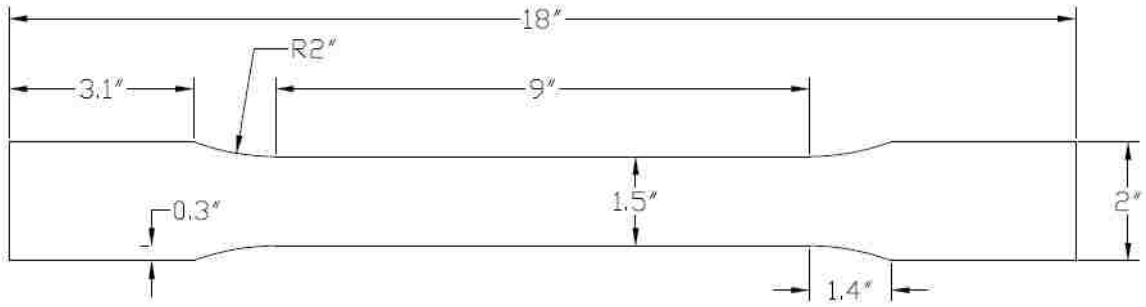

Figure 3.1. Coupon Dimensions

3.1.2. Carbon Fiber. Carbon FRP was used in all of the coupon tests. The FRP used was a CF 130 high strength carbon. Properties of this FRP along with the primer and saturant can be found in Table 3.1. The FRP applied had dimensions of 11 in long by 0.9 in wide. The strips of FRP were cut longitudinally so that the fibers ran lengthwise down the coupon. This ensured that the maximum strength would be achieved. The FRP strip was centered in coupon width and length wise. Each end was left with 3.5 in of exposed steel, with no FRP, primer, or saturant applied. This was done intentionally to

ease the application and testing processes. Steel coupons were put into tension during the application process of FRP. Therefore, it would be impossible to get FRP under the loading grips. Even if FRP were attached to the entire length of the coupon, FRP under the grips would be damaged when testing.

Table 3.1. Material Properties

	Properties			
Material	Ultimate Strength (ksi)	Ultimate Strain (in/in)	Modulus of Elasticity (ksi)	Thickness (in)
CF 130 Carbon	550	0.017	33000	0.0065
Primer	2.5	40	104	N/A
Saturant	8	7	260	N/A
Steel Coupon	78	0.011	24000	0.0598

3.2. FRP APPLICATION PROCESS

The procedure for applying FRP sheets to the steel coupon is as follows. For these coupon tests, only primer and saturant were used in the application process. First, the coupons were wiped down with rubbing alcohol to remove any grease from the construction and handling. Then, primer was mixed according to manufacturer's instruction and a thin layer was rolled onto the coupon. The primer was allowed to semi-dry until it was tacky to the touch, about 15 minutes. While the primer was curing, the saturant was prepared. Precut FRP strips were impregnated with saturant prior to being applied to the coupon. The strips were coated with saturant and then a heavy, grooved roller was rolled over the sheet to ensure that the fibers were fully saturated. The roller was used in the direction of the fibers to avoid damage. Next, a thin layer of saturant was rolled onto the exposed surface of the coupon, over the primer, and then the saturated FRP sheet was applied to the coupon. The FRP was smoothed out and centered. The coupons were allowed to cure for up to 24 hours at room temperature. All coupons with FRP followed this same process for mixing, saturating, and application.

Using an Instron 4485 as shown in Figure 3.2, preloading in the FRP was achieved by putting the steel coupon into tension. The FRP could then be applied to the surface so that when the load was released the FRP would be in compression. The

Instron 4485 uses an electric motor that provided a more constant load over the duration of the curing process opposed to a machine using hydraulics. This was important to ensure that the preloaded FRP would cure to a correct final load so the appropriate starting compressive strain was reached. The coupons were loaded to either 1.65 k or 3.2 k. The loading of 1.65 k represents 30% of yielding of the steel coupon while 3.2 k represents 60% of the yielding of steel. These values were based on a set of control coupons that was tested prior to the FRP application process. A coupon during the application phase is shown in Figure 3.3.

A steel coupon can be strengthened on two sides with different FRP applications. FRP installed under preloading was first applied to one side of the coupon. Once cured, the conventional FRP with no preloading was applied to the other side of the coupon. Strain gages were applied to the coupons after both sides of preloaded and non-preloaded FRP were installed. Location and number of gages are described in detail below depending on individual coupon tests.

Figure 3.2. Instron 4485 Machine

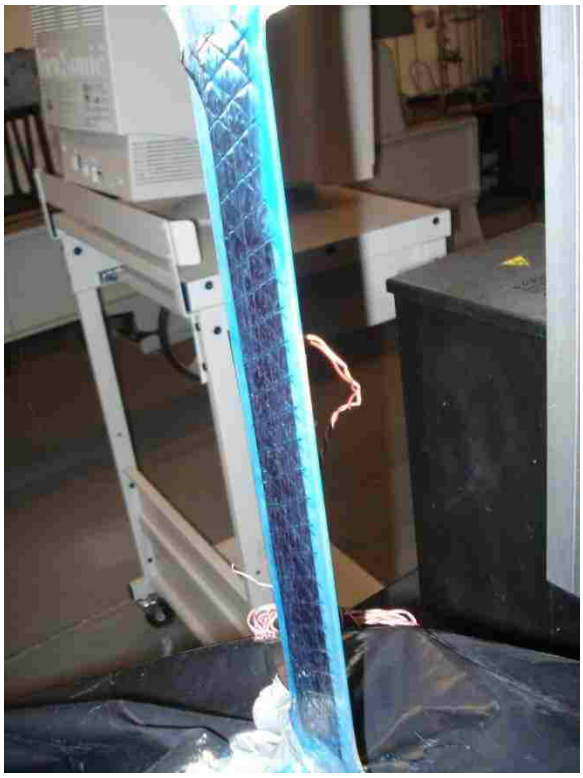

Figure 3.3. Coupon during Application

3.3. TEST PROCEDURE

The FRP coupons were tested to failure in a MTS 880 machine. The grips provided about 2500 lbs of force. The machine was set to displacement control with a rate of 0.063 in/min. Strain gages were hooked up so the strain can be constantly measured and recorded. Force and displacement were also logged during the test. An example of a coupon being tested is shown in Figure 3.4. Individual results are discussed below.

3.4. ORIGINAL COUPON TEST

Initially, nine coupons were tested with four separate loading conditions. The first set of three was a control test for the steel, with no FRP applied on either side. These control coupons, without FRP, were not sandblasted before testing. This was tested for the baseline steel properties since the yield strength was a major point of interest. After the control set was tested to failure, the yield force was established at 5.5 k. One coupon was strengthened with non-preloaded FRP on both sides. This set

provided data about the relationship between the non-preloaded FRP and steel needed for comparison in the loaded coupons. The third set of two coupons had FRP applied at a load of 30% of the yield strength of the steel, while the other side had non-preloaded FRP. The final set of three had FRP loaded to 60% yield of steel on one side, with the other side having non-preloaded FRP. Using the control coupons, the loading was determined to be 1.65 k for 30% yield of steel and 3.2 k for 60% yield of steel.

Figure 3.4. Coupon during Testing

These coupons were produced according to the procedure laid out above for the FRP application. Their curing time, starting loading, and final loading are shown in Table 3.2. Each coupon has a designation starting with FRP, followed by the FRP preloading on two sides, and completed by the specimen number under one condition. For example FRP 60,0 #2 means the second coupon specimen with FRP preloading of 60% of the yield force on one side and no preloading on the other side. Before the coupons were tested, strain gages were applied. One gage was applied to the center of each of the control coupons before tested to failure. Coupons with FRP had six gages

applied. Two gages were placed on the steel, two more on one side of FRP, and two more on the second side of FRP. The layout for the strain gages can be seen in Figure 3.5.

Table 3.2. FRP Coupon Loading and Curing Time

Coupon	Loading	Initial Load (k)	Final Load (k)	Curing (hrs)
FRP 60,0 #1	Preloaded	3.272	3.270	24
FRP 60,0 #2	Preloaded	3.237	3.202	24
FRP 60,0 #3	Preloaded	3.268	3.257	24
FRP 30,0 #1	Preloaded	1.672	1.656	19
FRP 30,0 #2	Preloaded	1.652	1.650	24
FRP 60,0 #1	None	0	0	24
FRP 60,0 #2	None	0	0	24
FRP 60,0 #3	None	0	0	24
FRP 30,0 #1	None	0	0	24
FRP 30,0 #2	None	0	0	24
FRP 0,0 #3	None	0	0	24
FRP 0,0 #3	None	0	0	24

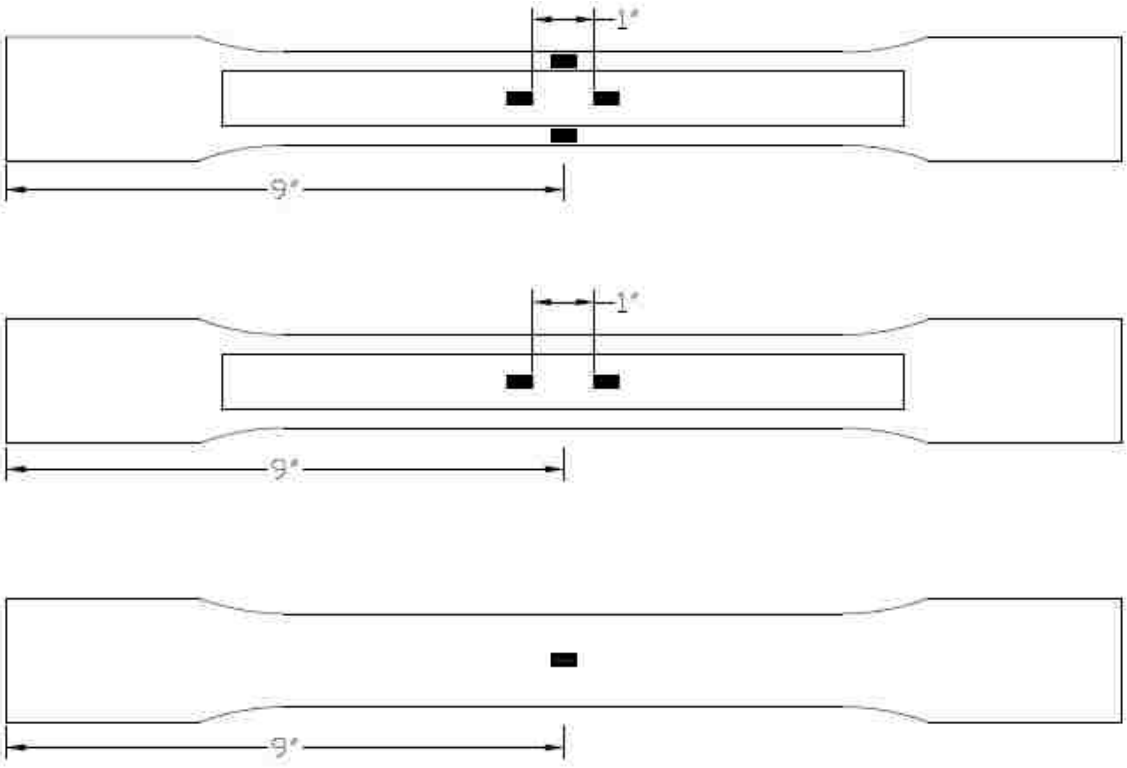

Figure 3.5. Strain Gage Locations: Preloaded, Non-Preloaded, Control

After several coupons were tested, a trend appeared. The steel was failing at the end of the coupon. This led to the FRP debonding from the ends towards the center. For this experiment, the fracture, not debonding, of the FRP was critical to determining the effectiveness of the process. From this point forward coupons had the center cross sectional area reduced, in both the steel and FRP. This helped to force the failure to occur in the center of the coupon and not at the end. To reduce the area, semi-circular holes were drilled on each side of center of the coupon. The diameter of the semi-circle was 1 in. The failure of each material is summarized in Table 3.3.

Table 3.3. Failure Mode of Each Material in FRP Coupons

Coupon	Material	Failure
Control #1	Steel	Fracture at End
Control #2	Steel	Fracture near Center
Control #3	Steel	Fracture 6 in from End
FRP 60,0 #1	Steel	Fracture at End
	60 FRP	Debonding at Steel Failure
	0 FRP	Debonding at Steel Failure
FRP 60,0 #2	Steel	Fracture at End
	60 FRP	Debonding at Steel Failure
	0 FRP	Debonding 1/2 Length of FRP
FRP 60,0 #3	Steel	Fracture in Center
	60 FRP	Debonding to End
	0 FRP	Debonding to End
FRP 30,0 #1	Steel	Fracture at End
	30 FRP	Debonding at Steel Failure
	0 FRP	Debonding at Steel Failure
FRP 30,0 #2	Steel	Fracture in Center
	30 FRP	Fracture in Center
	0 FRP	Fracture in Center
FRP 0,0 #3	Steel	Fracture at End
	30 FRP	Debonding 1/2 Length of FRP
	0 FRP	Debonding at Steel Failure

3.5. TEST RESULTS

3.5.1. Control Coupons. The control coupons were the first to be tested to determine the baseline for steel properties used for preloaded coupons. This set showed typical ductile behavior, as expected. The maximum load reached was 7000 lb prior to failure. The load displacement and load strain curves are shown in Figures 3.6 and 3.7, respectively.

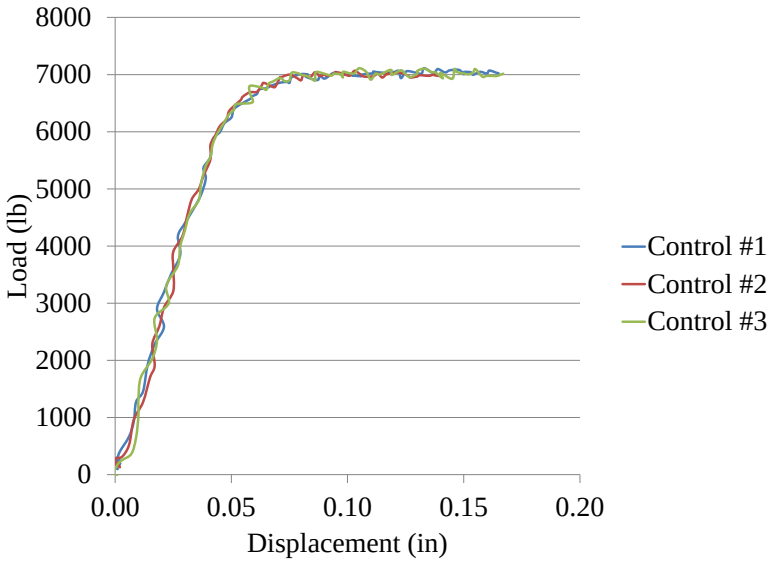

Figure 3.6. Load-Displacement: Control

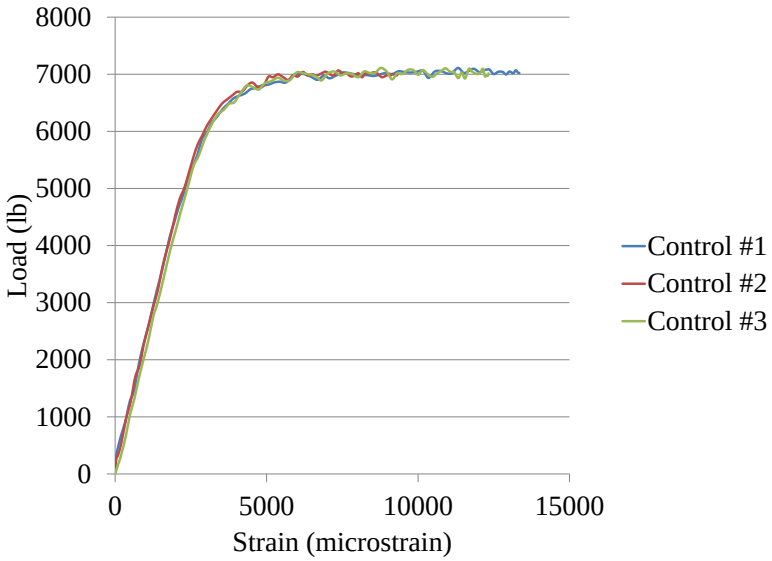

Figure 3.7. Load-Strain: Control

3.5.2. Preloaded 60% Coupons. The desired shape of this curve is to have a break of the non-preloaded FRP causing a drop in the load, then a recovery portion where the preloaded FRP picks up the load before failing. Ultimately, the preloaded FRP should be able to increase the amount of load back to the level before the break occurred.

This preloaded set of coupons tested had one side preloaded to 60% yield of the steel, while the other side was applied with no preloading. As shown in Figure 3.8, each of the load-displacement curves shows a drop in load. The use of FRP added 1000 lb to the overall maximum strength.

To determine the behavior of each material at the drop, the load strain curves were analyzed. For FRP 60,0 #1 as shown in Figure 3.9, the strain shows that each of the materials failed at the same loading. The preloaded layer did not pick up the load after the non-preloaded layer failed. The strain in the preloaded layer also did not show a delay between initial loading and engaging the FRP, as was anticipated. This was a coupon that failed at the end so the FRP debonding occurred which is not ideal.

For FRP 60,0 #2 as shown in Figure 3.10, the non-preloaded layer clearly breaks first. The steel and preloaded FRP are seen recovering slightly before failing. This is much closer to the behavior anticipated. Even with debonding on both FRP sheets the preloading layer takes the load after the non-preloaded sheet breaks showing the desired behavior. There does not appear to be any delay between when the load is added and when the preloaded FRP becomes engaged.

For FRP 60,0 #3 as shown in Figure 3.11, the non-preloaded layer appears to have supported more load after the initial drop than the preloaded layer. Again, both layers of FRP debonded, which may have been part of the reason for the reversal. This curve also shows the preloaded FRP layer engaged as soon as the test starts. These curves were not as expected. Only one of three had the preloaded layers taking load after the non-preloaded layer.

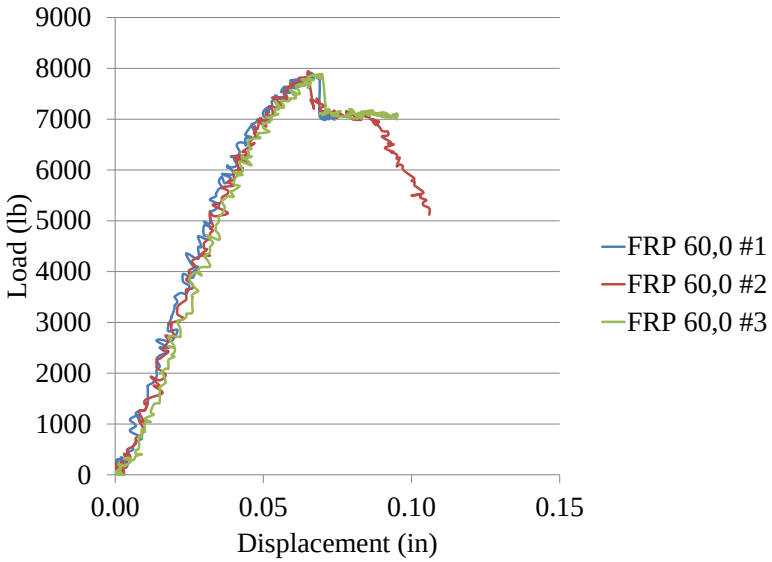

Figure 3.8. Load-Displacement: FRP 60,0

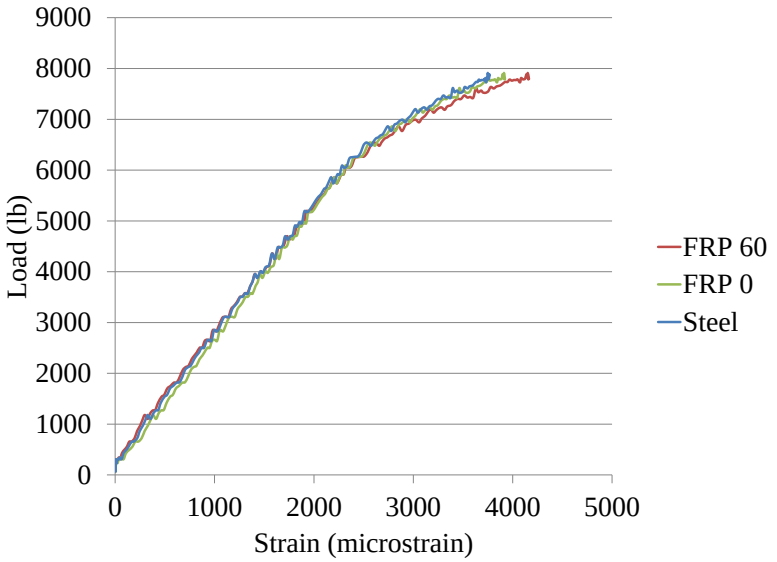

Figure 3.9. Load-Strain: FRP 60,0 #1

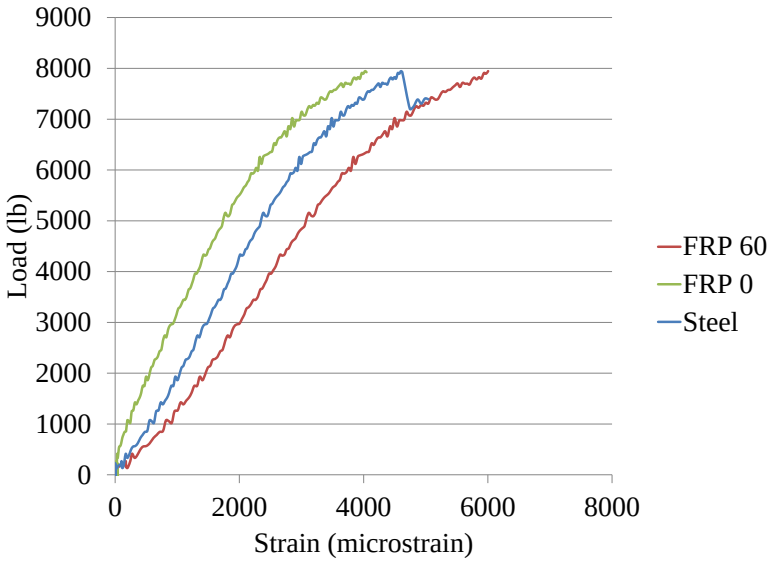

Figure 3.10. Load-Strain: FRP 60,0 #2

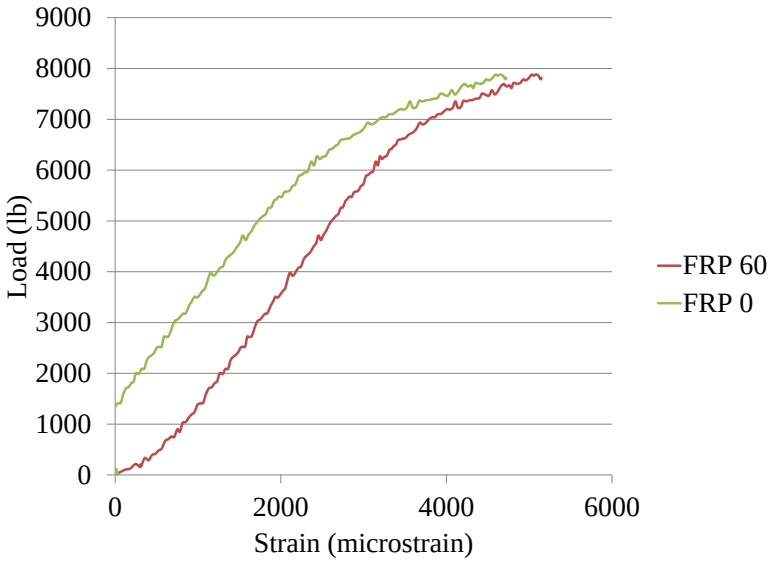

Figure 3.11. Load-Strain: FRP 60,0 #3

3.5.3. Preloaded 30% Coupons. This set of specimens was with preloaded FRP to 30% of yielding of the steel on one side and non-preloaded FRP on the other. As shown in Figure 3.12, for FRP 30,0 #1, the load-displacement curve had no visible drops in the load. Another specimen, FRP 30,0 #2, had the more predictable shape with the main drop but no load recovery. FRP 30,0 #2 was the first coupon that had the semi-circles in the center to force the failure to occur at that location. This is why the maximum load reached is much lower than the other coupons tested thus far.

It can be seen from the load-strain curves in Figure 3.13 that both of the FRP levels in FRP 30,0#1 and the steel all failed at the same time. This was most likely caused by the steel fracturing at the end which led to both sides of FRP to debond. This is the first case where the preloaded FRP does not immediately engage with the addition of loading. As shown in Figure 3.14, both layers of FRP in FRP 30,0 #2 have failed at the same point. Neither adds to the ability to carry load after the failure at 4500 lb. It seems that the recovery as indicated in Figure 3.12 was most likely from the steel before it finally fractured.

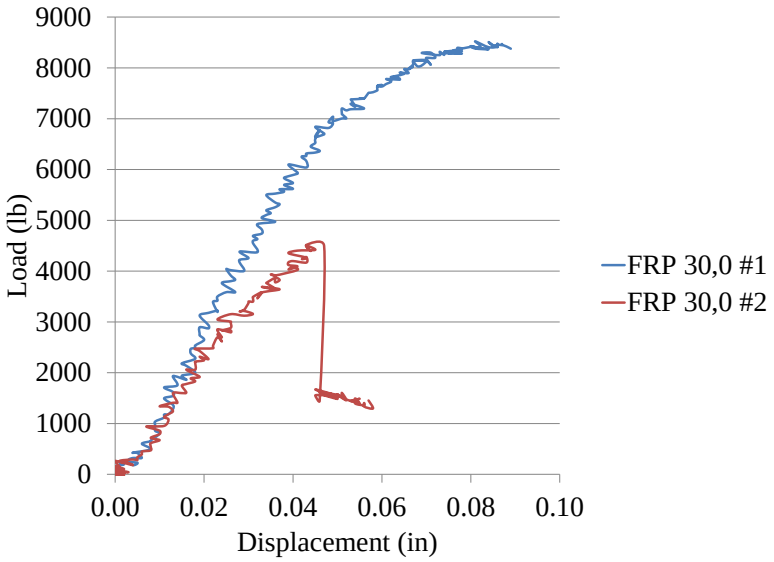

Figure 3.12. Load-Displacement: FRP 30,0

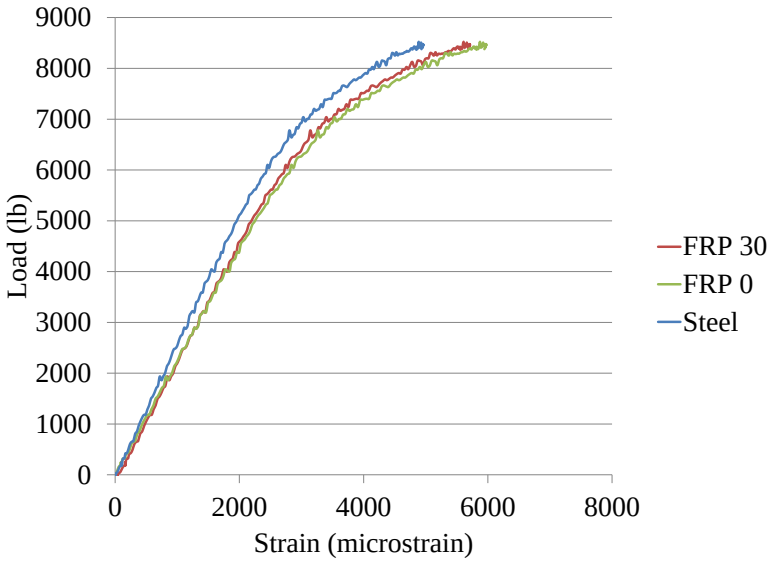

Figure 3.13. Load-Strain: FRP 30,0 #1

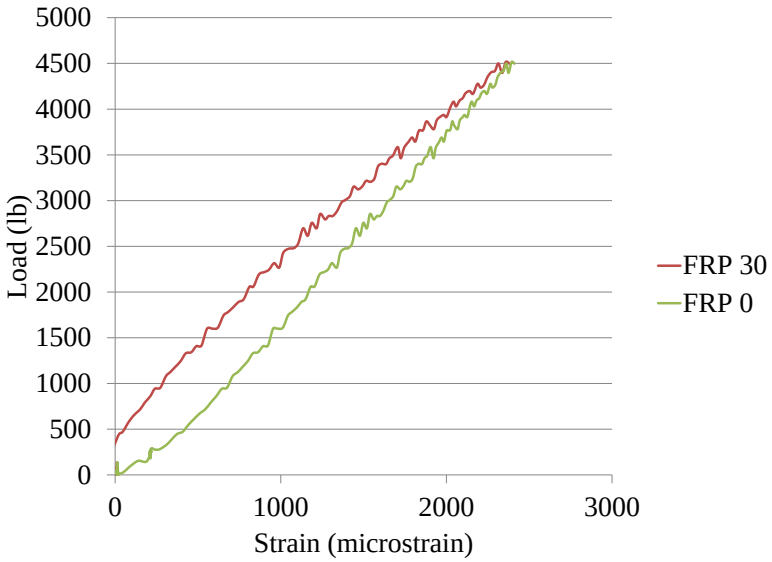

Figure 3.14. Load-Strain: FRP 30,0 #2

3.5.4. Non-Preloaded Coupon. The final coupon tested had two sides with non-preloaded FRP. For this setup, the curve should have each of the sides failing at the same point since they are both applied without preloading. This coupon did not have a reduced cross sectional area. As shown in Figure 3.15, the load-displacement curve for FRP 0,0 #1 had a drop in load and then recovery. This set achieved a 1500 lb increase in strength over the control coupons. From the load-strain curve as shown in Figure 3.16, one layer of the non-preloaded FRP fails, and then the other layer and steel pick up the load. The other layer and steel almost reach to the same load prior to any layer of FRP failing.

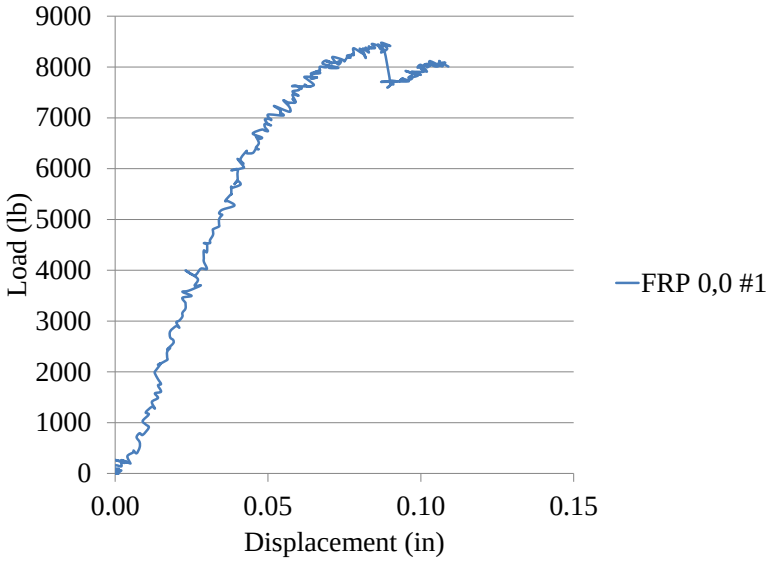

Figure 3.15. Load-Displacement: FRP 0,0

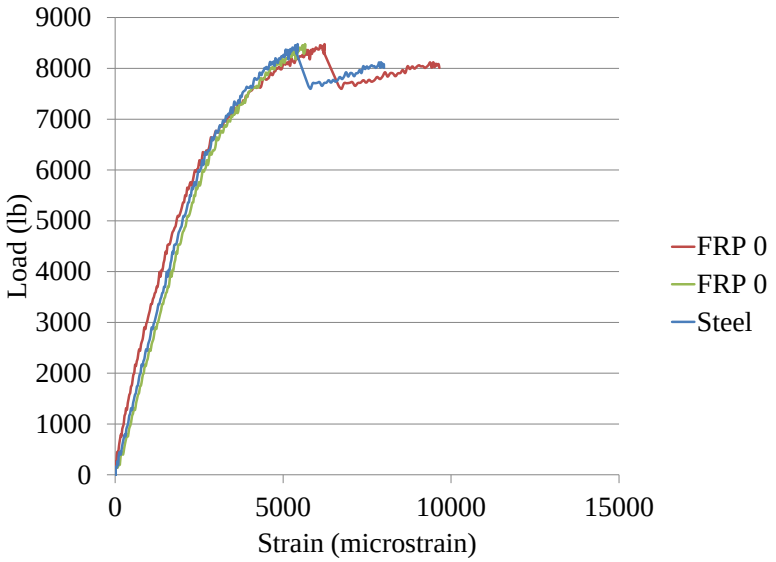

Figure 3.16. Load-Strain: FRP 0,0 #1

3.5.5. Concluding Remarks. Overall, the results were fairly inconclusive since only one specimen out of the six tested produced the preloaded layer to fail before the non-preloaded layer. Also, the two sides with non-preloaded FRP achieved the best shaped curve. This does not support the objective of failing the non-preloaded layer and then the preloaded layer consistently enough for a definitive conclusion. Another factor that should have occurred more than once in six specimens was the delayed engagement of the preloaded layer of FRP. In general, this preloading method did not produce consistent results.

3.6. SECOND COUPON TEST

After the initial coupons were tested, a second set of coupons was constructed. A phenomenon in the initial set was that bubbling occurred at fairly consistent locations on the coupons. The bubbling occurred shortly after the coupons were released from the loading and where not present prior to unloading. They appeared at about 3.5 in from each end of the FRP strip. The bubbles did not appear on the coupons with non-preloaded FRP. The coupons were given an appropriate amount of time for curing, so this was not a factor in the formation of the bubbles. From here it was concluded that the compression force on the FRP was the cause of the bubbles. A second set of coupons were created to force wrinkle formation at that position.

This wrinkle coupon set was constructed with an intentional wrinkle in the FRP to mimic the bubbling action. The wrinkle was put in under the FRP during application, 3.5 in from the end of the FRP strip, seen in Figure 3.17. This was achieved by wrapping a thin plastic wire over the surface of the coupon where the FRP was to be applied. The wire was secured in place by taping the ends of the wire to the back side of the coupon. The wire had a diameter of 0.0185 in. Markings on the coupons were drawn at specific dimensions to make sure that the FRP and wires were placed correctly. The wires were removed before the epoxy was fully cured to ensure that they could easily be removed. It was removed to not interfere with the FRP during testing. The curing time, initial loading, and final loading were recorded in Table 3.4. Each specimen is designated with a prefix W, signifying the importance of wrinkles.

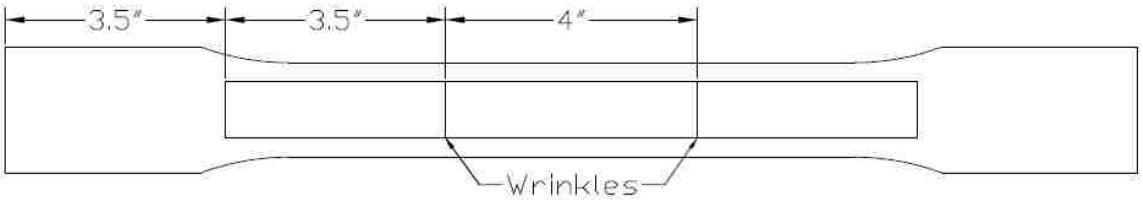

Figure 3.17. Wrinkle Locations

Table 3.4. Wrinkle FRP Coupon Loading and Curing Time

Coupon	Loading	Initial Load (k)	Final Load (k)	Curing (hrs)	Wire Removed (hrs)
W FRP 60,0 #1	Preloaded	3.199	3.169	24	20
W FRP 60,0 #2	Preloaded	3.229	3.219	24	18
W FRP 60,0 #3	Preloaded	3.223	3.179	24	18
W FRP 30,0 #1	Preloaded	1.650	1.700	24	17
W FRP 30,0 #2	Preloaded	1.782	1.621	24	17
W FRP 30,0 #3	Preloaded	1.588	1.453	24	17
W FRP 60,0 #1	None	0	0	24	-
W FRP 60,0 #2	None	0	0	24	-
W FRP 60,0 #3	None	0	0	24	-
W FRP 30,0 #1	None	0	0	24	-
W FRP 30,0 #2	None	0	0	24	-
W FRP 30,0 #3	None	0	0	24	-

After this set was constructed and cured, semi-circles were once again cut into the FRP and steel. The diameter was 1 in. There were some issues that arose when the semi-circles were cut out of this set of coupons. These cuts were not manufactured to the same standard as the initial set. The first problem with these semi-circles was that they were not made exactly in the center of the coupon. There was a difference of up to 0.25 in within the entire set. Also, the two semi-circle cuts were not lined up with each other width wise. The two semi-circles should have been parallel to each other but that was not always the case.

Another problem with the FRP near the cuts is that it was damaged in several ways. First, the FRP was not completely cut all the way through. There were still fibers that were attached to both sides of the semi-circle. The portion on the sides of the circle near the edge of the coupon had some delamination problems on certain coupons. The FRP in the testing area, between the semi-circles, appeared to not have any delamination issues.

Another problem encountered was heat. Damage can occur in FRP and saturant when the temperature reaches 140°F to 180°F depending on the manufacturer (ACI 440). On many of the coupons it appears that this limit was exceeded. Various signs included discoloration from the normal blue to a green-yellow color, and changes in finish from glossy to dull. The list of observed damage for each individual coupon was recorded and shown in Table 3.5. The decision was made to go ahead and test the coupons even with the damage to determine if any conclusions could be drawn. The entire set of 9 coupons is seen in Figure 3.18.

After this, strain gages were added to the coupons. Two strain gages were applied to each side of the FRP, with no gages on the steel itself. Each coupon had a total of four strain gages. A second set of control coupons without FRP were also produced. These were sandblasted and had the same semi-circles cut into them. This set had two strain gages applied to the steel surface. This set provided a new baseline for the FRP set with semi-circles. Strain gage locations are seen in Figure 3.19. The coupons were then tested and the mode of failure for each material is described in Table 3.6.

Table 3.5. Wrinkle Coupon Damage

Coupon	Damage
W FRP 60,0 #1	Dull (Both Sides), Discolored, Fibers Damaged
W FRP 60,0 #2	Dull (Non-Preloaded Side), Discolored
W FRP 60,0 #3	Dull (Both Sides)
W FRP 30,0 #1	Dull (0% Side)
W FRP 30,0 #2	Dull (Both Sides)
W FRP 30,0 #3	Dull (Both Sides), Discolored, Fibers Damaged

Figure 3.18. Wrinkle Coupon Set

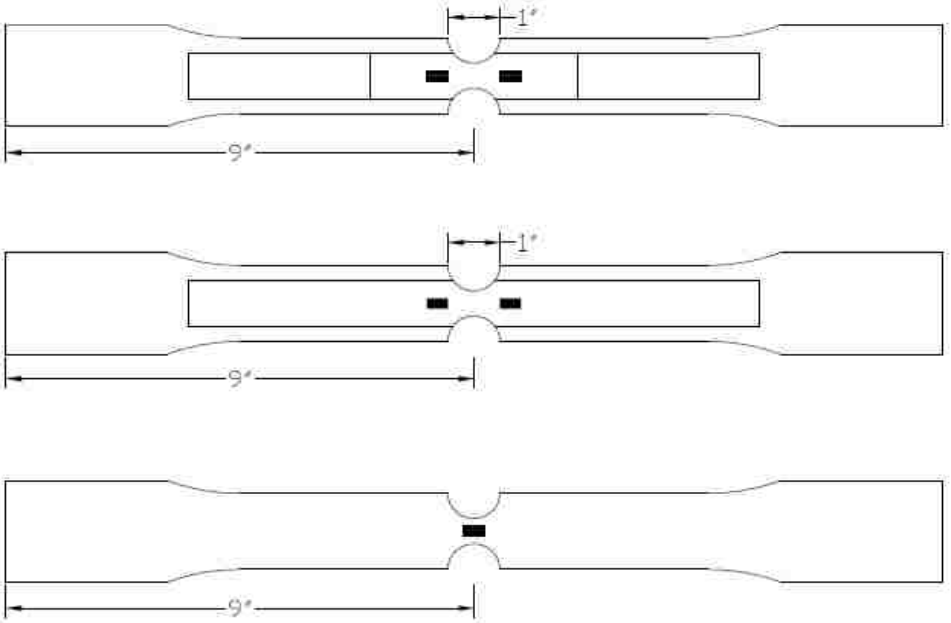

Figure 3.19. Wrinkle Strain Gage Locations: Preloaded, Non-Preloaded, Control

Table 3.6. Failure Modes of Each Material in W FRP Coupons

Coupon	Material	Failure
Control #1	Steel	Fracture in Center
Control #2	Steel	Fracture in Center
Control #3	Steel	Fracture in Center
W FRP 60,0 #1	Steel	Fracture in Center
	60 FRP	Fracture in Center
	0 FRP	Debonding from End
W FRP 60,0 #2	Steel	Fracture in Center
	60 FRP	Debonding from End
	0 FRP	Fracture in Center
W FRP 60,0 #3	Steel	Fracture in Center
	60 FRP	Fracture below Center
	0 FRP	Fracture in Center
W FRP 30,0 #1	Steel	Fracture in Center
	30 FRP	Fracture in Center
	0 FRP	Fracture in Center
W FRP 30,0 #2	Steel	Fracture in Center
	30 FRP	Fracture in Center
	0 FRP	Debonding/Fracture from Wrinkle
W FRP 30,0 #3	Steel	Fracture in Center
	30 FRP	Debonding/Fracture from Wrinkle
	0 FRP	Fracture in Center

3.7. TEST RESULTS

3.7.1. Control Coupons. This group of control coupons had reduced cross sections so that they could more accurately be compared to the FRP coupons. Figures 3.20 and 3.21 present the load-displacement curves and the load-strain curves, respectively. This set shows the ductile behavior of the steel and an average maximum load of 1750 lb.

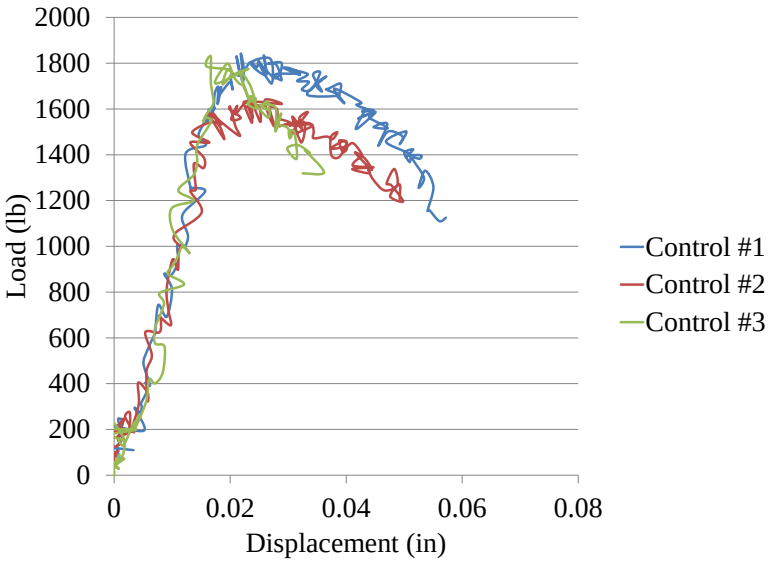

Figure 3.20. Load-Displacement: Control

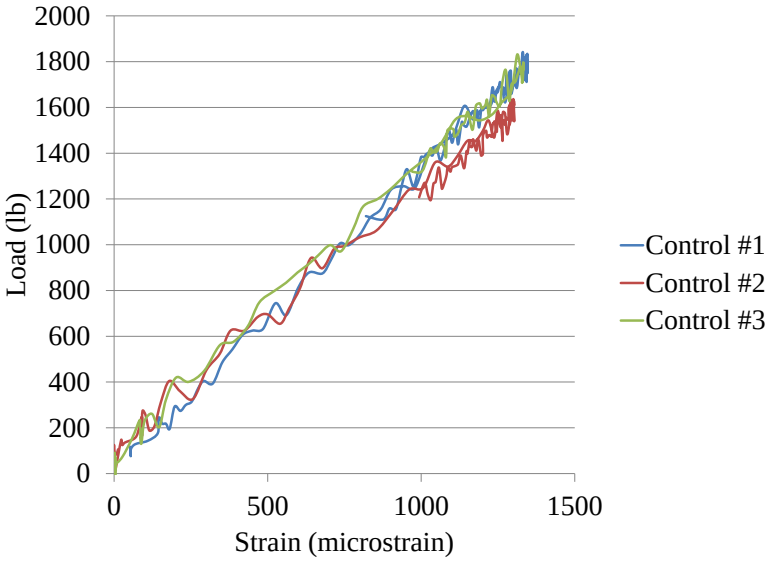

Figure 3.21. Load-Strain: Control

3.7.2. Preloaded 60% Coupons. The next coupons to be tested had one side with a preloaded level of 60% of yield of steel and the other without any preloading. As shown in Figure 3.22, the load-displacement curves each had one major drop and then some recovery before completely failing. The FRP created an average maximum load of 3500 lb instead of 1750 lb. This is double the load of the original steel coupons.

Using the load strain graphs as shown in Figures 3.23-3.25, the cause of the drop and recovery was discovered. For W FRP 60,0 #1, the preloaded layer was actually the one to break first. The non-preloaded layer picked up the load before finally failing. The preloaded layer becomes engaged as soon as the load is added, which is not ideal. W FRP 60,0 #2 appears to have the same situation. The preloaded level fails first followed by the non-preloaded level. In this case, it even appears that the non-preloaded layer does not initially engage instead of the preloaded FRP. The non-preloaded FRP is acting like the preloaded FRP. For W FRP 60,0 #3, the non-preloaded layer was the one to fail first. It had some recovery from the preloaded layer before finally failing. Again, the preloaded FRP becomes engaged as soon as load is added. Out of 3 specimens tested, only one produced positive results. The implementation of wrinkles was not very successful.

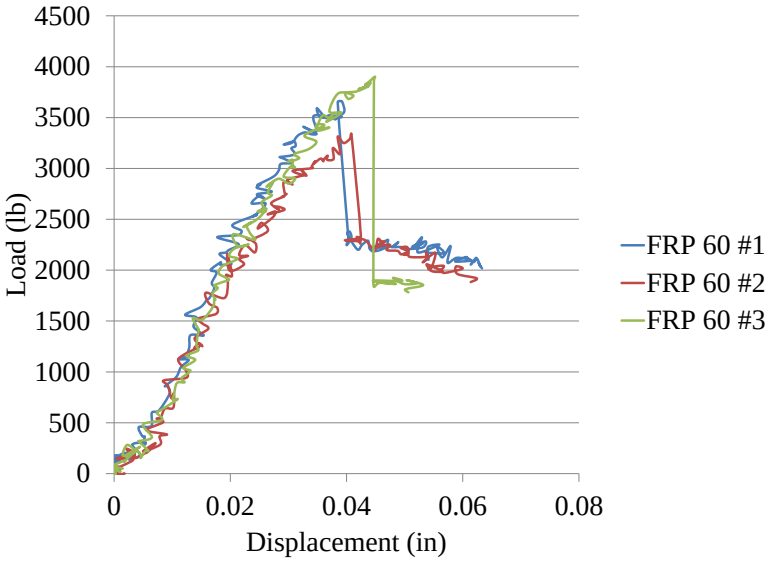

Figure 3.22. Load-Displacement: W FRP 60,0

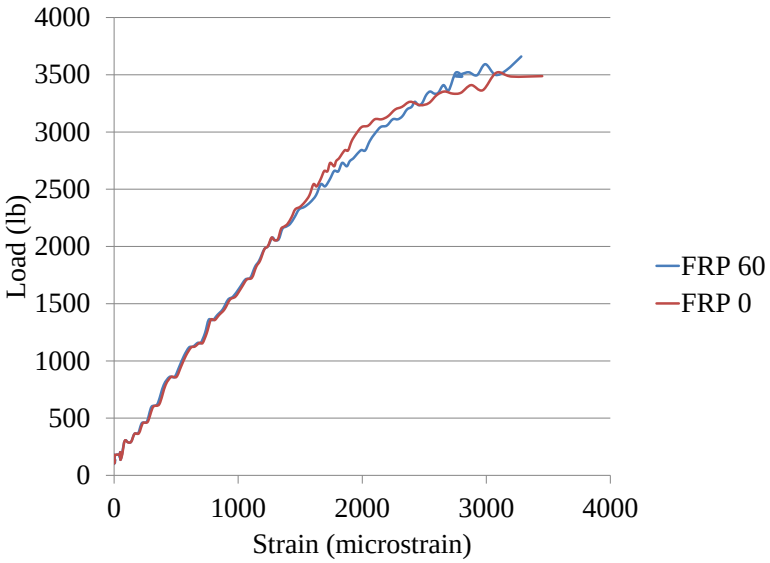

Figure 3.23. Load-Strain: W FRP 60,0 #1

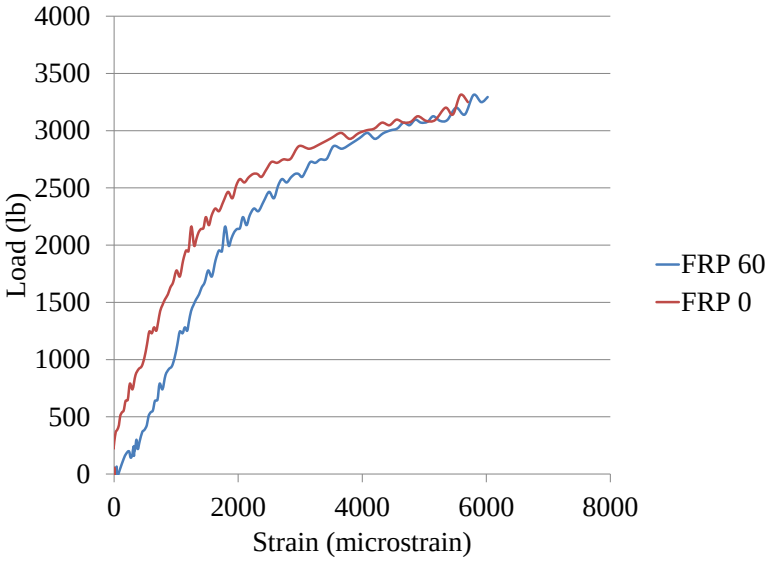

Figure 3.24. Load-Strain: W FRP 60,0 #2

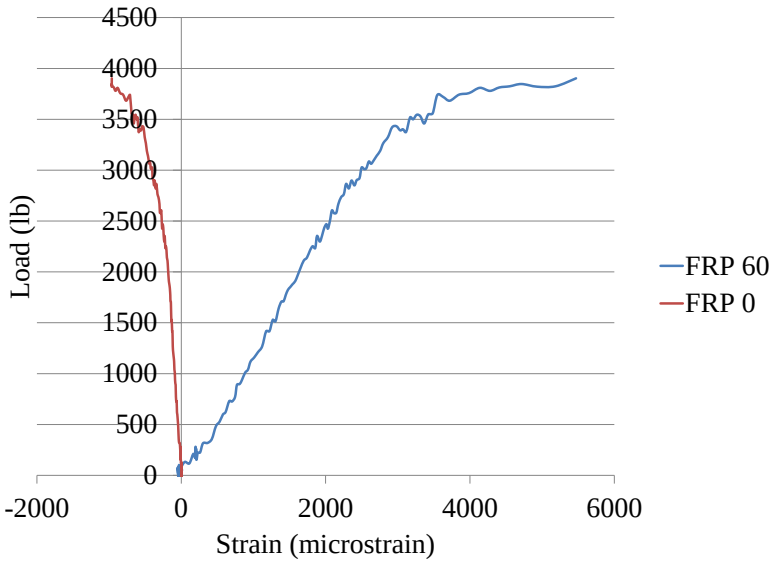

Figure 3.25. Load-Strain: W FRP 60,0 #3

3.7.3. Preloaded 30% Coupons. These coupons had one side preloaded to 30% of yielding of steel and the other side with non-preloaded FRP. This set produced average maximum loads of 4500 lb. This is more than double the strength of the control coupons. As shown in Figure 3.26, the load-displacement curves have one large drop of all three specimens and then appear to have a decreasing stair step where the recovery should be. The load-strain curves of the three specimens are presented in Figures 3.27-3.29. For W FRP 30,0 #1, the non-preloaded level fails where the large drop occurs. The preloaded level is the portion taking load before fracturing. W FRP 30,0 #2 has the preloaded layer failing first. The non-preloaded layer is the only FRP taking load that contributes to the recovery. For W FRP 30,0 #3, both layers take load after an initial drop with the preloaded layer lasting slightly longer than the non-preloaded layer. All specimens in this set have initially engaged the preloaded FRP contrary to the desired behavior.

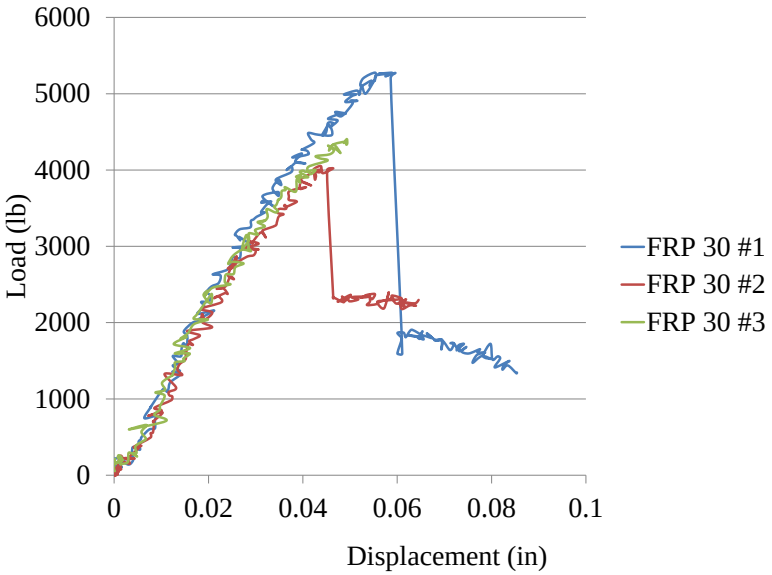

Figure 3.26. Load-Displacement: W FRP 30,0

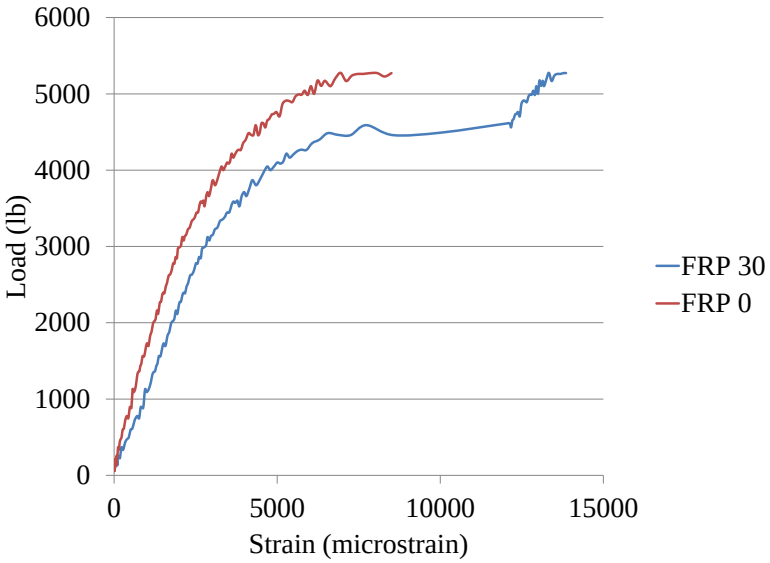

Figure 3.27. Load-Strain: W FRP 30,0 #1

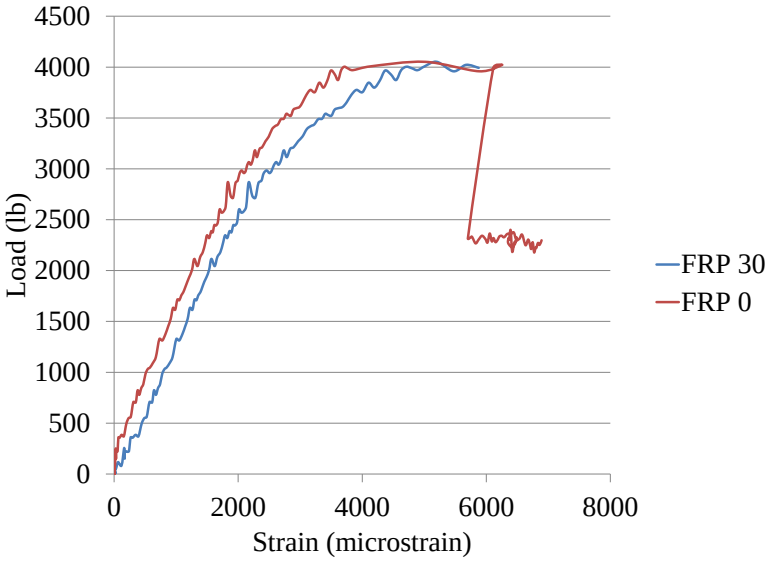

Figure 3.28. Load-Strain: W FRP 30,0 #2

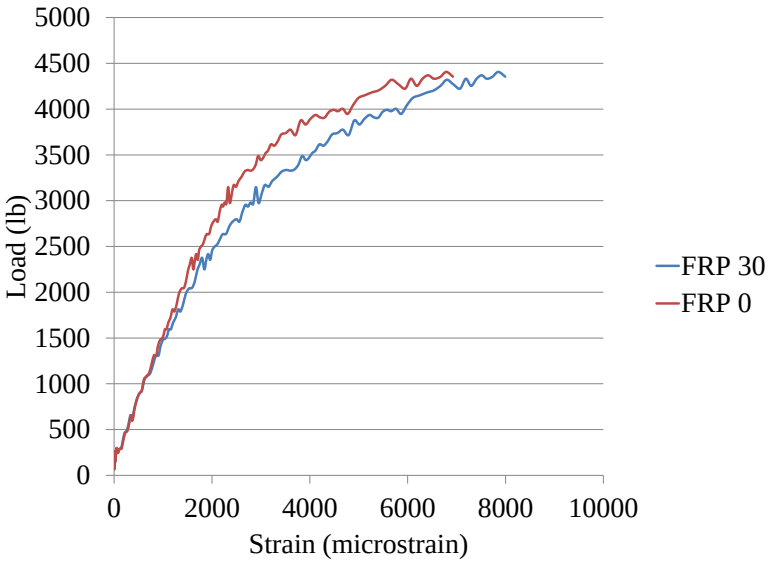

Figure 3.29. Load-Strain: W FRP 30,0 #3

3.7.4. Concluding Remarks. For this set of coupons, the results were slightly better than the initial set. Half of the specimens showed the desired behavior. The results could have been even more improved if the heat and damage encountered in the production were avoided. Even considering possible damage, this method of preloading is not effective and another method should be considered.

3.8. THIRD COUPON TEST

In this case, the preloaded FRP was intentionally left unbound in the center 2 in. This was done to attempt to allow the FRP to act independently of the steel until it became engaged. This was not consistently achieved in the other two sets of coupons. A total of six coupons were produced for this test.

These coupons were produced similarly to the first two tests. Coupons were marked to show the position of the FRP and of the portion left unbound. The unbound portion was on the preloaded side only. The unbound side of the coupon is shown in Figure 3.30. The non-preloaded side was bound to the entire length of the FRP strip. To achieve the unbound portion, a piece of plastic sheet was cut 2 in long by 1.5 in wide and attached to the center portion of the coupon. This plastic prevented the FRP from adhering to the steel underneath. The entire length of the FRP sheet was saturated in epoxy. The unbound portion came from the plastic and not a lack of saturant. The non-

preloaded side of the FRP was then applied and allowed to cure in the same lab conditions as the preloaded FRP. The final and initial loadings, displacement, and curing times are given in Table 3.7. Each specimen is designated by a prefix U.

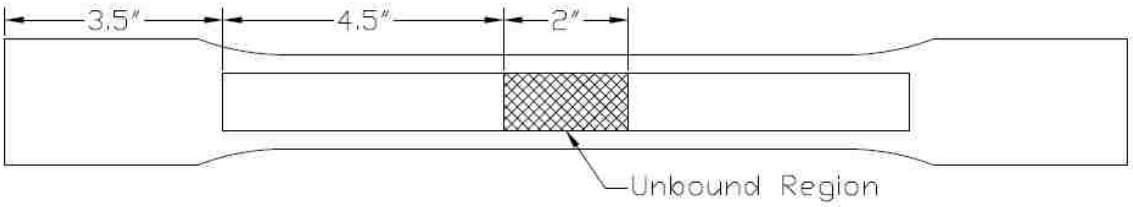

Figure 3.30. Unbound FRP Location

Table 3.7. Unbound FRP Coupon Loading and Curing Time

Coupon	Loading	Initial Load (k)	Final Load (k)	Dry Time (hrs)	Deflection (in)
U FRP 60,0 #1	Preloaded	3.275	3.327	23	0.081
U FRP 60,0 #2	Preloaded	3.248	3.238	23	0.061
U FRP 60,0 #3	Preloaded	3.276	3.224	24	0.068
U FRP 30,0 #1	Preloaded	1.732	1.734	23	0.059
U FRP 30,0 #2	Preloaded	1.689	1.730	24	0.038
U FRP 30,0 #3	Preloaded	1.647	1.735	24	0.042
U FRP 60,0 #1	None	0	0	23	-
U FRP 60,0 #2	None	0	0	24	-
U FRP 60,0 #3	None	0	0	23	-
U FRP 30,0 #1	None	0	0	24	-
U FRP 30,0 #2	None	0	0	24	-
U FRP 30,0 #3	None	0	0	24	-

After all the specimens were produced, semi-circles of 1 in diameter were cut into the center section of the coupon to force a break. One coupon was drilled and was damaged so badly it could not be tested. After that a new approach was tried. The semi-circles were punched instead of drilled. This created semi-circles without damage or debonding. A total of five were then tested from the original six created. From here, strain gages were applied to both sides of the FRP, two on each side, shown in Figure 3.31. Failure modes for each material are summarized in Table 3.8.

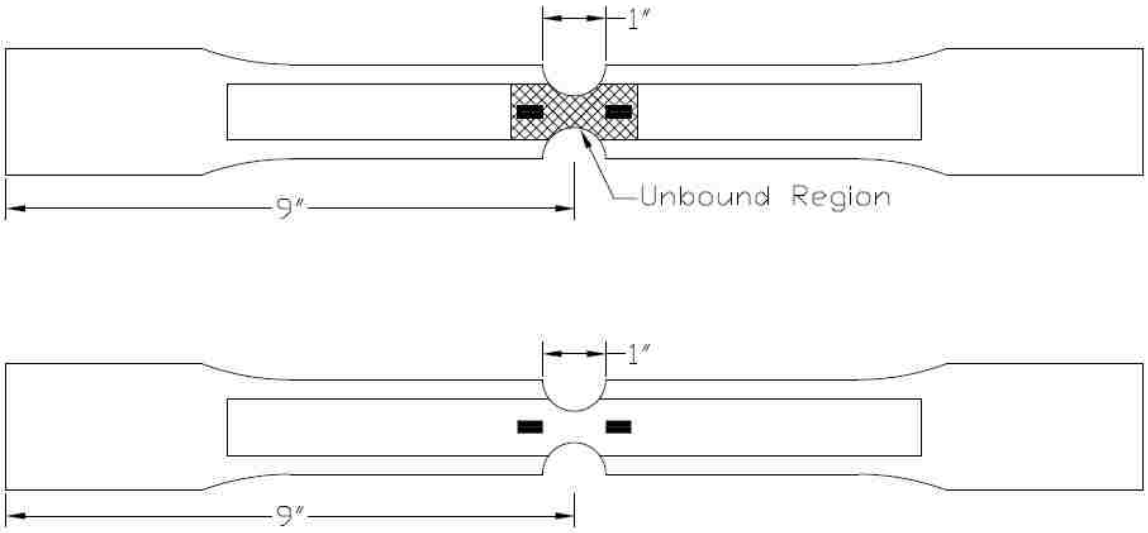

Figure 3.31. Unbound Strain Gage Location

Table 3.8. Failure Modes of Each Material in U FRP Coupons

Coupon	Material	Failure
U FRP 60,0 #1	Steel	Fracture in Center
	60 FRP	Debonding from End
	0 FRP	Debonding from End
U FRP 60,0 #2	Steel	Fracture in Center
	60 FRP	Fracture in Center
	0 FRP	Fracture in Center
U FRP 60,0 #3	Steel	Fracture in Center
	60 FRP	Fracture in Center
	0 FRP	Fracture in Center
U FRP 30,0 #2	Steel	Fracture in Center
	30 FRP	Fracture in Center
	0 FRP	Debonding/Fracture 3 in from End
U FRP 30,0 #3	Steel	Fracture in Center
	30 FRP	Fracture in Center
	0 FRP	Fracture in Center

3.9. TEST RESULTS

3.9.1. Preloaded 60% Coupons. From the load displacement graph, Figure 3.32, U FRP 60,0 #2 had one failure without any recovery. U FRP 60,0 #1 and #3 had recovery before finally failing. Compared to the control coupons with the reduced cross section, the average load increased from 1750 lb to 3000 lb.

From the load-strain curve of U FRP 60,0 #1 as shown in Figure 3.33, it is seen that the main drop does not appear to be caused by failure of either layer of FRP. The preloaded and non-preloaded FRP both recover for a while before the layers finally debond. The strain indicates that the preloaded FRP still becomes engaged as soon as load is added.

For U FRP 60,0 #2, the load-strain curve as shown in Figure 3.34 proves that both FRP levels break at the same load and no recovery occurs. U FRP 60,0 #3 has the most desired result of this set as shown in Figure 3.35. The preloaded layer contributes to the recovery, with the non-preloaded layer failing first. This curve also shows that the strain in the preloaded layer has a delay before becoming engaged.

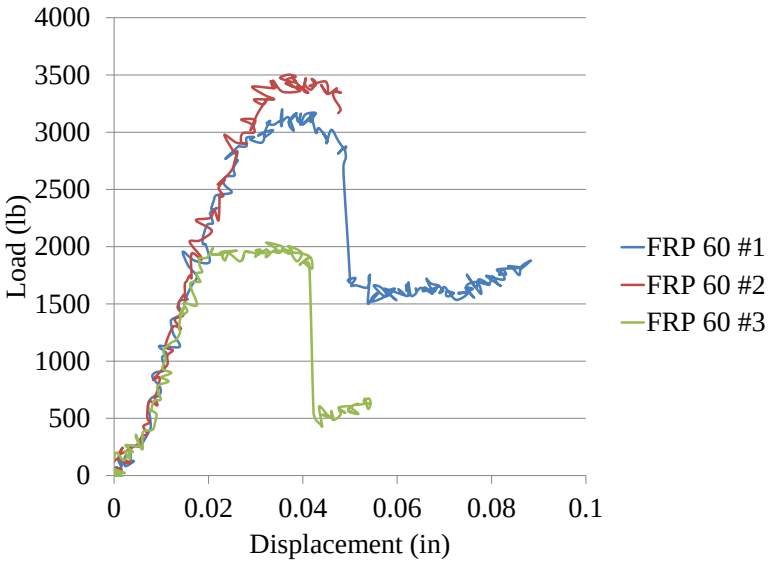

Figure 3.32. Load-Displacement: U FRP 60,0

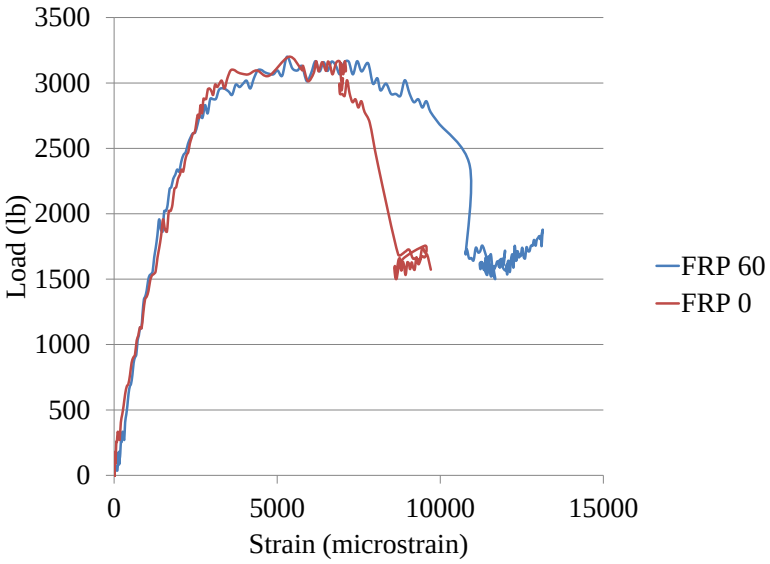

Figure 3.33. Load-Strain: U FRP 60,0 #1

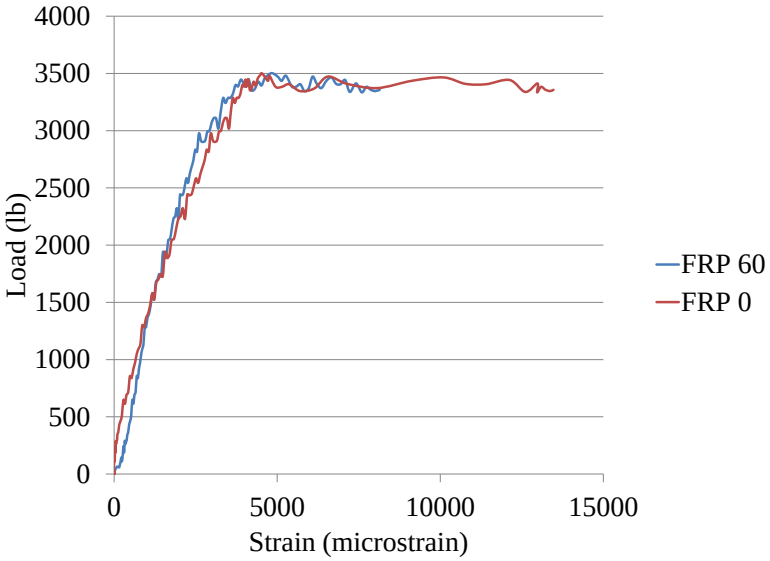

Figure 3.34. Load-Strain: U FRP 60,0 #2

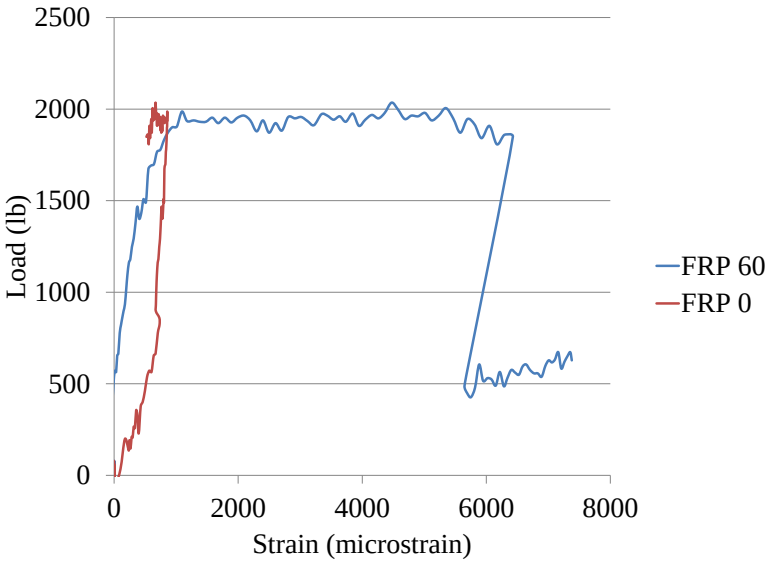

Figure 3.35. Load-Strain: U FRP 60,0 #3

3.9.2. Preloaded 30% Coupons. The coupons with a preloaded level of 30% of yielding of the steel and the non-preloaded level were the final set tested. U FRP 30,0 #1 was badly damaged when the semi-circles were cut. It was not tested. From the load-displacement graph, Figure 3.36, both U FRP 30,0 #2 and #3 encountered a large drop in load followed by a recovery that increased in load slightly. From the load-strain curve of U FRP 30,0 #2, Figure 3.37, it is seen that the recovery was unfortunately due to the contribution of the non-preloaded layer. So even though the load displacement curve showed a positive result, the load strain curve proves that it was really the non-preloaded layer providing the recovery. As for U FRP 30,0 #3, both the preloaded and non-preloaded levels failed at the same loading as illustrated in Figure 3.38. The recovery on this specimen is most likely from the steel before it fails. Even though the load displacement curve showed positive results, they were proven wrong when looking at individual materials.

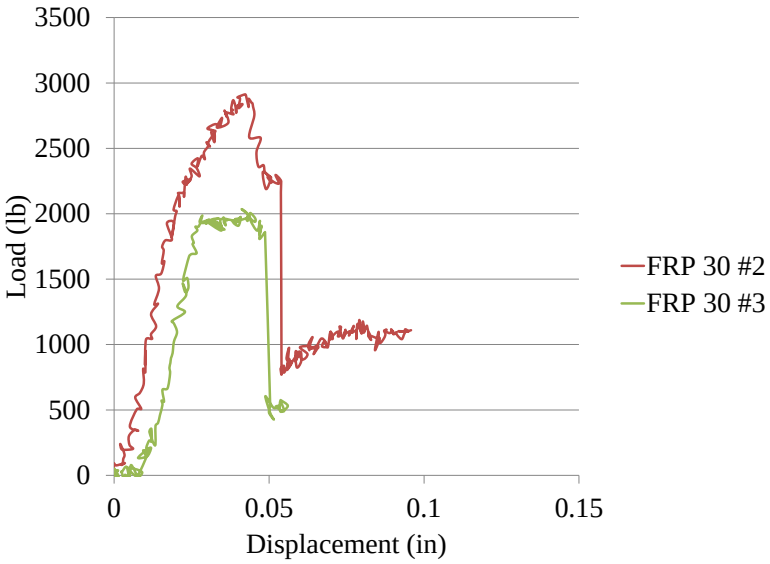

Figure 3.36. Load-Displacement: U FRP 30,0

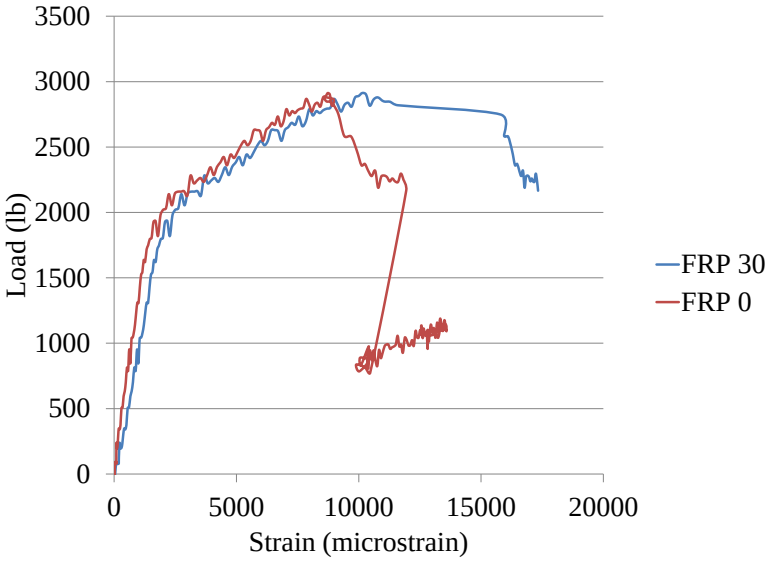

Figure 3.37. Load-Strain: U FRP 30,0 #2

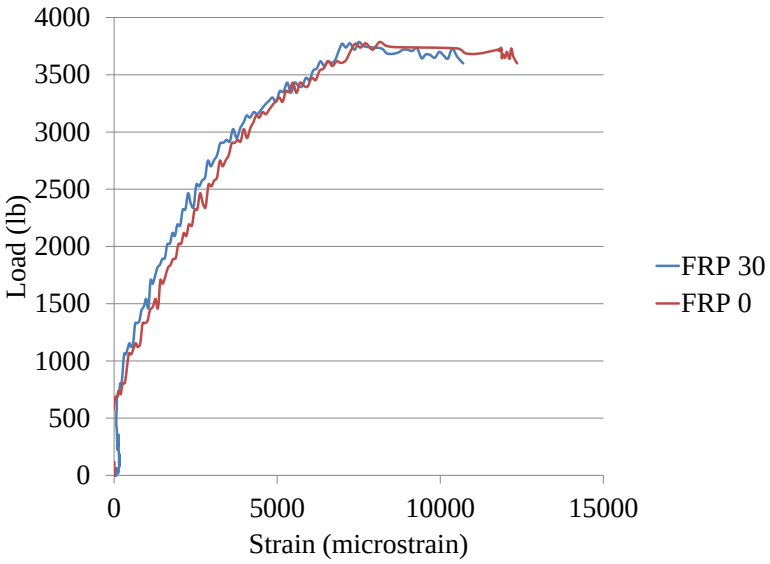

Figure 3.38. Load-Strain: U FRP 30,0 #3

3.9.3. Concluding Remarks. This unbound set of coupons only produced one positive result out of five specimens. The method of preloading that includes leaving a portion unbound in the center appears to be unreliable as well.

3.10. SUMMARY ON COUPON TESTS

The coupons tested did provide some insight into the behavior of preloaded FRP. The initial set of coupons had many issues with debonding and did not provide reliable results of the preloaded FRP. The wrinkle set of the coupons was the best preforming of the three sets, even with the damage encountered. This set still only achieved success 50% of the time. The unbound coupons received poor results, despite the high expectations for the set. Out of a total of seventeen coupons tested with FRP only five got a positive result. Even though the steel was sandblasted, it may not have been permeable enough of a surface to achieve sufficient bonding needed so that most of tested specimens reveal in premature failures. Moving from steel to concrete should provide improved results since the concrete is more porous and should provide greater bonding with the primer and saturant.

4. INTERMITTENT DEBONDING FRP SYSTEM WITH BEAM TESTS

4.1. GENERAL

In Section 3, preloading method was discussed with steel coupon tests. Due to limited strains induced under reduced service loads (30% and 60%), various FRP strips installed in stage were engaged at small strain differences, limiting the pseudo-ductility of a so-designed FRP system. In this section, an alternative to introduce strain differences in various FRP strips is developed to directly control the strain differences among the FRP strips with geometry designs. Since it is difficult to realize the geometry design of FRP strips on small scale coupon specimens, large-scale RC beams are tested instead. In addition, the use of RC materials in beam tests is appropriate for practical applications of the developed technology in RC structures.

Staged FRP strips are deployed in parallel on the tension side of a RC beam. The outer strips are installed on the tension side of the beam according to the conventional FRP installation procedure. The middle strips, however, are designed and installed with predetermined arches that are periodically distributed along the beam length so that they are engaged at higher loads than those for the side strips.

4.2. BEAM DESIGN

RC beams were designed and cast to test the proposed FRP application. As shown in Figures 4.1 and 4.2, each measured 11 ft long, 12 in wide, and 18 in deep. It was reinforced with four longitudinal, #6 rebar. The top two longitudinal bars measured 126 in long. At each end, the bottom bars had 90 degree bends that are 7 in long. Stirrups were created from #3 rebar. The stirrups had a width of 10.5 in and a depth of 15.5 in. A total of thirty stirrups were used in each beam. Spacing was set to 4 in between stirrups and 5 in from each end.

The two bottom longitudinal bars were instrumented with six strain gauges, three on each longitudinal bar. As illustrated in Figure 4.3, the three strain gauges were placed at the center and at 4 in on either side of the center, respectively. Chairs of 0.5 in were added to the bottom and sides to provide proper spacing between the cage and form.

Hooks were added to the top of the cage to assist in lifting the beams around the lab with a crane.

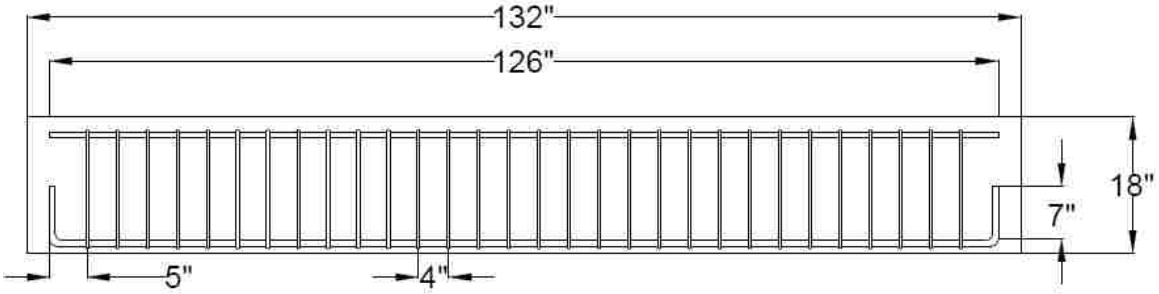

Figure 4.1. Beam Dimensions

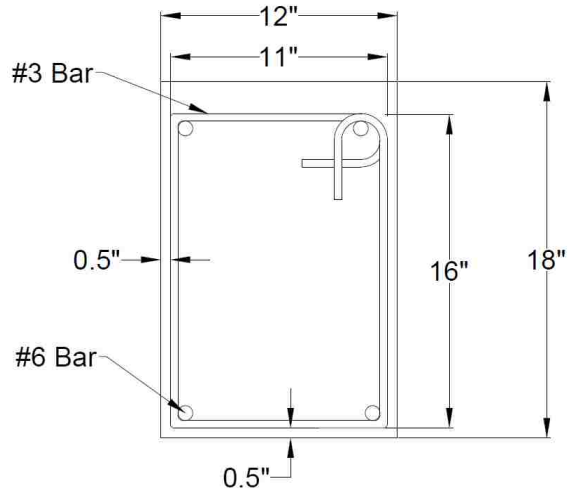

Figure 4.2. Stirrup Dimensions

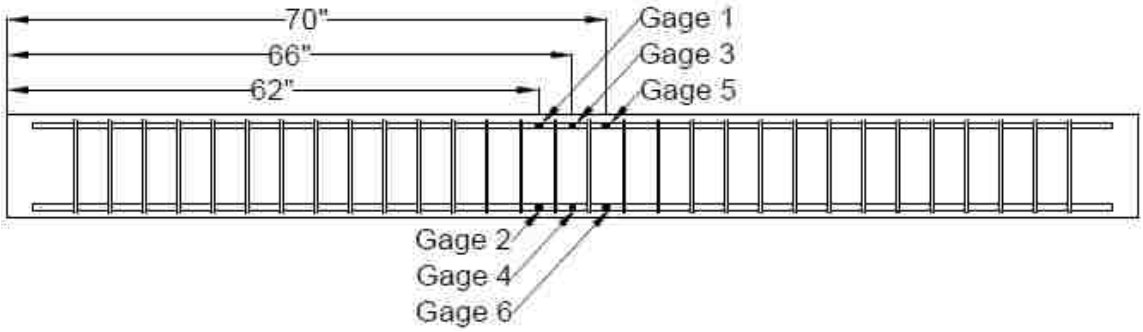

Figure 4.3. Steel Rebar Strain Gage Locations

After the rebar cages were completed, they were lowered into the steel forms. Concrete was placed in separate batches, due to the limited number of forms available.

The concrete placement is shown in Figure 4.4. Concrete was delivered from Rolla Ready Mix. Slump was measured to ensure proper workability. Once the concrete produced a slump around 4.5 in, it was placed in the forms and vibrated internally. The vibration, shown in Figure 4.5, is done to achieve consolidation and ensure no voids occurred. The beams were allowed to cure covered with wet burlap and plastic sheeting for the first day. The beams were then deformed and allowed to cure the rest of the time in the lab until they were used for FRP application.

Cylinders and flexure beams were also cast. The cylinders had a diameter of 4 in and were 8 in tall. Flexure beams measured 6 in by 6 in and 24 in long. They were allowed to cure and were then deformed. Cylinders were sulfur capped before being tested for the 28 day compressive strength of the concrete. Details on compressive strength can be found in the individual beam tests below.

Figure 4.4. Concrete Placement

Figure 4.5. Internal Vibration

4.3. FRP APPLICATION

This application process applies to all of the beams with FRP application. Strips of carbon fiber were cut to size according to the appropriate ratios needed for the staging. Specifications for each beam are described below in the individual tests. Surface preparation was required to level the bottom face of the beam and open the pores in the concrete to provide the best possible surface for adhesion. The beam was then labeled with locations of the FRP as well as the staging method used in that particular test. Primer was mixed and applied to the beam. It was allowed to dry until becoming tacky. Next, saturant was mixed. Both the saturant and primer were mixed per manufacturer's instructions. Strips were pre-impregnated with saturant before being applied to the beam. This procedure made it easier to ensure that the FRP was fully saturated while not interrupting the various staging that was in place.

Prior to testing, the FRP beams were given a minimum of 36 hours to cure. Strain gages were installed to the FRP surface in addition to the gages already in place on the steel rebar. Locations for the strain gages are described in individual tests.

4.4. TESTING PROCEDURE

All the beams were tested under four point loads as shown in Figure 4.6. The setup was housed in the High Bay Structures Lab. Support points were spaced at 9 ft

center to center and the load points were 3 ft center to center. Two actuators provided the loading rate of 0.05 in/min. All of the strain gages on the steel rebar and FRP sheets were recorded throughout the test. In addition to the strain gages, 2 DCVTs measured deflection at the center of the beam. At various levels of loading, cracks were marked on the beams to show the progression over time.

Figure 4.6. Beam Test Setup

4.5. FIRST PHASE BEAM TEST

In the first phase, three beams were tested with three different configurations of FRP. Beam 1 was a control with no FRP installed. Beam 2 had separate FRP sheets applied at two different stages. The middle strip was at stage 1, while the two outer strips were applied at stage 0. For this test, the highest level of staging is stage 1 while stage 0 refers to a conventionally installed FRP sheet. The FRP strips were installed side by side and are placed longitudinally along the length of the beam. Beam 3 had three different FRP stages. Like Beam 2, the FRP strips were arranged by staging with the highest staging, stage 2, being placed in the center. The next strips of FRP were installed at a lower stage, stage 1. The last strips, closest to the beam edges, were placed at stage 0.

None of the beams tested were loaded and did not have any cracks prior to having FRP applied. The test matrix for the first phase beam test is seen in Table 4.1. Further details are presented below.

Table 4.1. Test Matrix First Phase Beam Test

Beam	Pour	Description	Stage 0	Stage 1	Stage 2
1	1	Control-No FRP	-	-	-
2	2	2 Stage FRP	2-1.25 in wide	1-7.5 in wide	-
3	3	3 Stage FRP	2-1 in wide	2-1.5 in wide	1-5 in wide

Beam 2 had two levels of staged FRP. The goal of the two levels was to have the stage 0 FRP fail first, so that the stage 1 layer can recover the load before it finally fails. Staging was achieved using a strain difference of 0.04 in/in. A total width of 10 in was used on the bottom face of the beam. The ratio of the stage 1 to stage 0 FRP was also determined to be 75% for stage 1 to 25% for stage 0. This means that of the total 10 in FRP width, 7.5 in was of the stage 1 strip and the other 2.5 in was the stage 0 strip. This 2.5 in strip was split into two 1.25 in strips so that one would be placed on either side of the middle stage 1 section for symmetry. For the stage 1 and stage 0 strips, only one carbon fiber sheet of thickness was used. The total length of the FRP was 8 ft. The portion of the beam that was to have the staging was the middle 3 ft of the beam. So, the staged section there was a center 3 ft of FRP and two 2.5 ft ends were fully bonded and did not contain staging. A layout of the FRP is shown in Figure 4.7. In this set of beams plastic wires were used to create the staged effect. For the correct applied staging, the spacing of the wire was determined. The wire thickness was 0.125 in. From here it was determined that a spacing of 2.6 in was required for the correct staging. This 2.6 in was a 60% increase of the calculated spacing to account for some possible error in the application process. The final strain used for the staged layer was 0.06 in/in.

Beam 3 used three levels of staging in an attempt to achieve ductile behavior. The strain difference for stage 1 was 0.03 in/in and stage 2 was 0.07 in/in. The width ratio of different staged levels was also an important factor. The percentages used were 20% for the stage 0 level, 30% for stage 1, and 50% stage 2. The total width of the combined FRP strips was 10 in with one layer thick of the carbon fiber sheets. For this

beam, a 5 in strip stage 2 was placed in the middle, followed by two 1.5 in strips of stage 1, and then two 1 in stage 0 sheets near the edges of the beam. A diagram of the FRP positions is shown in Figure 4.7. For the staged section, The 3 ft center section was strengthened with the staged FRP layers. Final strains, after the 60% increase for possible application errors, were found to be 0.05 in/in for stage 1 and 0.11 in/in for stage 2. Spacing of 3.3 in and 1.4 in was used, respectively.

The strips were placed on the beam in order of staging levels. The levels were installed on separate days to ease application. The middle strip was first applied and allowed to dry then the plastic wires were removed. This allowed the FRP to retain the predetermined arches locally. The wire was removed to leave space for the FRP as it was put into tension. A picture of the application of the middle strip of FRP is shown in Figure 4.8. The FRP was allowed to fully cure before the next stage was applied.

For Beam 2, a total of ten gages were installed: five gages on the stage 1 strip and the other five gages on the stage 0 strip. Beam 3 had fifteen total gages, five on each staged level. Locations for the gages are shown in Figure 4.9.

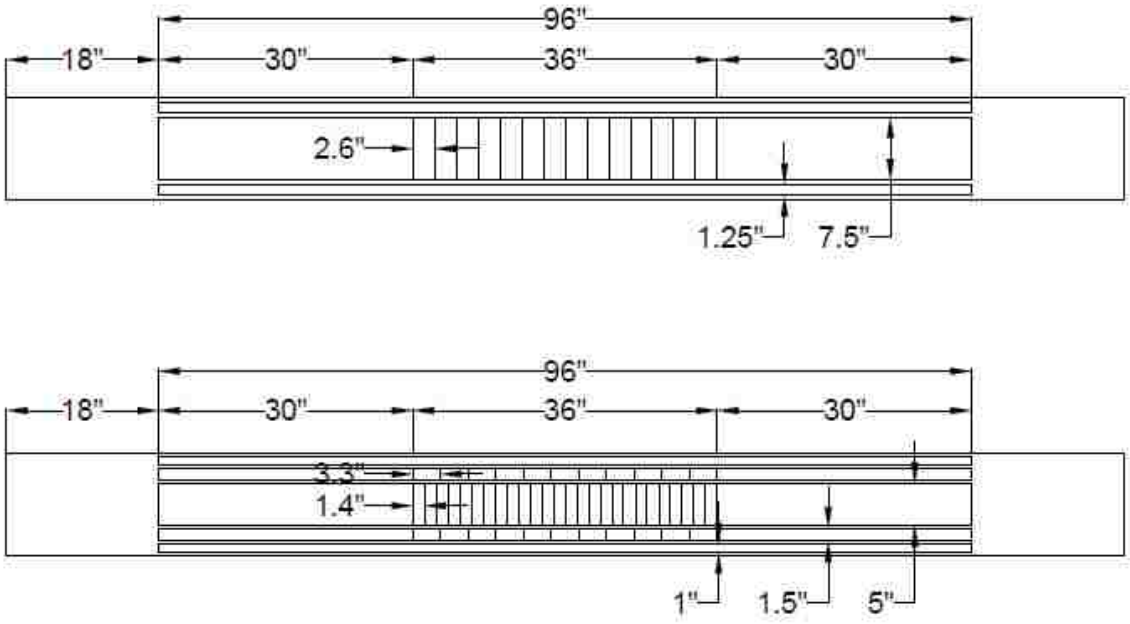

Figure 4.7. FRP Dimensions: Beam 2 and Beam 3

Figure 4.8. During FRP Application

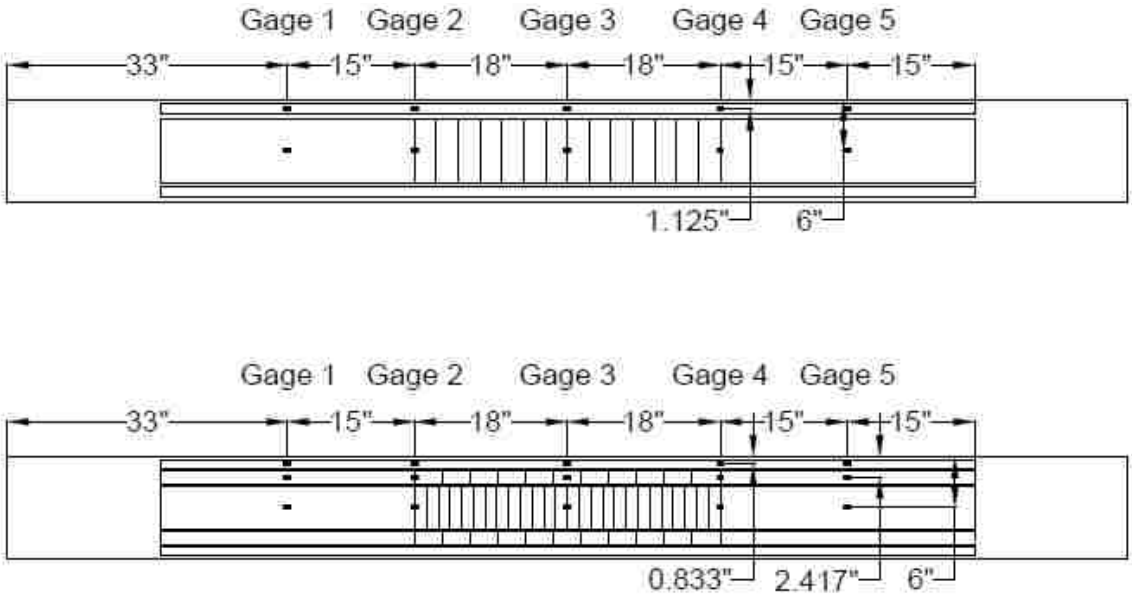

Figure 4.9. FRP Strain Gage Location: Beam 2 and Beam 3

4.6. FIRST PHASE BEAM TEST RESULTS

This set provided the first attempt at staging FRP in order to create a ductile FRP system. While the overall concept was proven some fine-tuning needs to be done in order to get a longer time between when the non-staged layers and staged layers fail.

4.6.1. Control Beam. Beam 1 was the control beam without FRP. The failure is seen in Figure 4.10. The load-displacement curve, Figure 4.11, shows that the beam was cracked around 15 k and began yielding around 54 k. The maximum load reached was 73 k. The load-strain graph for the steel rebar in the control beam is found in Figure 4.12.

Figure 4.10. Failure of Beam 1

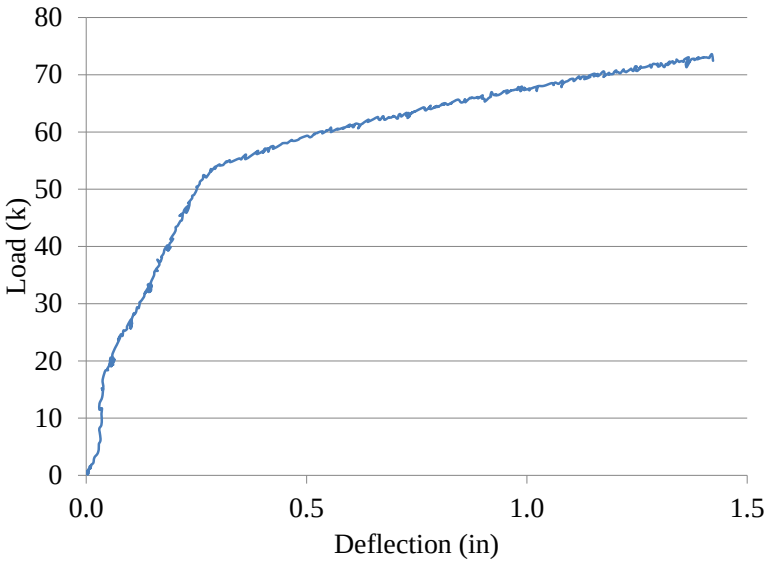

Figure 4.11. Load-Deflection: Beam 1

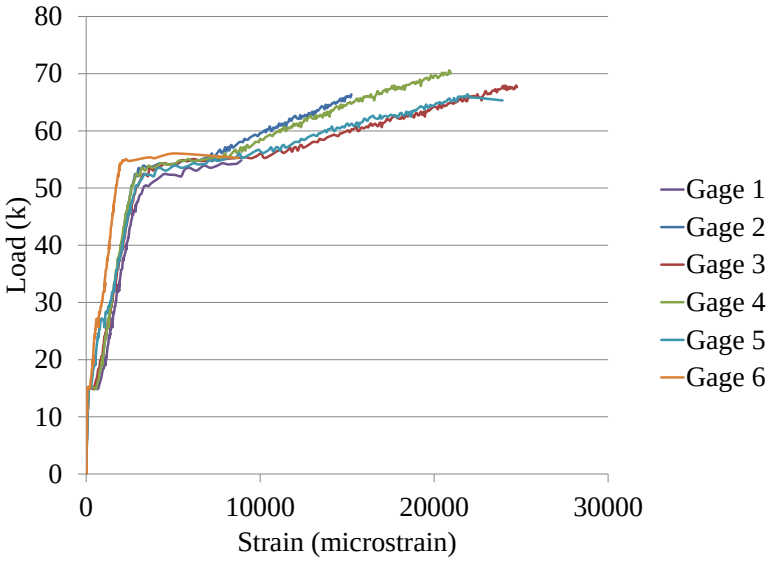

Figure 4.12. Load-Strain: Steel Rebar

4.6.2. Two Staged FRP. The goal of Beam 2 was to achieve a failure of the stage 0 layer, followed by a recovery in load by the stage 1 layer, and finally the failure of the stage 1 layer. The FRP on this beam failed due to the fracture of the FRP sheets as seen in Figure 4.13. There was some debonding present from the fracture locations towards the ends of the beam. This was most likely due to high stresses developed at locations of flexure cracks. The load-displacement curve, Figure 4.14, shows the beam reached a peak load of 85 k before stage 0 failed.

As shown in the load-strain curves, Figures 4.15-4.17, the stage 1 layer of FRP fractured after the stage 0 layer although the difference was negligible. The stage 1 layer showed a drop and then a small recovery in load. This was very brief before failure. The stage 0 layer failed at 85 k. Looking at the initial strain difference between the stage 1 and stage 0 layers, it is shown that the strain in the stage 1 layer does not increase until about 20 k. The stage 0 layer increases in strain as soon as load is added. This is positive because the stage 1 layer did not engage initially. After testing the FRP on the bottom of the beam was examined and it was determined that the FRP did not stretch out flat while in tension. It still had the shape of the arches present. This could be one reason why the FRP did not behave as expected.

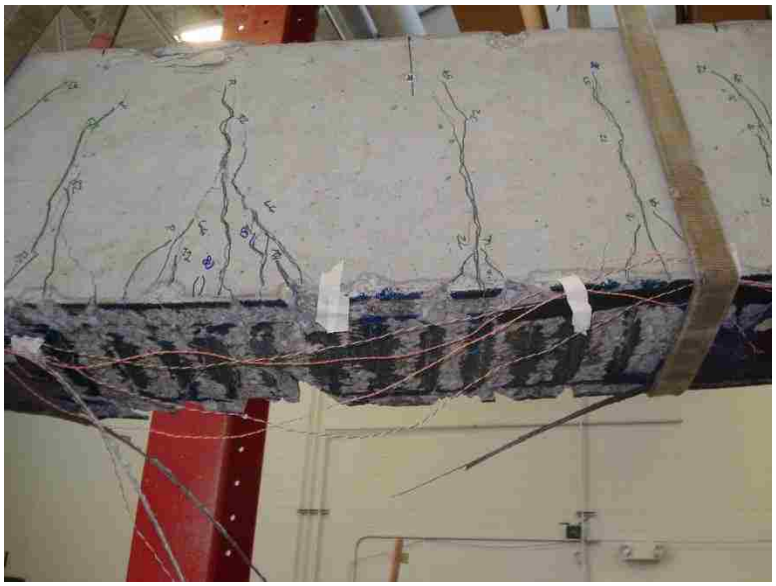

Figure 4.13. Failure of Beam 2

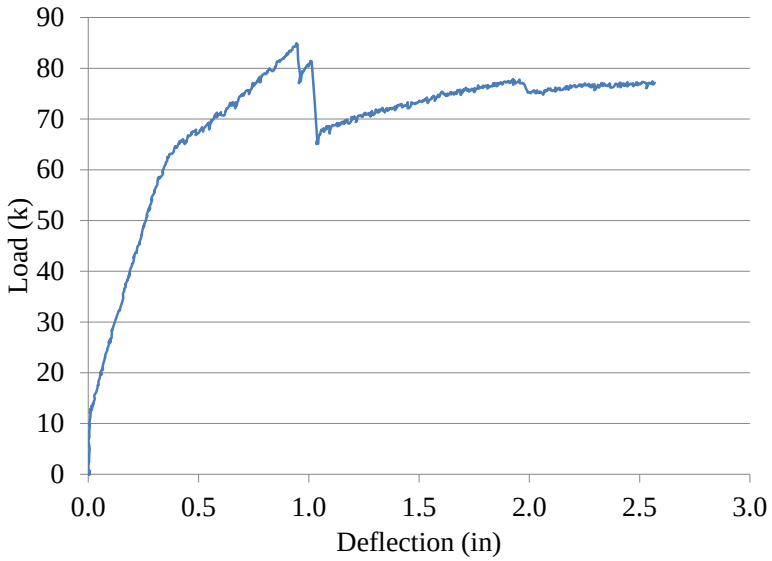

Figure 4.14. Load-Deflection: Beam 2

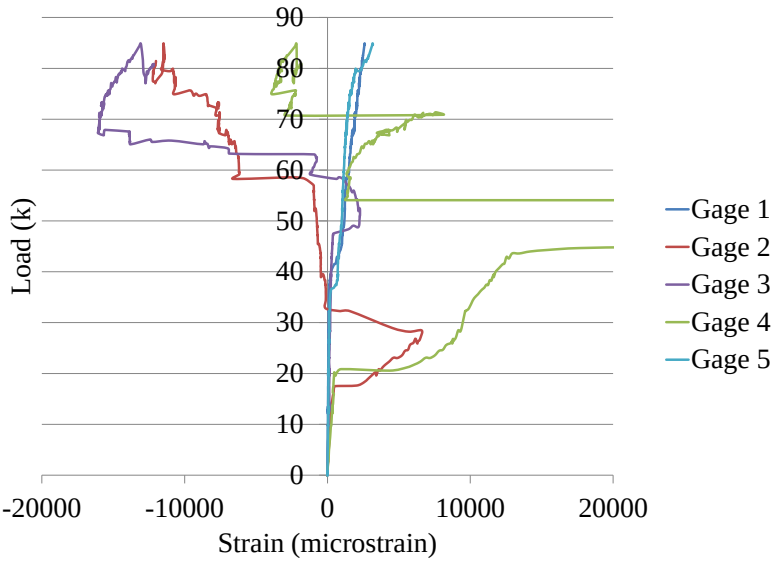

Figure 4.15. Load-Strain: Stage 1 FRP

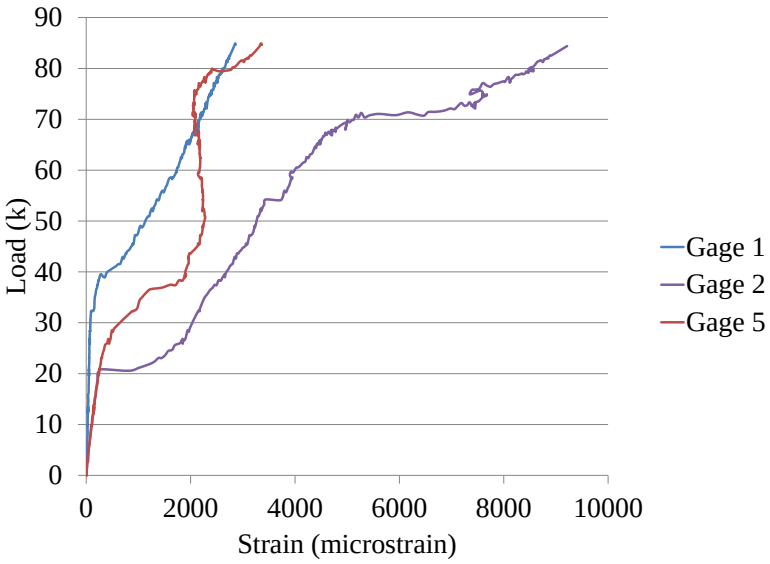

Figure 4.16. Load-Strain: Stage 0 FRP

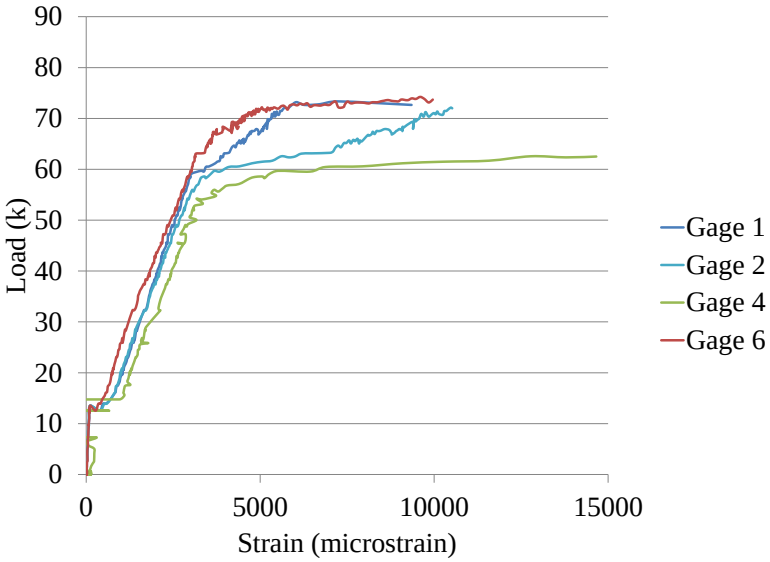

Figure 4.17. Load-Strain: Steel Rebar

4.6.3. Three Stage FRP. The final beam of this set was Beam 3. This FRP had fracture as the main failure mode seen in Figure 4.18. Although debonding was observed near the flexural cracks, it did not reach to end of the beam. This showed an excellent bond at the end of the FRP sheets. The load-displacement curve can be seen in Figure 4.19. The curve shows that the beam reached a maximum load of 80 k. This is 5 k less than the last beam with two staged levels of FRP. This could be due to the arrangement of the FRP. When FRP fractures it does so perpendicular to the direction of the fibers so the smaller the width, the smaller the number of fibers needed to fracture before complete failure.

The load-strain curves, Figures 4.20-4.23, were examined next. The stage 2 layer of FRP contributed little to recovery prior to failure of the beam. This sheet fractured at 80 k. The initial strain is very close to zero until 15 k showing that there was a delay between when the load was added and when the FRP became engaged.

The stage 1 FRP did not become engaged until a load of over 20 k. This layer appears to be the reason for the second small peak at 79 k of load. After the stage 2 level failed, the stage 1 layer picked up the load for a very short time. This is not ideal, but it is still promising to see that a staged layer was able to take load over a stage 0 layer.

The stage 0 FRP is slightly engaged from the time that the load is added, more so than the stage 1 or 2 layers. The end of the stage 0 layer did not have any part in the recovery. This is expected since this layer is the stage 0 layer.

Figure 4.18. Failure of Beam 3

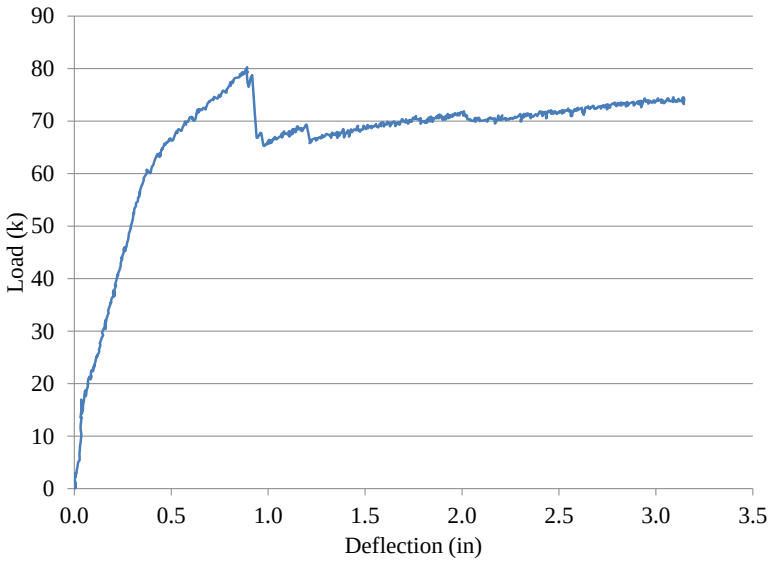

Figure 4.19. Load-Displacement: Beam 3

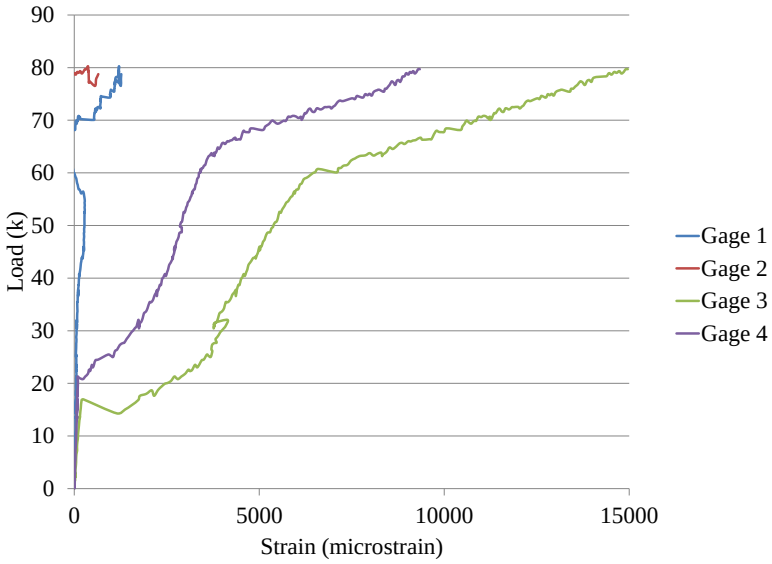

Figure 4.20. Load-Strain: Stage 2 FRP

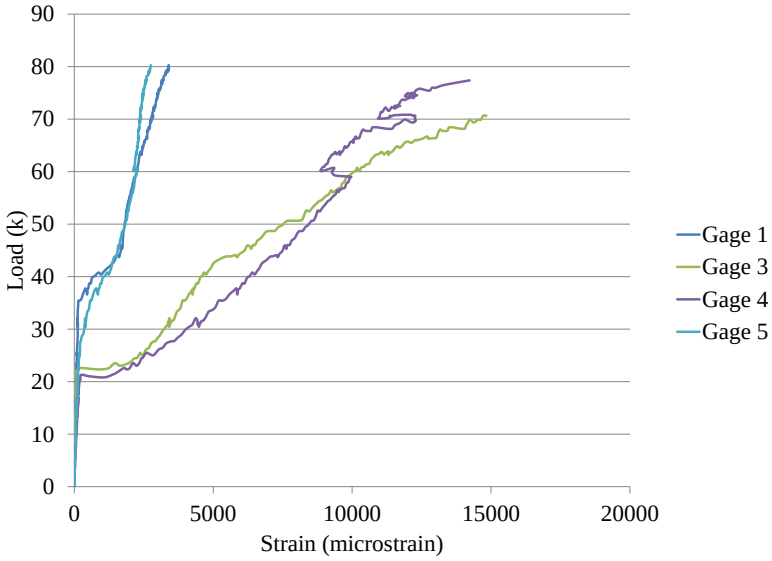

Figure 4.21. Load-Strain: Stage 1 FRP

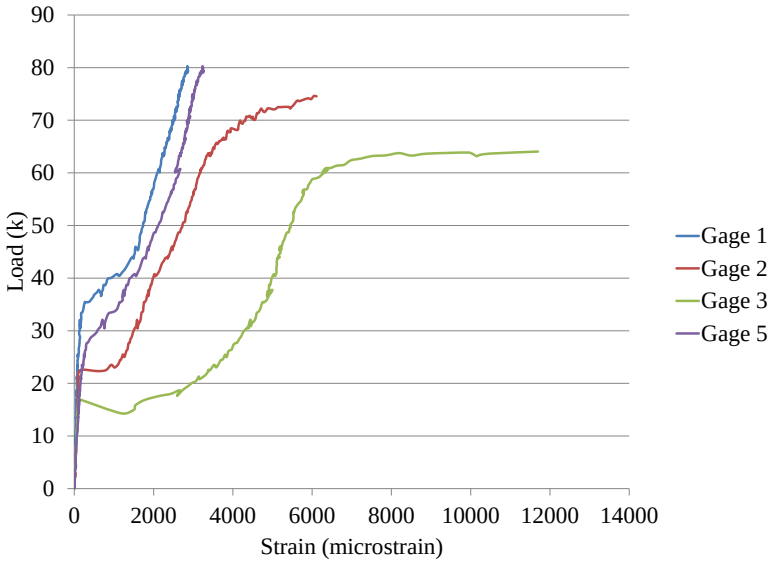

Figure 4.22. Load-Strain: Stage 0 FRP

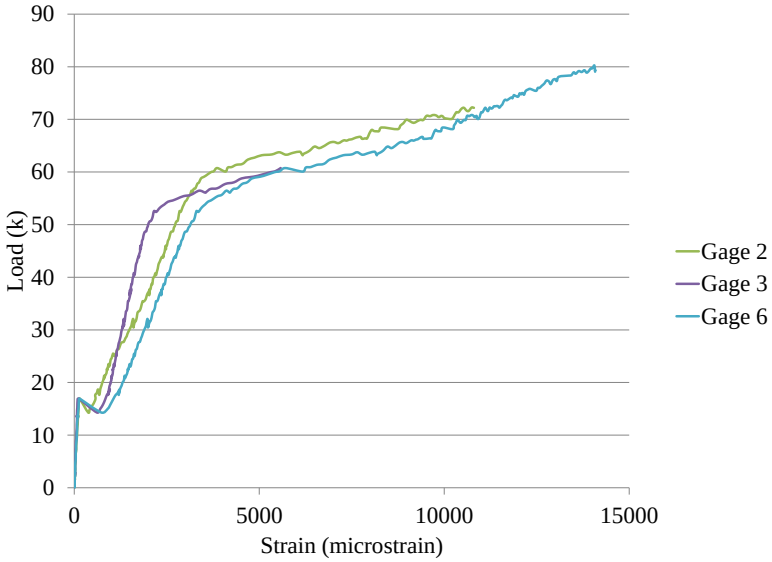

Figure 4.23. Load-Strain: Steel Rebar

4.7. SECOND PHASE BEAM TEST

4.7.1. General. Another set of 12 beams was used to further test the staged FRP theory based on the results gathered from the first phase beam test. These beams were constructed to the same specifications as described in Section 4.2. Beams were cast in two separate batches. Cylinders were cast along with the full scale beams. A total of fifteen cylinders were cast. The cylinders were sulfur capped before being tested for compressive strength. A graph of the compressive strength over time is shown in Figure 4.24. The 28-day compressive strength is approximately 4,400 psi.

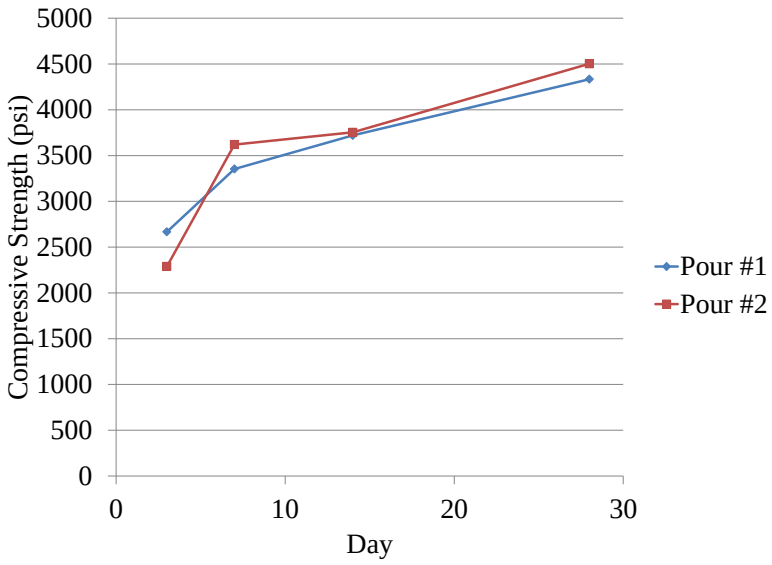

Figure 4.24. Compressive Strength

Of the twelve beams tested, two were control beams with no FRP application at all. One 0 stage beam had FRP on the bottom to act as a baseline for conventionally installed FRP. Four more had 2 staged levels of FRP. The final five had 3 staged levels of FRP. The test matrix can be seen in Table 4.2. Note that Beam #8 was tested with the incorrect setup and thus not included in the following discussions.

On Beam 3, the FRP that was applied was as similar as possible to the staged beams for comparison. The sheet was cut to 8 ft long and 10 in wide. Only 1 layer thick was applied. Beam 3 is shown in Figure 4.25.

Foam was used to create individual arches in both the beam with two layers and the beam with three layers of staging. The foam was stiff enough to hold the arches of

the FRP layers during FRP applications but flexible enough to become flattened when the FRP was put into tension. Therefore, the foam did not need to be removed before testing, like the previously used wire.

Table 4.2. Test Matrix Second Phase Beam Test

Beam	Pour	Description	Stage 0	Stage 1	Stage 2
1	1	Control-No FRP	-	-	-
2	2	Control-No FRP	-	-	-
3	1	0 Stage FRP	10 in wide	-	-
4	1	2 Stage FRP	2-1.25 in wide	1-7.5 in wide	-
5	2	2 Stage FRP	2-1.25 in wide	1-7.5 in wide	-
6	1	2 Stage FRP	2-1.125 in wide	1-7.75 in wide	-
7	2	2 Stage FRP	2-1.125 in wide	1-7.75 in wide	-
8	1	3 Stage FRP	2-1 in wide	2-1.5 in wide	1-5 in wide
9	2	3 Stage FRP	2-1 in wide	2-1.5 in wide	1-5 in wide
10	2	3 Stage FRP	2-1 in wide	2-1.5 in wide	1-5 in wide
11	1	3 Stage FRP	2-0.875 in wide	2-1.625 in wide	1-5 in wide
12	2	3 Stage FRP	2-0.875 in wide	2-1.625 in wide	1-5 in wide

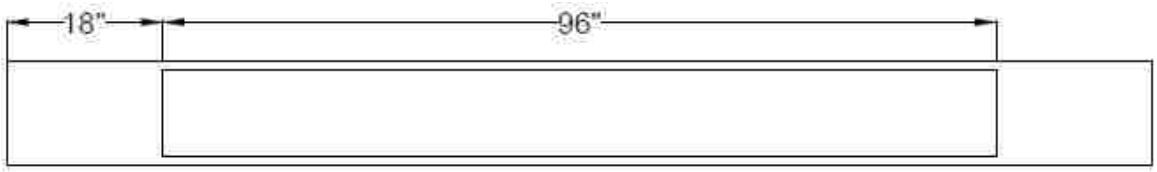

Figure 4.25. FRP Configuration: Beam 3

4.7.2. 2 Stage FRP Beams. Beams 4 and 5 were identical in FRP application to determine if the width of the foam changed depending on the FRP configuration on the beam. The height of the foam remained constant at 0.125 in. A total length of 8 ft of FRP was used for both beams. The width of the strips totaled 10 in, with 7.5 in of the stage 1 FRP and 2.5 in for the stage 0 layer. The 0 stage layer was split into two 1.25 in strips placed on either side of the stage 1 layer. The 3 ft section of the FRP was the only portion to contain staging. Tape was used every 4 in on center to provide a debonded portion in stage 1 only. On top of that, 0.5 in width of foam was glued in place. A total of nine debonded/foam regions were added within the stage 1 section.

Beams 6 and 7 were identical 2 stage beams as well. These beams used an overall length of 8 ft with 1 layer thick of FRP. Stage 0 had two strips of FRP each with a width

of 1.125 in. This stage had no debonded or foam sections; it was fully bonded to the beam. Stage 1 was 7.75 in wide. The debonded portions were placed in the center 3 ft with a spacing of 4 in on center. The debonded portions had a length of 1 in, which was created by placing 0.5 in wide foam strips on the surface of the beams in the debonded areas. Nine of the foam/debonded regions were placed. FRP layouts for Beams 4, 5, 6, and 7 are shown in Figure 4.26.

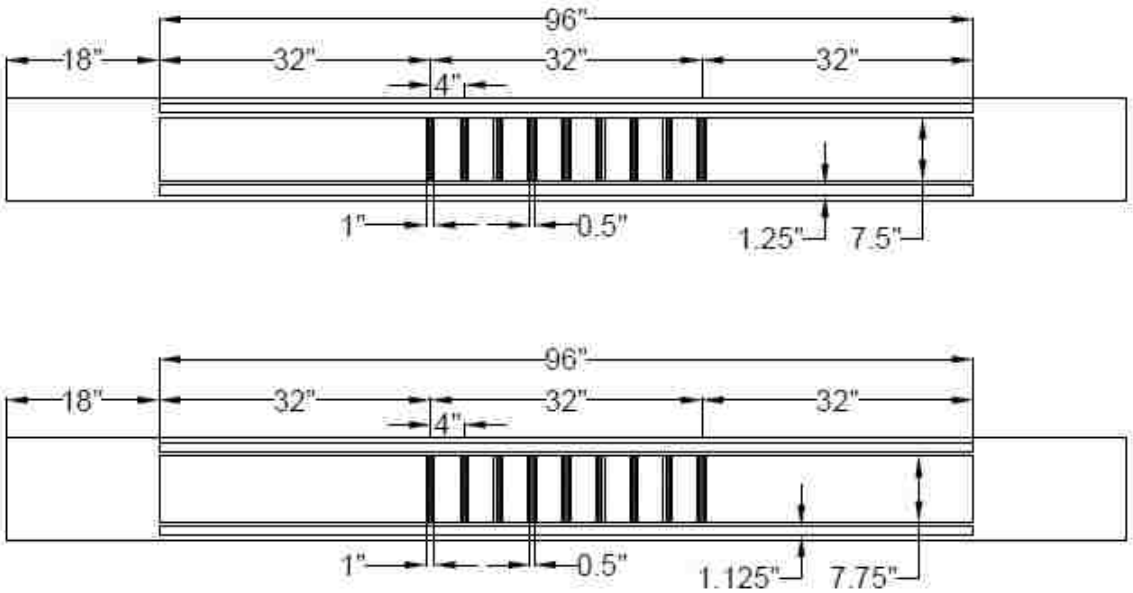

Figure 4.26. FRP Configuration: Beams 4, 5 and Beams 6, 7

4.7.3. 3 Stage FRP Beams. Beams 8 and 9 used the same foam to accomplish three staged levels of FRP. The total width of the FRP was again 10 in. Stage 2 was 5 in wide, had 1 in long debonded spaces every 4 in, which was created by placing 0.5 in wide foam every 4 in. Again, the foam was placed on top of the debonded areas and only the center 3 ft of FRP contained the debonded portion. Stage 1 had a 3 in wide strip, that was divided into two 1.5 in strips placed on either side of stage 2. Stage 1 FRP had 1 in debonded length every 4 in and 0.25 in foam placed on top of these debonded areas. The debonded areas were created with tape to prevent saturant from bonding with the concrete surface. The last layer of FRP added to the beam was stage 0. This layer consisted of two 1 in wide strips that were positioned on the outsides of the stage 1 layers. This layer was fully bonded to the beam.

Beam 10 was similar to Beams 8 and 9 except in the width of the foam used to create the staging. The total width was kept at 10 in wide. Stage 2 was at 5 in wide with 1 in long debonded portions spaced at 4 in on center. The foam in this layer was 0.5 in wide placed on top of the debonded spaces at 4 in on center. Stage 1 consisted of two 1.5 in strips with 1 in long debonded spaces 4 in on center. The stage 1 foam was 0.375 in wide. Stage 0 had two 1 in wide sections with no debonded sections or foam.

Beams 11 and 12 were the last of the 3 stage beams to be tested. They used different widths of FRP to create 3 stage FRP applications. Stage 2 had a width of 5 in with debonded sections and foam in the center 3 ft. The debonded sections were 1 in long spaced at 4 in on center while the foam was 0.5 in wide centered on top of the debonded section. Stage 1 had two strips each with a width of 1.625 in. The debonded sections for this layer were still 1 in long while the foam was 0.375 in wide. Both were placed at 4 in on center. Stage 0 was 0.875 in and fully bonded to the beam. The FRP layout for all of the 3 stage beams is seen in Figure 4.27.

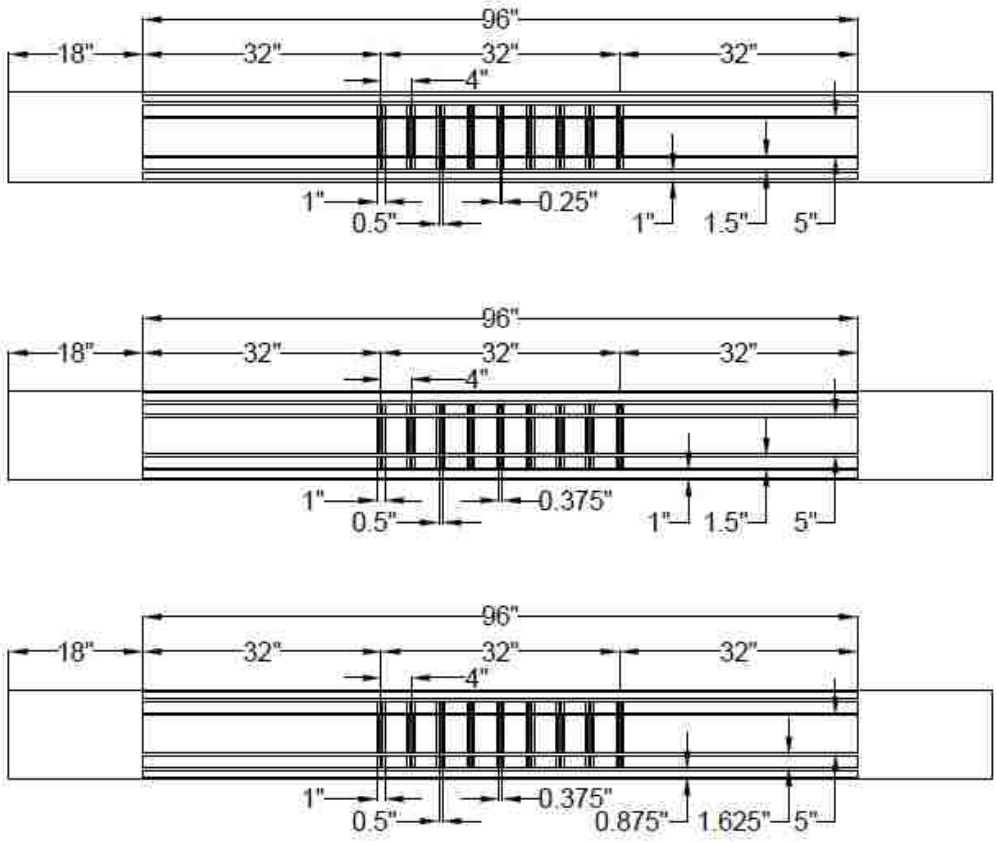

Figure 4.27. 3 Stage FRP Configurations: Beams 8, 9 and Beam 10 and Beams 11, 12

4.8. FRP APPLICATION

The FRP application involved labeling the beam at locations of the debonded and foam sections before the primer was applied but after the surface preparation was finished. The tape was then laid out and the foam was glued to the top of the tape, shown in Figure 4.28. This prevented it from shifting during the application of the FRP sheet. The primer was then rolled over the surface of the concrete, tape, and foam. A bath of saturant was made to pre-impregnate the sheets of FRP. This ensured that the fibers were fully saturated without flattening the foam, already in place on the beam. Sheets were saturated and then laid in the proper locations. A grooved roller was used to ensure proper bonding between the concrete and FRP sheets. An area of concern was between each of the foam pieces. Extra care was given to roll the fibers here to aid in bonding, shown in Figure 4.29.

Strain gages were added to the FRP sheets after the sheets had fully cured. Five gages were added to each sheet of staged and stage 0 FRP. Locations for gages are seen in Figure 4.30. Testing was done to the same standard as described in Section 4.4.

Figure 4.28. Layout of Foam Prior to FRP Application

Figure 4.29. Ensuring Proper Bonding

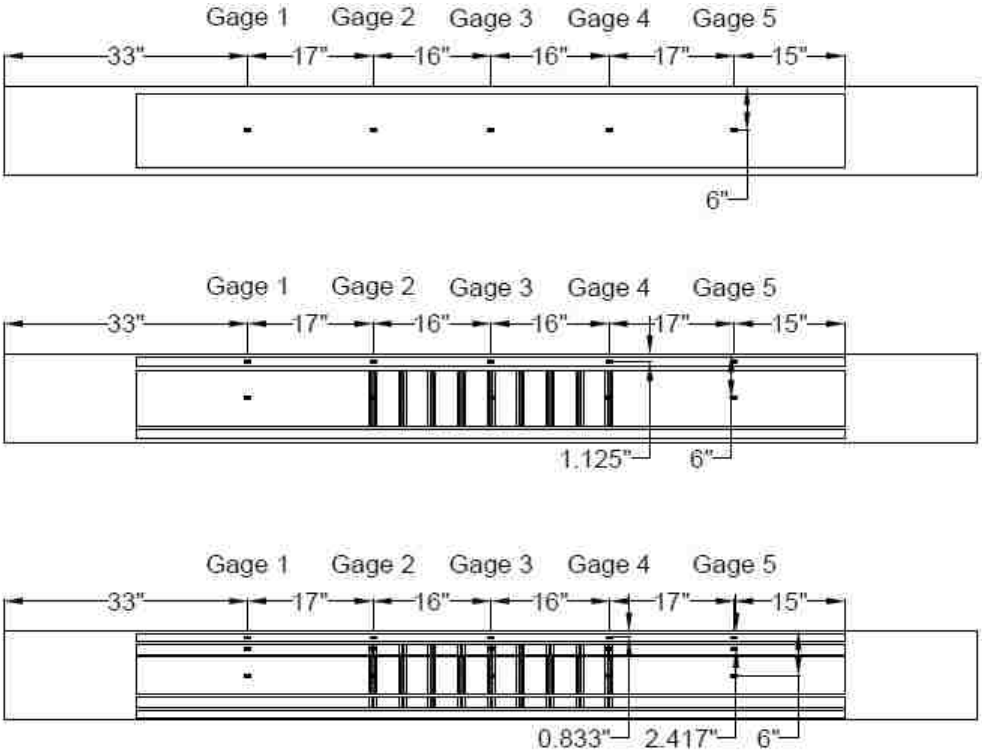

Figure 4.30. Stain Gage Locations: 0 Stage, 2 Stage, and 3 Stage

4.9. SECOND PHASE BEAM TEST RESULTS

4.9.1. Control Beams. The failure of Beam 1 is seen in Figure 4.31. The yielding and deflection were similar to the other control beams tested. This beam began yielding at 58 k as shown in the load-deflection curve in Figure 4.32. The maximum load achieved was 77 k. Concrete crushing occurred at 1.5 in deflection causing a drop in the load. The load-strain graph of the steel rebar is seen in Figure 4.33.

Figure 4.31. Failure of Beam 1

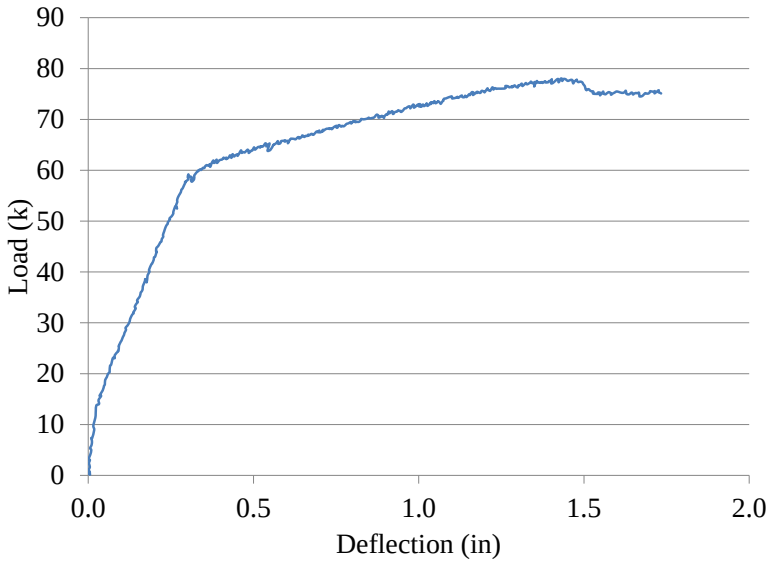

Figure 4.32. Load-Deflection: Beam 1

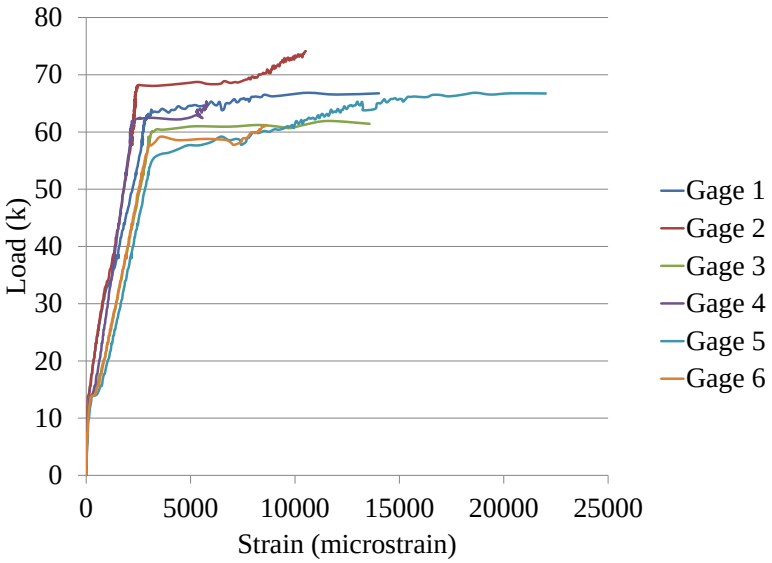

Figure 4.33. Load-Strain: Steel Rebar

Beam 2 was the control beam from the second concrete pour. The failure of this beam can be seen in Figure 4.34. Shown in the load-deflection curve, Figure 4.35, the steel began yielding at 58 k. Beam 2 reached an ultimate load of 73 k. The load-strain curve for the steel rebar is shown in Figure 4.36.

Figure 4.34. Failure of Beam 2

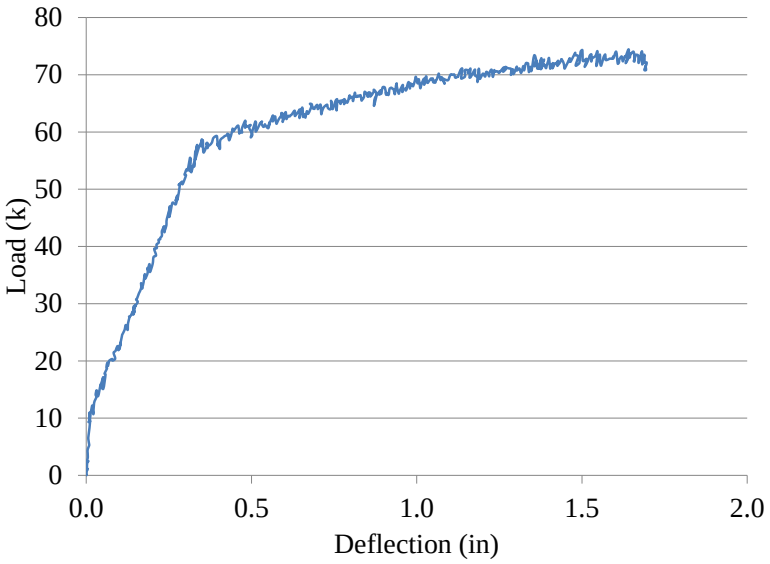

Figure 4.35. Load-Deflection: Beam 2

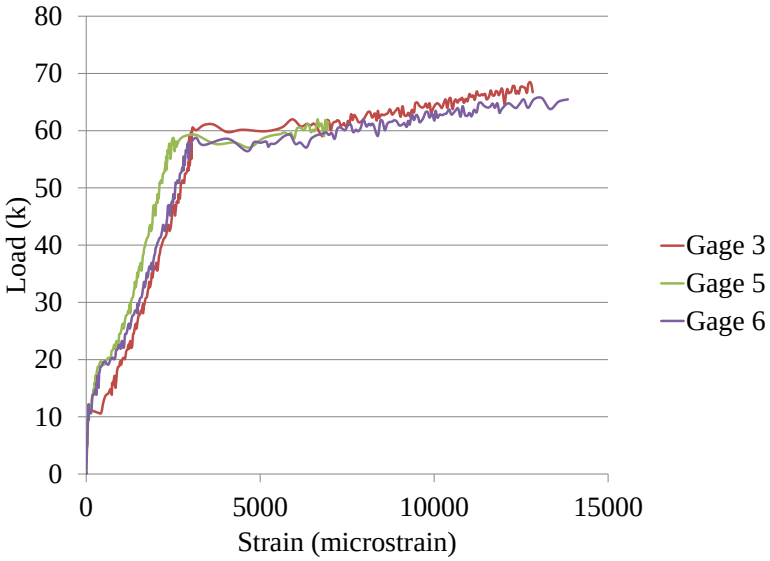

Figure 4.36. Load-Strain: Steel Rebar

4.9.2. 0 Staged FRP Beam. Beam 3 had one single sheet of stage 0 FRP applied to the bottom face. The FRP failed due to debonding from the end of the sheet. This debonding can be seen in Figure 4.37. A small 1 in wide strip did fracture near the center but the majority of the sheet failed from debonding. The load-deflection graph is shown in Figure 4.38. This beam achieved a steel yielding load of 67 k and a maximum load of 88 k. The FRP failed at 88 k causing the load to drop to 65 k. There is no load recovery in this beam because there are no additional staged FRP levels to take the load. The second drop in load that occurs at 1.4 in of deflection is due to concrete crushing of the entire compression zone.

The load-strain curve of the 0 stage FRP, Figure 4.39, backs up the failure of the FRP at 88 k. The layers are engaged from the start of the test to when the sheet fails. The load-strain curve for the steel rebar is seen in Figure 4.40.

Figure 4.37. Failure of Beam 3

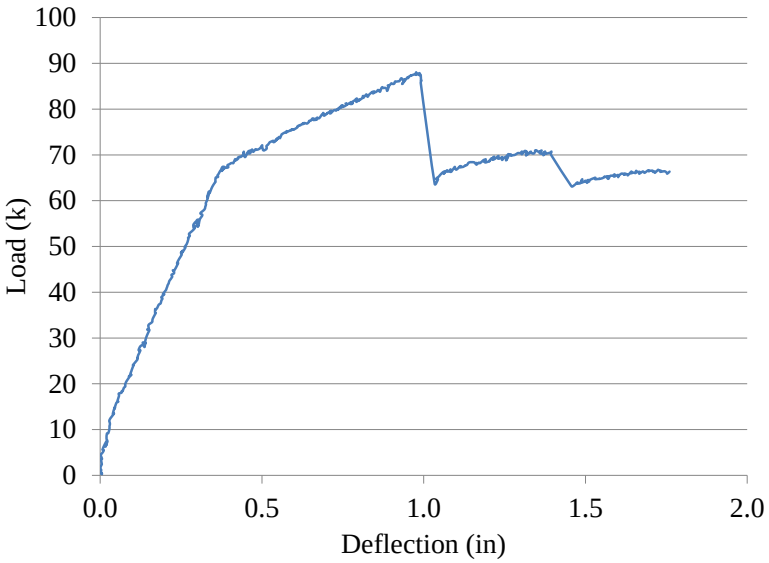

Figure 4.38. Load-Deflection: Beam 3

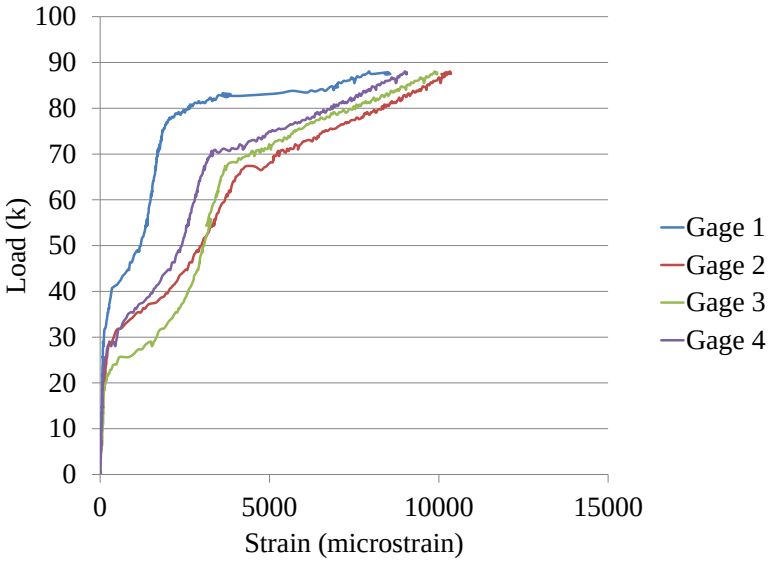

Figure 4.39. Load-Strain: Stage 0 FRP

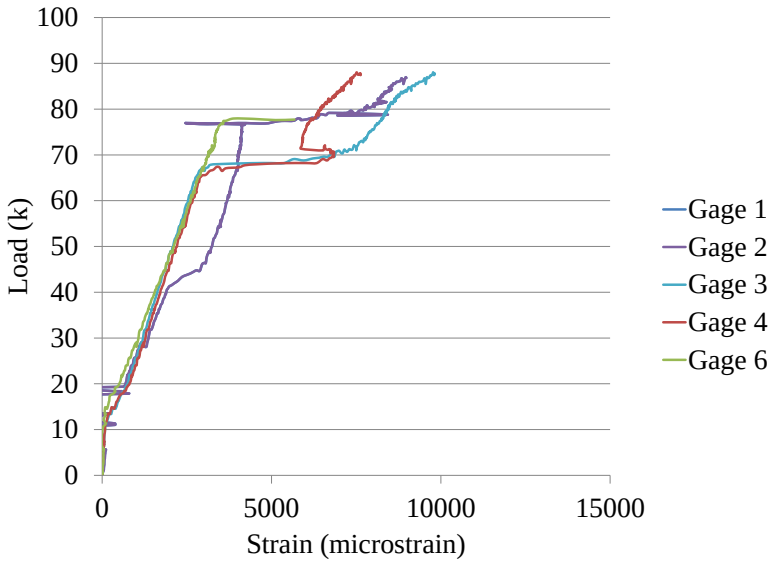

Figure 4.40. Load-Strain: Steel Rebar

4.9.3. 2 Staged FRP Layers. Beam 4 had two levels of staging applied with the stage 1 middle sheet and the stage 0 outer strips. All the strips fractured near the middle of the beam, seen in Figure 4.41. The foam can still be seen in tact on the FRP strips. The load-deflection curve, Figure 4.42, shows that this beam began yielding at 65 k and reached an ultimate strength of 85 k.

The load-strain curves, seen in Figures 4.43-4.45, show that the stage 0 FRP strips broke at the first 85 k peak. The stage 1 strip recovered the load to 84 k again after the stage 0 failed. Stage 1 then failed at the 84 k peak. After this failure the load dropped back to 70 k. Concrete crushing occurred at 1.4 in of deflection causing an additional 5 k drop in load. Both the stage 0 and stage 1 layers appear to have delayed engagement of the FRP. The layers do not become engaged until 20 k.

Figure 4.41. Failure of Beam 4

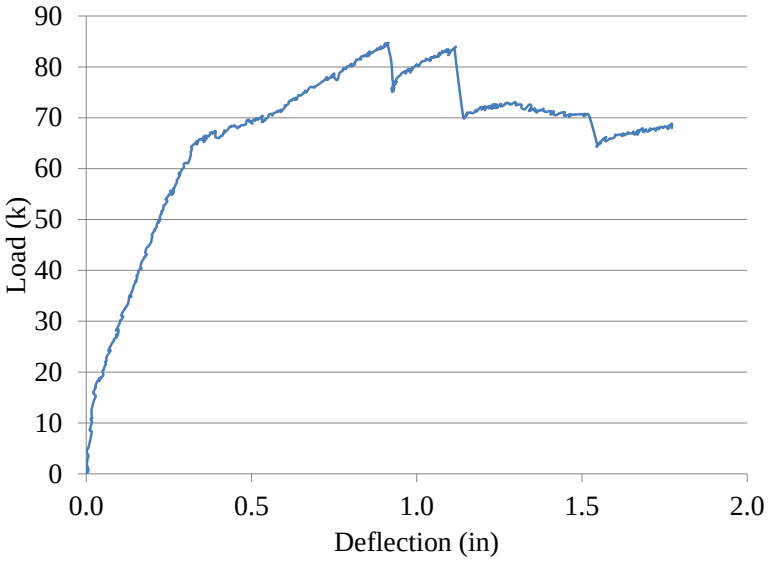

Figure 4.42. Load-Deflection: Beam 4

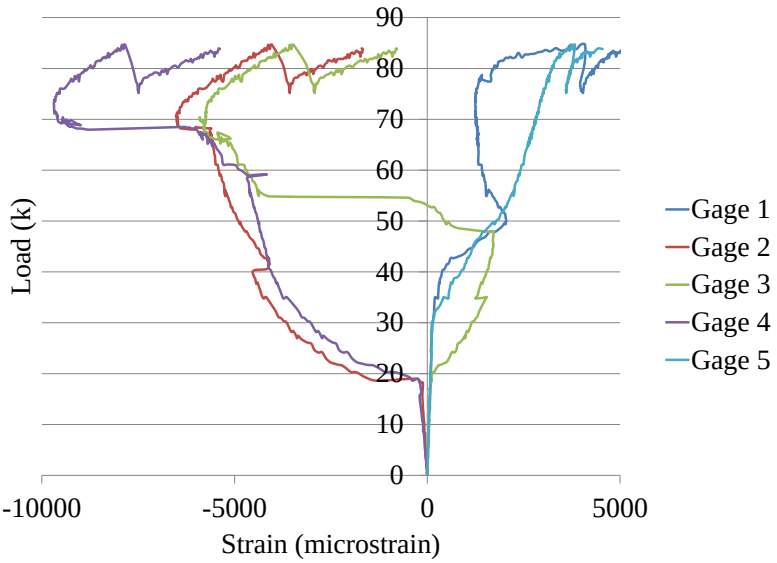

Figure 4.43. Load-Strain: Stage 1 FRP

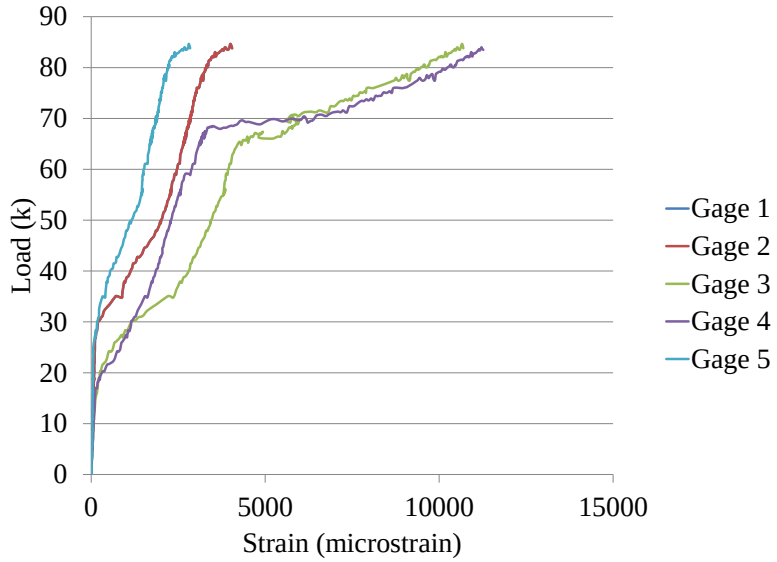

Figure 4.44. Load-Strain: Stage 0 FRP

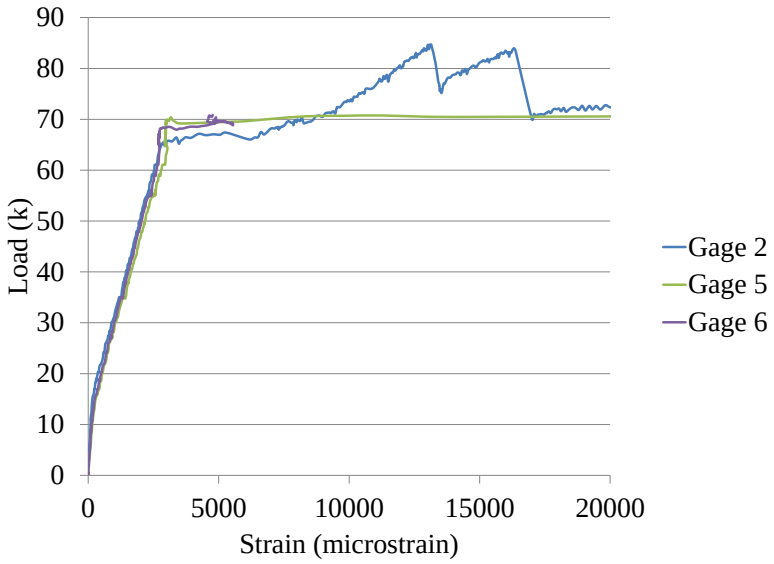

Figure 4.45. Load-Strain: Steel Rebar

Beam 5 was from the second concrete pour and had the same test parameters as beam 4. The failure of this beam can be seen in Figure 4.46. Stage 1 failed due to debonding propagating from the end of the sheet. Stage 0 had a fracture of the fibers near the center of the beam. The load-deflection curve, Figure 4.47, shows that this beam was able to achieve 88 k before failing FRP. This beam had the stage 0 strips failing at separate times. Stage 1 then debonded a short time later. A greater separation in the failure of the different staged levels would be optimal.

The load-strain curves, Figures 4.48-4.50, were examined to determine exactly when the levels debonded. It is clearly seen here that the stage 0 levels broke prior to the debonding of stage 1. The stage 0 and stage 1 levels of FRP do not begin to engage until around 20 k.

Figure 4.46. Failure of Beam 5

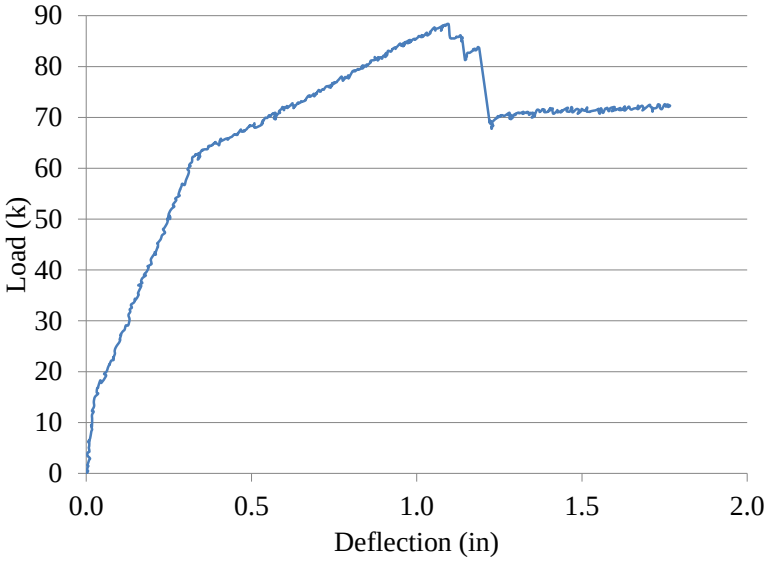

Figure 4.47. Load-Deflection: Beam 5

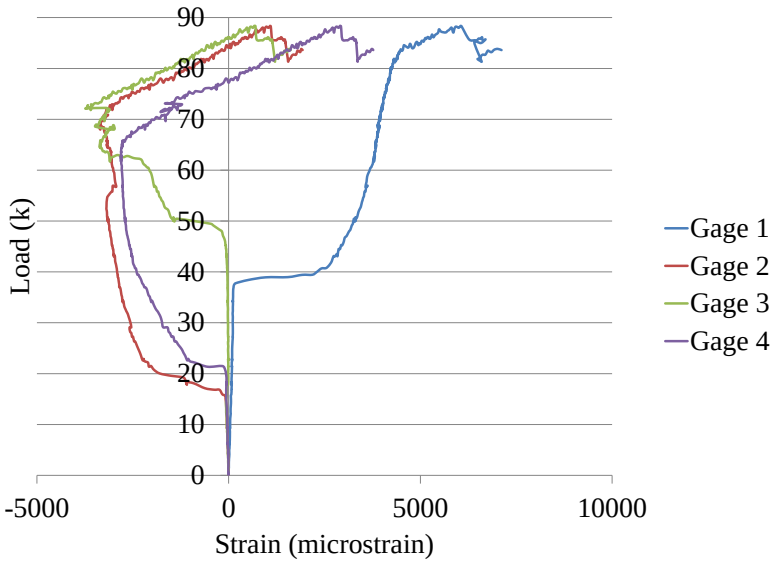

Figure 4.48. Load-Strain: Stage 1 FRP

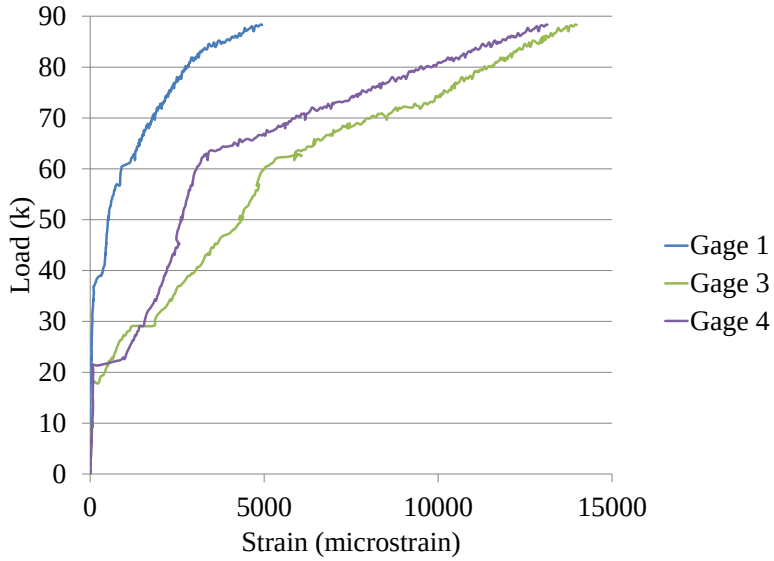

Figure 4.49. Load-Strain: Stage 0 FRP

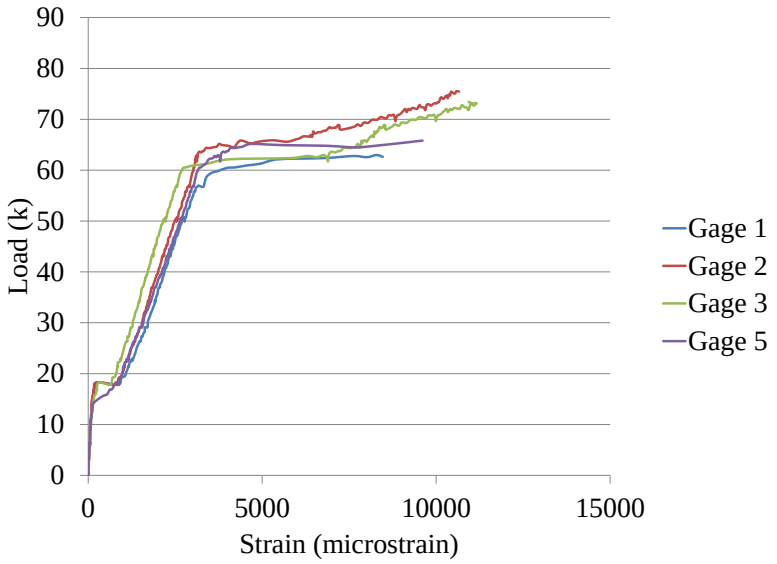

Figure 4.50. Load-Strain: Steel Rebar

Beam 6 had two stages of FRP applied. Stage 1 was increased to 7.75 in wide while stage 2 was decreased to 2.25 in wide. This beam had all the FRP fracture near the center of the beam, as seen in Figure 4.51. From the load-deflection curve, Figure 4.52, it can be seen that the steel began yielding at 66 k and reached an ultimate strength of 88 k. Concrete crushing was the cause of the drop in load at 1.5 in of deflection.

The load-strain curves, Figures 4.53-4.55, were examined to confirm when each of the FRP strips failed. Visually it was seen that one side of the stage 0 strips failed at 81 k. The second stage 0 strip visually fractured at 88 k, which is backed up by Figure 4.54. Stage 1 held the load shortly after the second stage 0 strip failed. Stage 1 failed at 87 k. Both stages 0 and 1 did not engage until about 20 k. Only the stage 1 layer should be delayed.

Figure 4.51. Failure of Beam 6

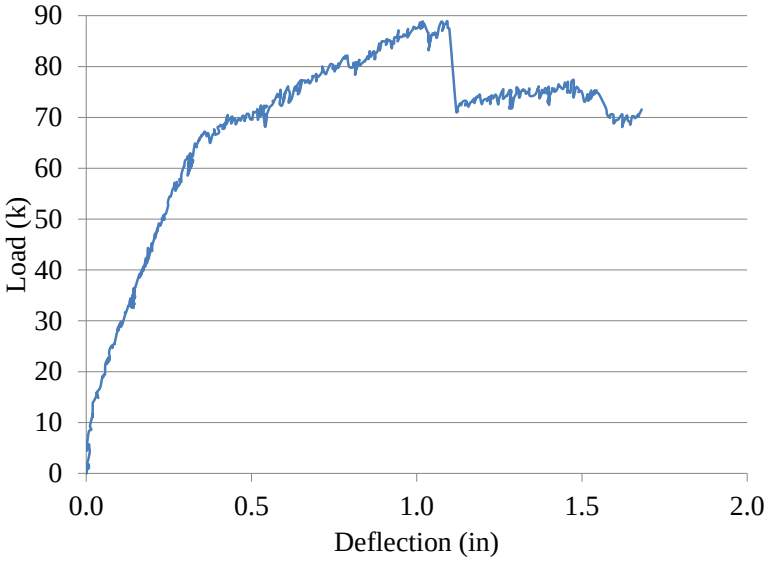

Figure 4.52. Load-Deflection: Beam 6

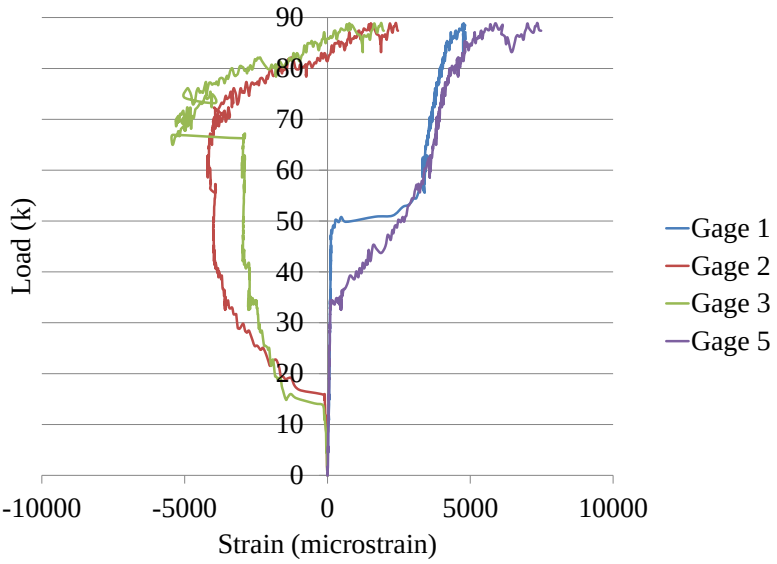

Figure 4.53. Load-Strain: Stage 1 FRP

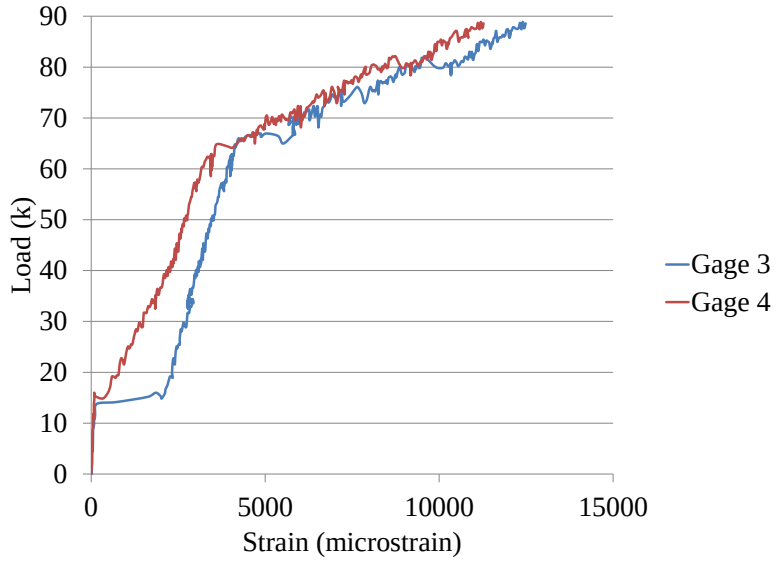

Figure 4.54. Load-Strain: Stage 0 FRP

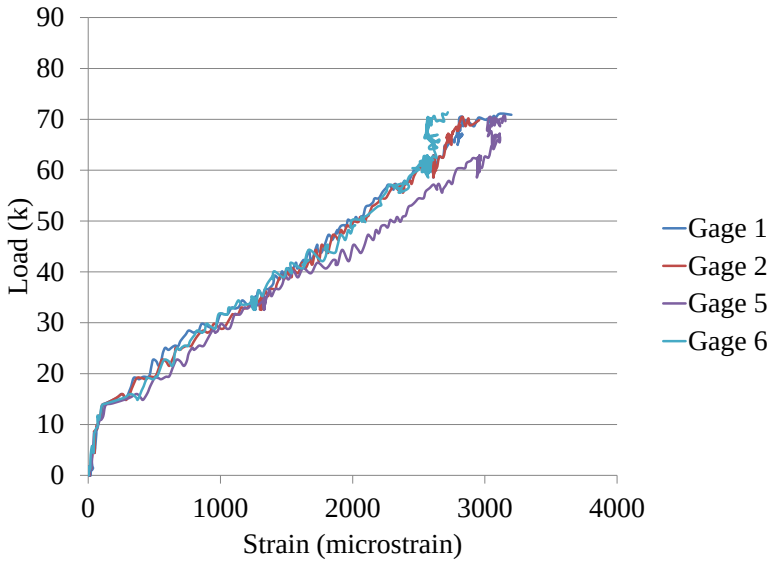

Figure 4.55. Load-Strain: Steel Rebar

Beam 7 has the same FRP staging as Beam 6. The failure of the FRP is shown in Figure 4.56 with fracture of the stage 0 strips and debonding of the stage 1 strip. Figure 4.57 shows the load-deflection curve. This beam had steel yielding beginning around 65 k and an ultimate strength of 91 k. This graph appears to have a more ductile curve than Beam 6 because the FRP fails between 1.10 in and 1.30 in of deflection.

The load-strain curves, Figures 4.58-4.60, were needed to determine exactly when each of the strips failed because it was not visually obvious for each strip. One strip of the stage 0 failed at 91 k. The next to fail was the second stage 0 strip at 91 k after a short recovery. Stage 1 was the last layer to debond at 90 k. It appears that the stage 1 FRP becomes engaged well before the stage 0 FRP.

Figure 4.56. Failure of Beam 7

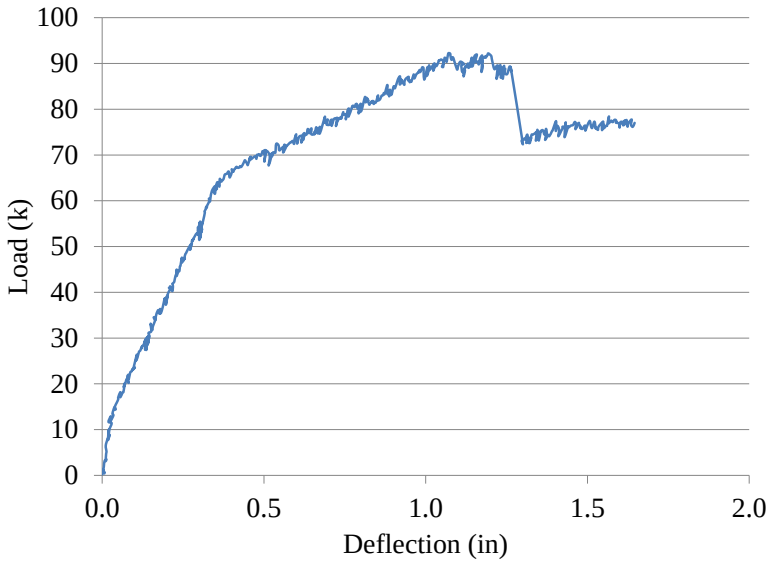

Figure 4.57. Load-Deflection: Beam 7

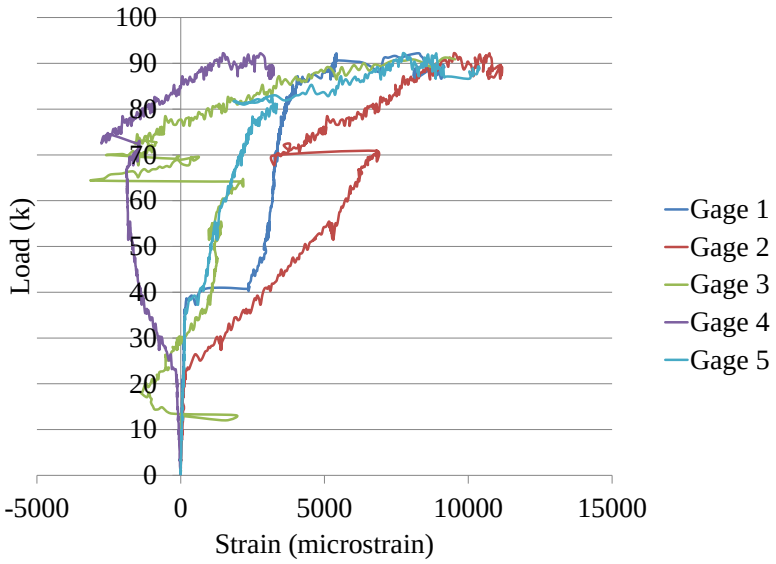

Figure 4.58. Load-Strain: Stage 1 FRP

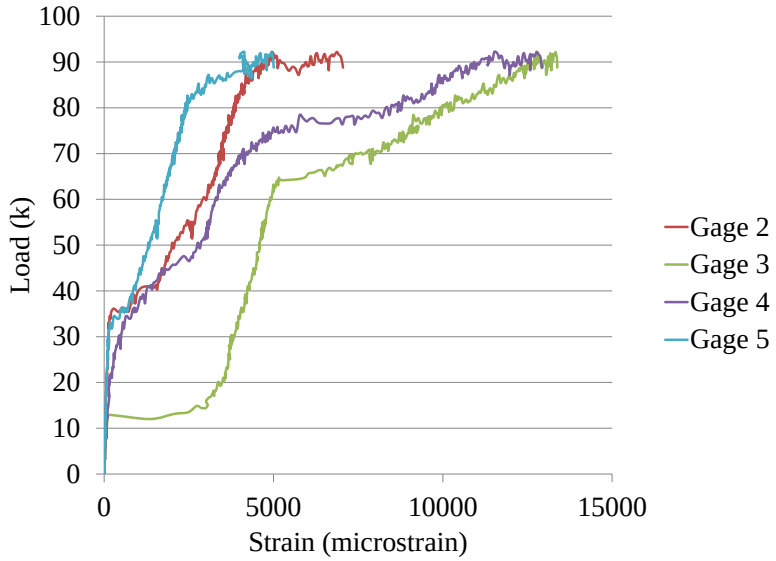

Figure 4.59. Load-Strain: Stage 0 FRP

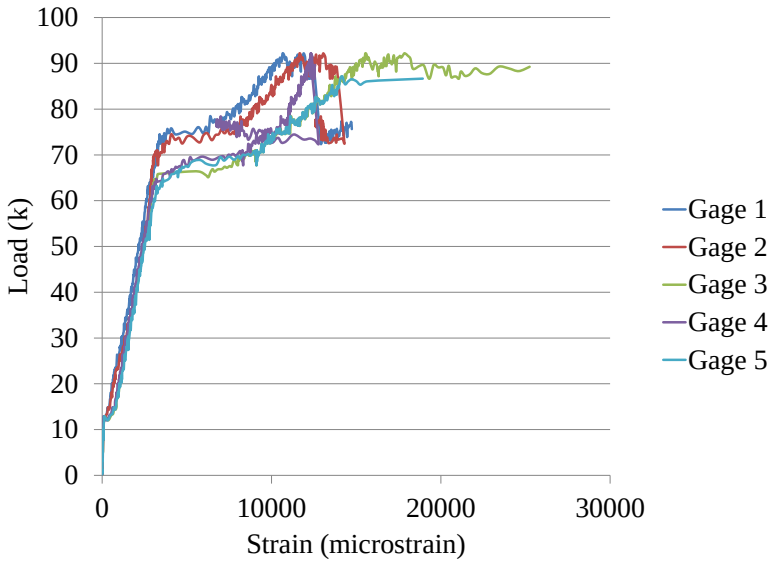

Figure 4.60. Load-Strain: Steel Rebar

4.9.4. 3 Staged FRP Layers. Beam 8 was tested in a different setup and thus not discussed further in this study. Beam 9 had each of the FRP strips fractured as a means of failure, Figure 4.61. It began yielding at 66 k with an ultimate load of 89 k shown in the load-displacement curve, Figure 4.62.

Load-strain graphs are shown in Figures 4.62-4.66. The fracture of the stage 0 strips were determined visually and audibly to have failed at 81 k and 85 k. This was confirmed by the load-strain curve of the stage 0 FRP. The next strip of FRP that failed was stage 2 followed shortly by both strips of stage 1. Concrete crushing occurred at 1.5 in of deflection.

Figure 4.61. Failure of Beam 9

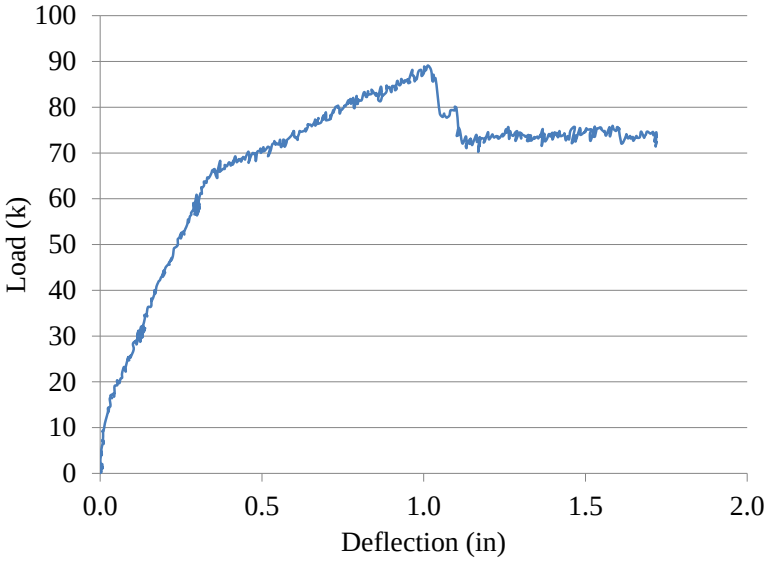

Figure 4.62. Load-Deflection: Beam 9

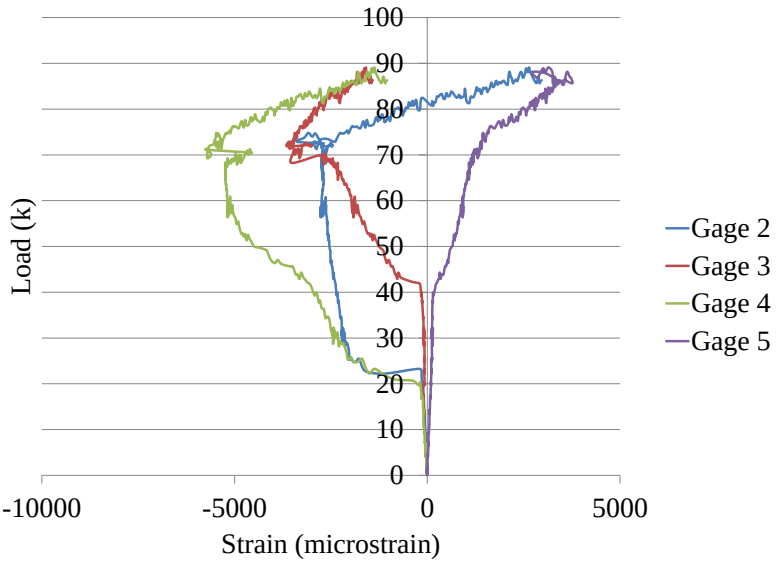

Figure 4.63. Load-Strain: Stage 2

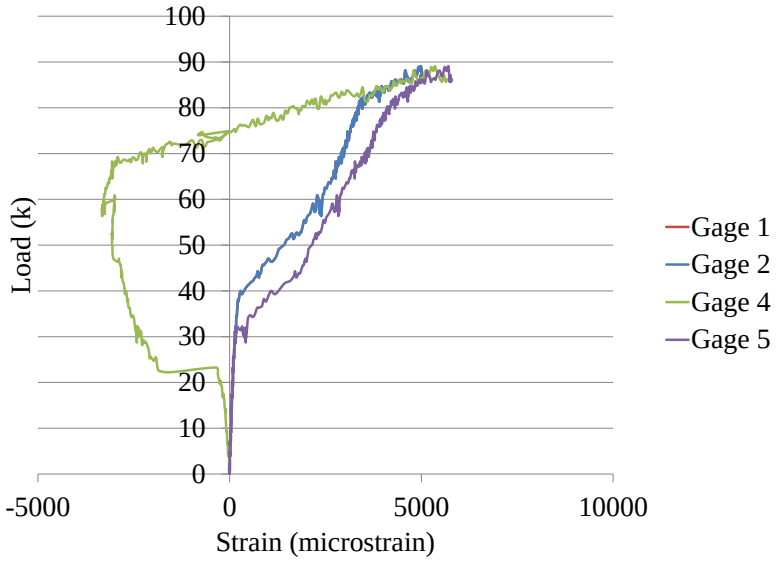

Figure 4.64. Load-Strain: Stage 1 FRP

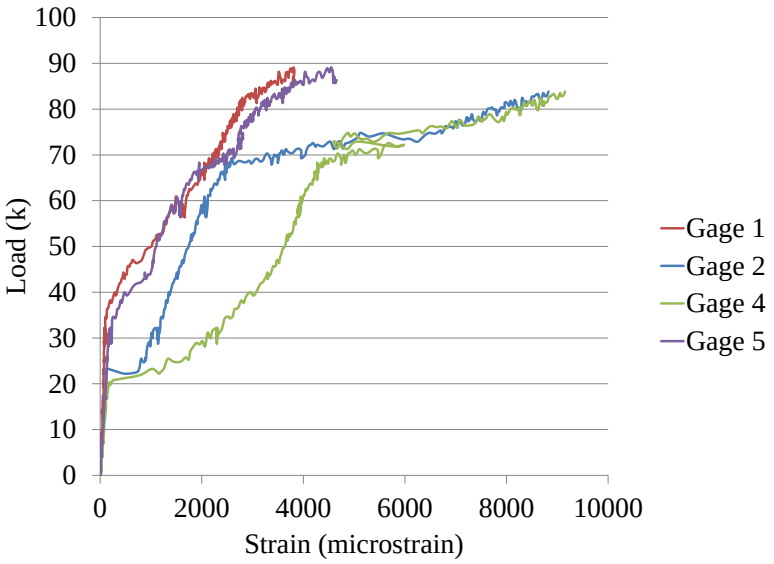

Figure 4.65. Load-Strain: Stage 0 FRP

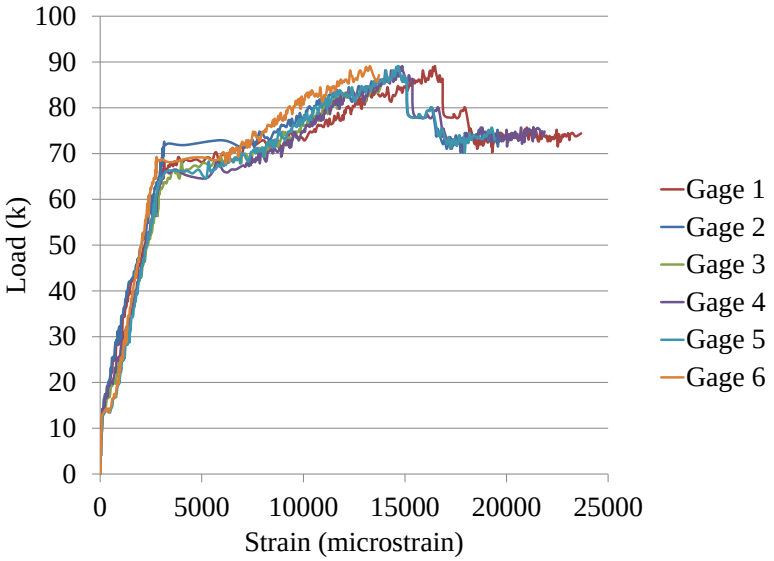

Figure 4.66. Load-Strain: Steel Rebar

Beam 10 had a slight variation in the width of the foam compared to Beam 9. The failure of this beam is seen in Figure 4.67. All of the stages of FRP fractured. Stage 2 fractured near the end of the strip while stages 0 and 1 fractured closer to the center of the beam. The load-deflection curve, shown in Figure 4.68, shows that an ultimate load of 87 k was reached.

The load-strain curves, Figures 4.69-4.72, were needed to determine when the FRP strips failed. Stage 0 was first to break at 82 k. From the cracking sounds and visual inspection during the test it was determined that the stage 0 strips partially fractured before a complete failure. Stage 1 reached 87 k before fracture. Stage 2 failed at the 85 k peak before the load dropped to 75 k. Concrete crushing caused the final drop in load at 1.5 in in deflection.

Figure 4.67. Failure of Beam 10

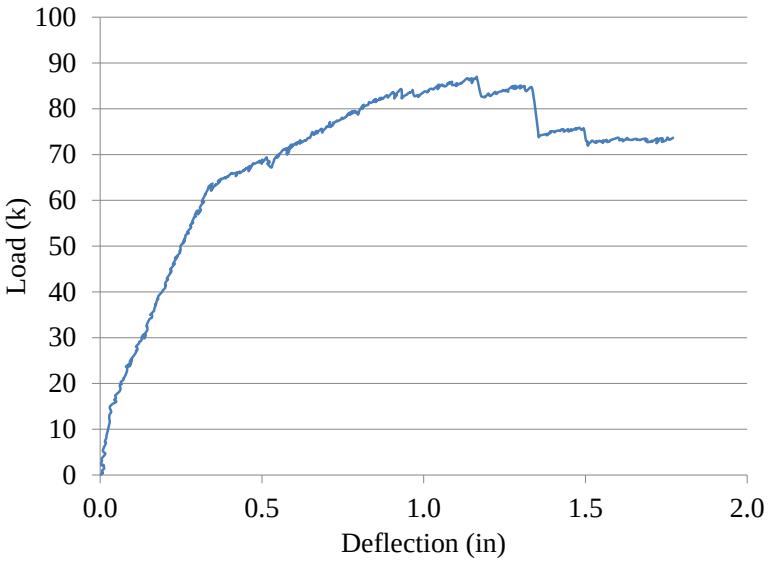

Figure 4.68. Load-Deflection: Beam 10

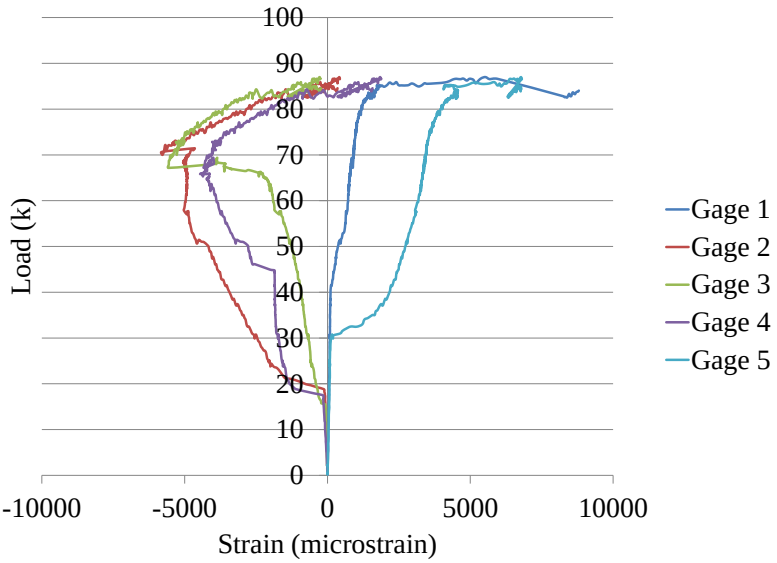

Figure 4.69. Load-Strain: Stage 2 FRP

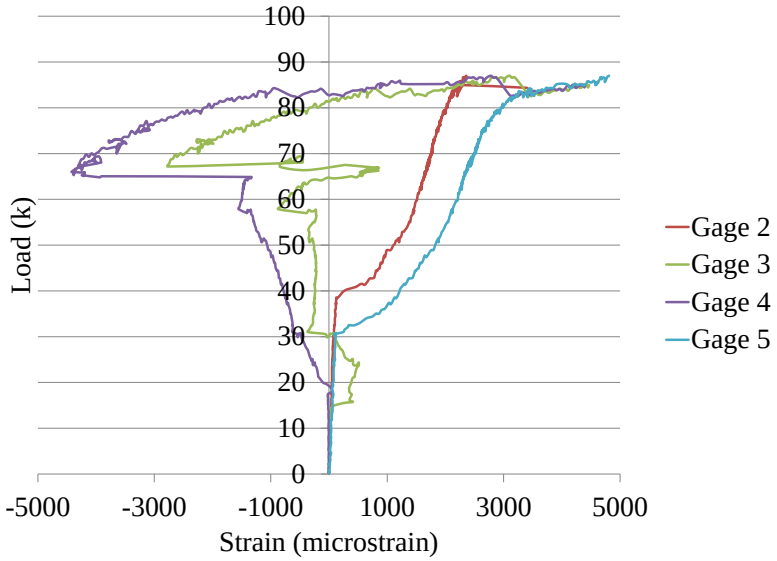

Figure 4.70. Load-Strain: Stage 1 FRP

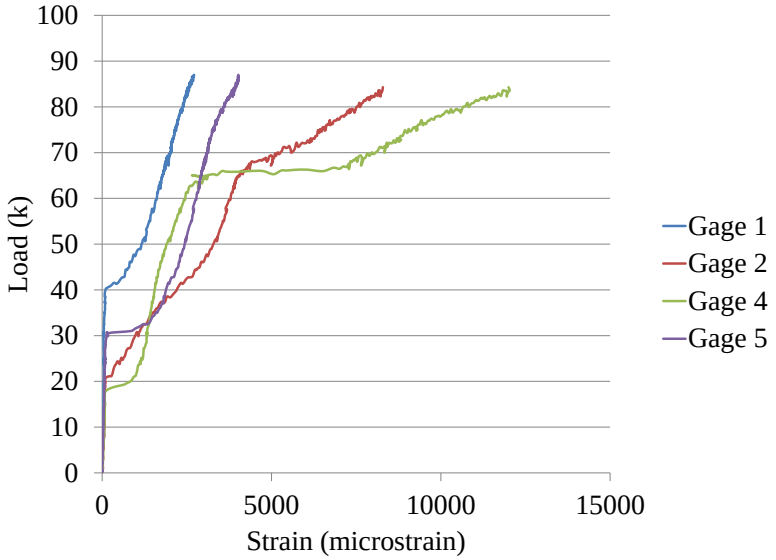

Figure 4.71. Load-Strain: Stage 0 FRP

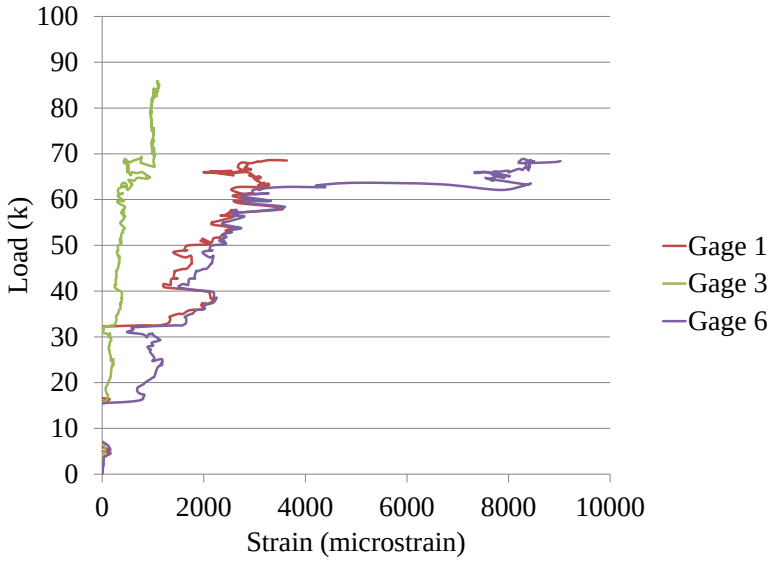

Figure 4.72. Load-Strain: Steel Rebar

Beam 11 had three stages of FRP applied to the bottom face. As seen in Figure 4.73, this beam fractured at the stage 0 and stage 1 strip while the stage 2 strip debonded. The load-deflection curve, Figure 4.74, shows that yielding began around 59 k. Beam 11 reached an ultimate strength of 87 k.

The load-strain graphs are found in Figures 4.75-4.78. The stage 0 strips of FRP visually failed first at 77 k and 79 k. One strip of the stage 1 FRP was the next to fail at

85 k. There was a recovery to 85 k again before stage 2 and second strip of stage 1 failed.

Figure 4.73. Failure of Beam 11

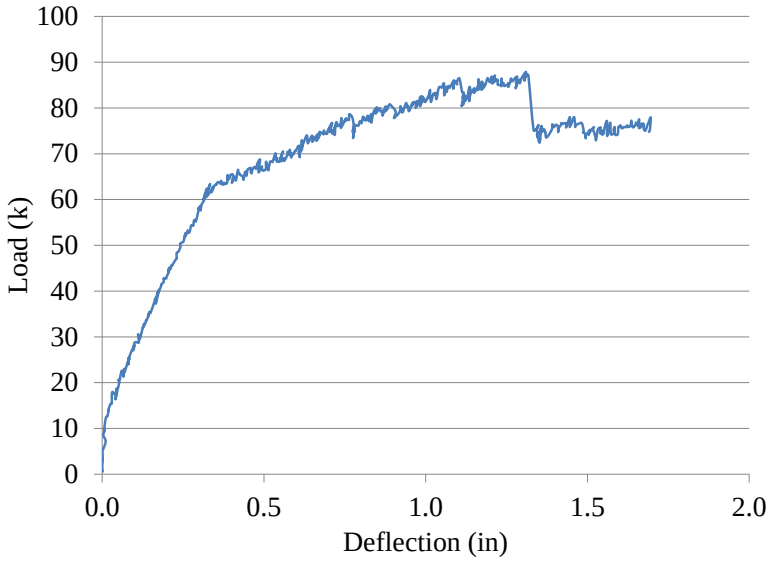

Figure 4.74. Load-Deflection: Beam 11

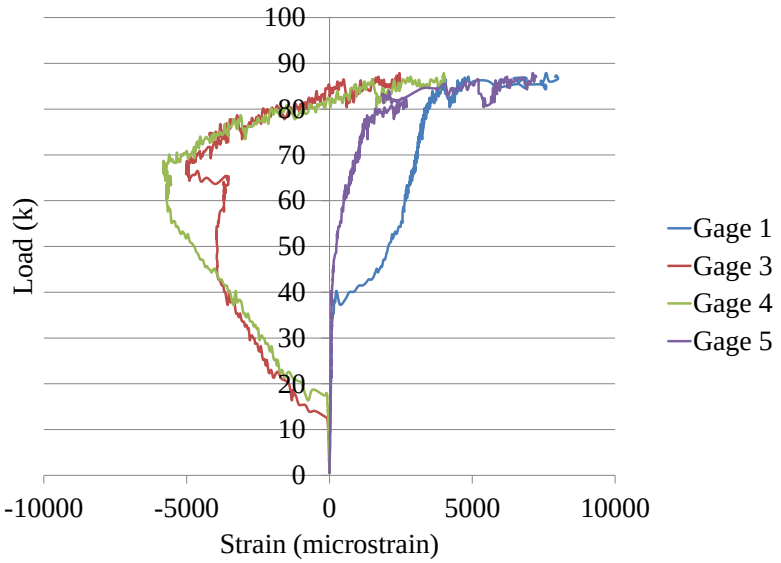

Figure 4.75. Load-Strain: Stage 2 FRP

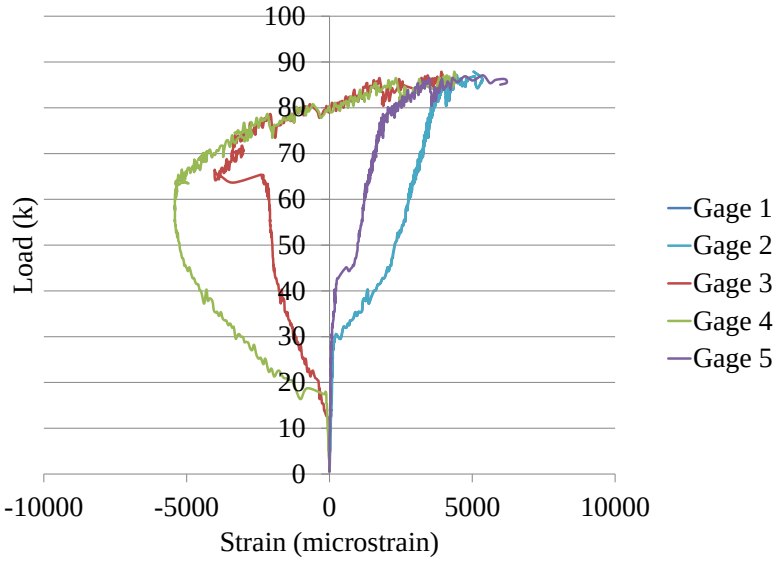

Figure 4.76. Load-Strain: Stage 1 FRP

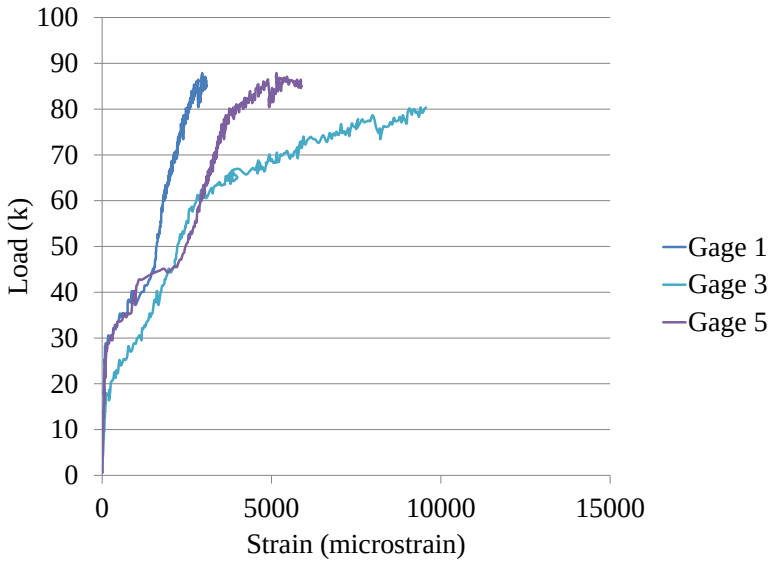

Figure 4.77. Load-Strain: Stage 0 FRP

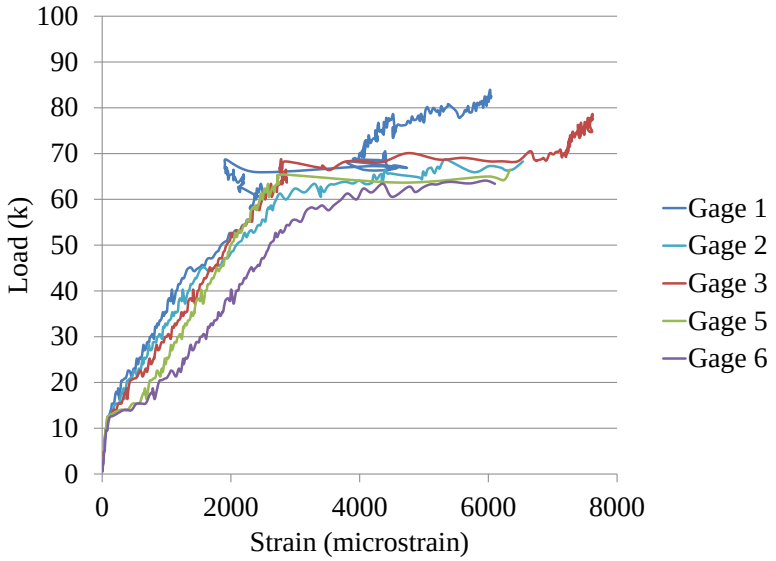

Figure 4.78. Load-Strain: Steel Rebar

Beam 12 had the exact same FRP configuration as Beam 11. The failure of Beam 12 is shown in Figure 4.79. The stage 0 and stage 1 strips fractured and the stage 2 strip debonded from the end. The load-deflection curve in Figure 4.80 shows that Beam 12 reaches an ultimate strength of 84 k. The overall shape of the curve for Beams 11 and 12 are very similar to each other. This appears to be a fairly accurate repeat of results between two separate beams.

The load-strain curves, Figures 4.81-4.84, show the order in which the FRP stages fail. The stage 0 strips visually failed first at 77 k and 79 k. This failure is identical to the failure of the stage 0 strips in beam 11. One of the stage 1 strips failed at 83 k. There was recovery before the second stage 1 strip and the stage 2 strip failed at 84 k.

Figure 4.79. Failure of Beam 12

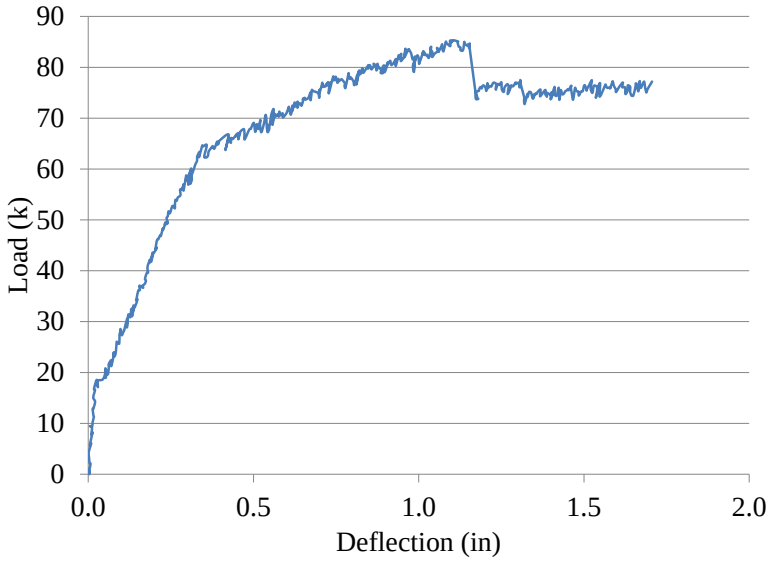

Figure 4.80. Load-Deflection: Beam 12

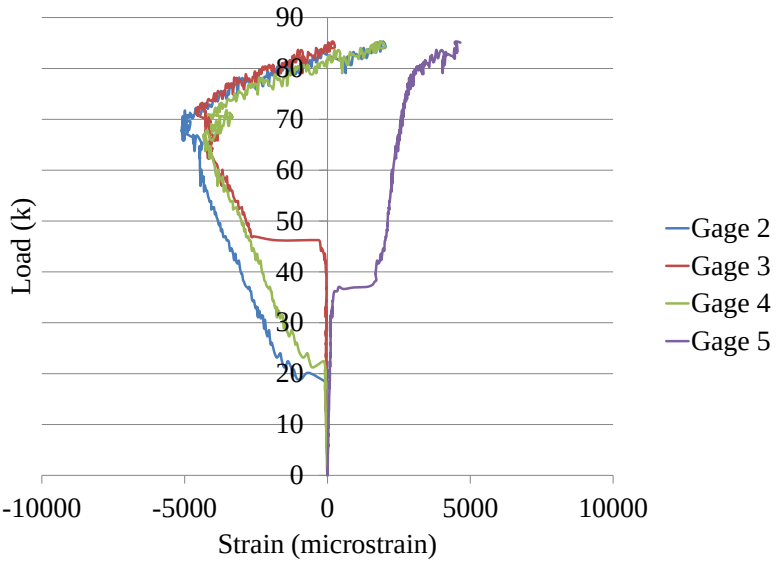

Figure 4.81. Load-Strain: Stage 2 FRP

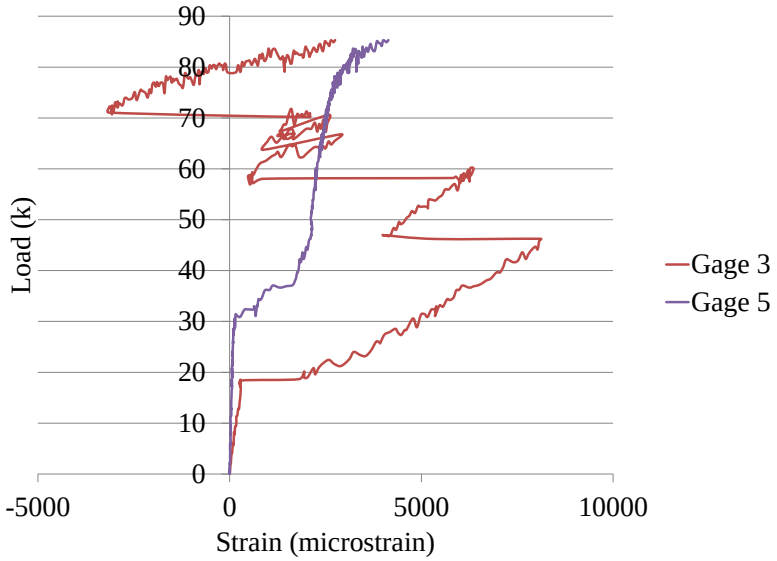

Figure 4.82. Load-Strain: Stage 1 FRP

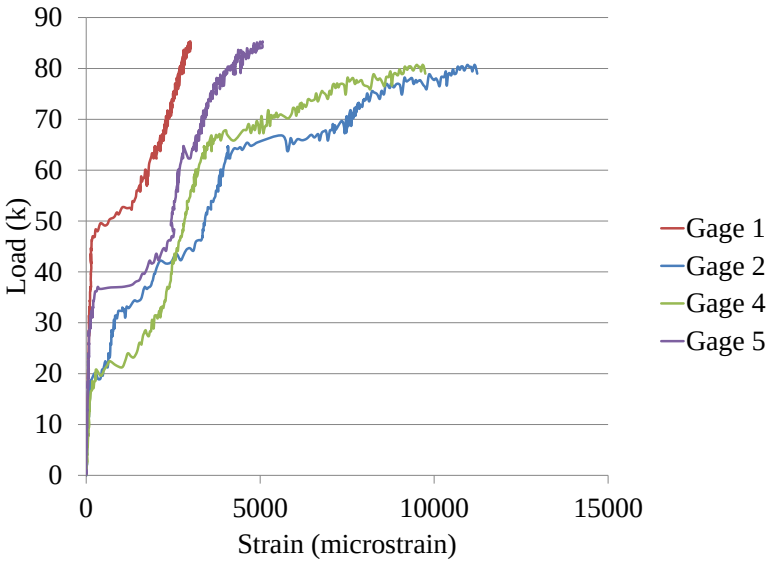

Figure 4.83. Load-Strain: Stage 0 FRP

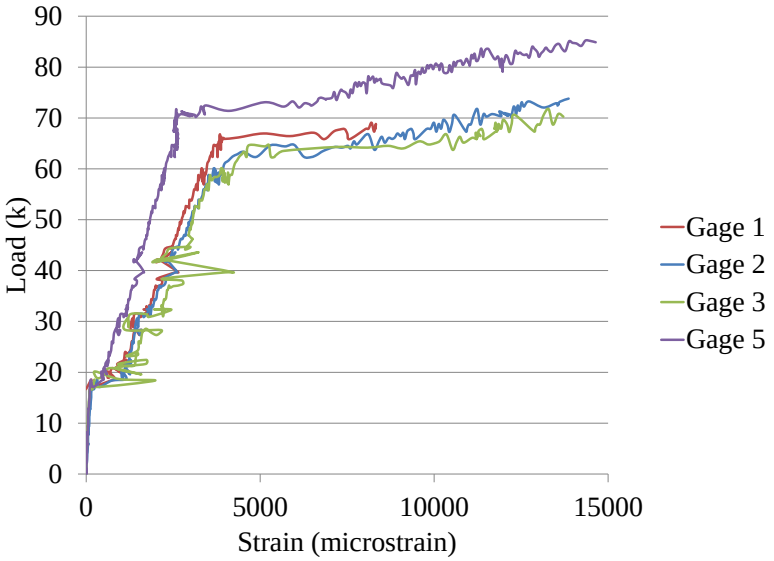

Figure 4.84. Load-Strain: Steel Rebar

4.10. SUMMARY ON BEAM TESTS

Overall, 14 beams were tested in two phases with various levels of staged FRP. The first phase and the second phase include three and eleven beams, respectively. For the first phase, local arches in FRP layers were created by embedding and pulling out plastic wires before the primer for FRP installation becomes completely dry. For the

second phase, local arches in FRP layers were created by periodically embedding foam between the concrete beam and FRP layers.

4.10.1. First Phase Beam Test. The load-deflection curves of the first three beams are compared in Figure 4.85. Beam 1 served as a control with no FRP applied. Beam 2 had two layers of staging applied. Beam 3 had three levels of staging. Beams 2 and 3 had concrete crushing occur at 2 in of deflection which is the reason for the slight drop in load. These beams did not produce ideal results. Beam 2 had the stage 0 layer fail before the stage 1 layer but the difference was insignificant. Beam 3 had the stage 0 and stage 2 layers failing at the same time. The small recovery in load was all due to the stage 1 FRP.

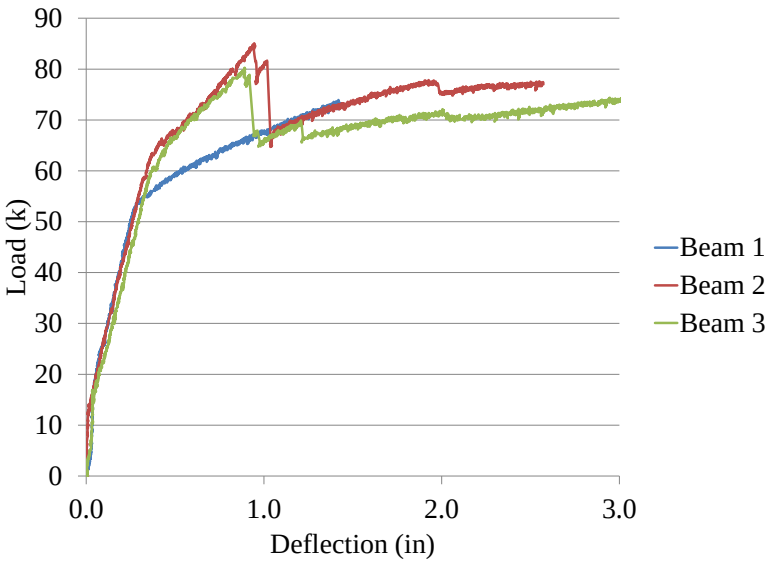

Figure 4.85. Load-Deflection: First Phase Beam Tests

The use of the plastic wires could have been the cause for the beams not to behave as well as expected. Since the wires were round they allowed saturant to accumulate in what should have been a void. Even when the wire was removed, there was hardened saturant trapped under the FRP. This did not allow the FRP to flatten out when put into tension. This is the reason for the switch to foam in the second set of beams.

4.10.2. Second Phase Beam Test. The second set of staged beams included 11 beams ranging from no FRP to three stages of FRP. These beams used form to create predetermined FRP arches locally. The load-deflection curves of Beams 1, 2, and 3 are compared in Figure 4.86. Beams 1 and 2 represent controls from each batch of concrete. Beam 3 had a conventional strip of 10 in wide FRP adhered to the bottom face of the beam. This shows the increase in ultimate load with the use of FRP. A minimum 10 k increase is seen. However, the deflection corresponding to the peak load was reduced from approximately 1.5 in for the non-strengthened beams to approximately 1.0 in with FRP strengthening. The brittle fracture nature of FRP also caused a sudden drop of load capacity at 1.0 in. The decreases in load at 1.5 in of deflection are due to concrete crushing not failing FRP.

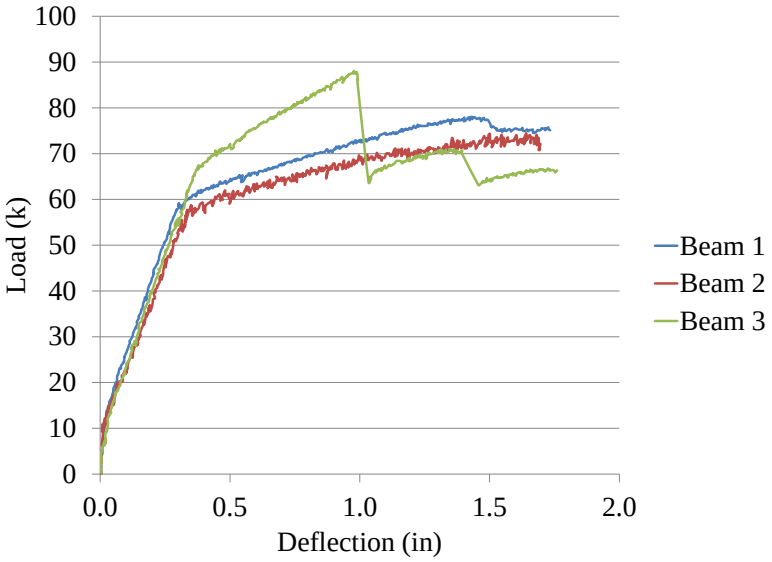

Figure 4.86. Load-Deflection: Beams 1, 2, and 3

Beams 4 and 5 both have the same two stage FRP configurations. As shown in Figure 4.87, the load-deflection curves are very similar until the failure of the FRP. Beam 4 has two distinctive failures in the stages of FRP followed by concrete crushing. Beam 5 seems to have separate failures of each of the stage 0 strips followed by debonding. Both beams did have FRP failure in the correct order of staging. Even though these beams were manufactured to the same standard, they have very different load deflection curves. These beams seem to show that the proposed technique is very

sensitive to the fabrication process and requires further investigation for practical applications.

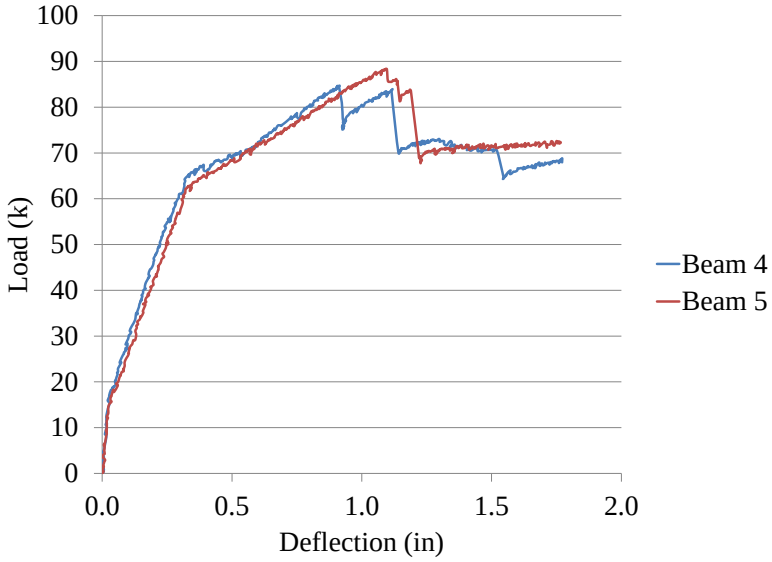

Figure 4.87. Load-Deflection: Beams 4 and 5

Beam 6 and 7 are identical with two levels of staged FRP. As shown in Figure 4.88, the load-deflection curves have a similar overall shape to the curves. The main difference was the deflection at when the FRP failed. The main drop was similar in load although it occurred at a deflection difference of 0.3 in.

Beams 9 and 10 were similar in the FRP configuration but not identical. The foam for the stage 1 FRP in Beam 10 is 0.125 in wider than in Beam 9. As shown in Figure 4.89, the load-deflection curves become very different when the FRP begins to fail. Beam 10 has a much more ductile shape than Beam 9 as expected since a larger difference in strains when the two FRP layers are respectively engaged was used in Beam 10.

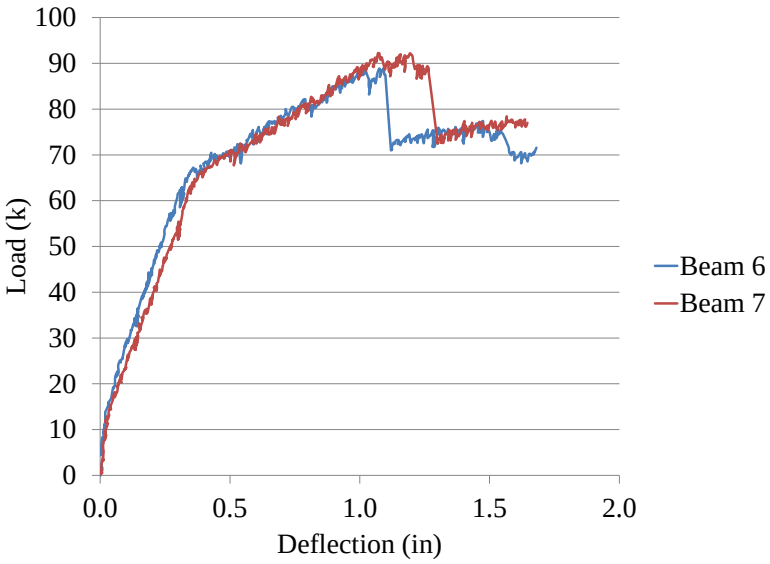

Figure 4.88. Load-Deflection: Beams 6 and 7

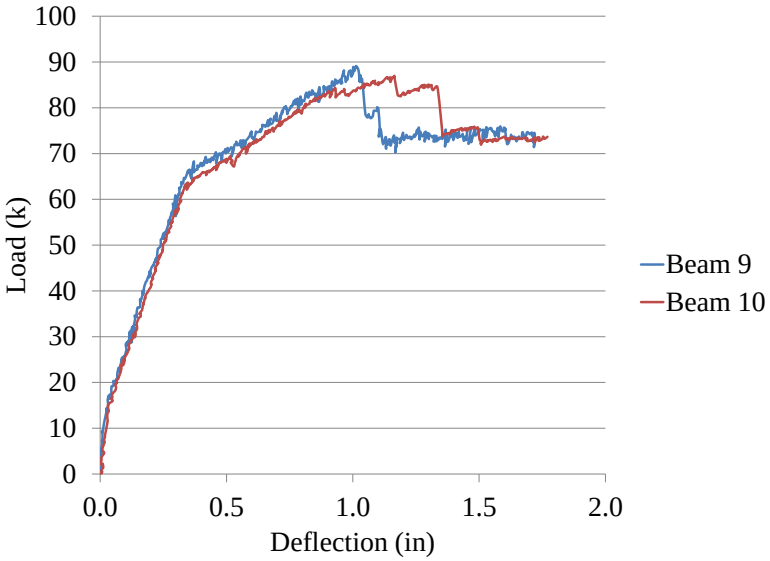

Figure 4.89. Load-Deflection: Beams 9 and 10

Beams 11 and 12 have the most identical load-deflection curves of all of the beams compared as illustrated in Figure 4.90. Beam 11 reached a few kips higher in load before failing FRP. Beam 12 lead the FRP failure by 0.2 in of deflection. Other than that, the curves are very consistent.

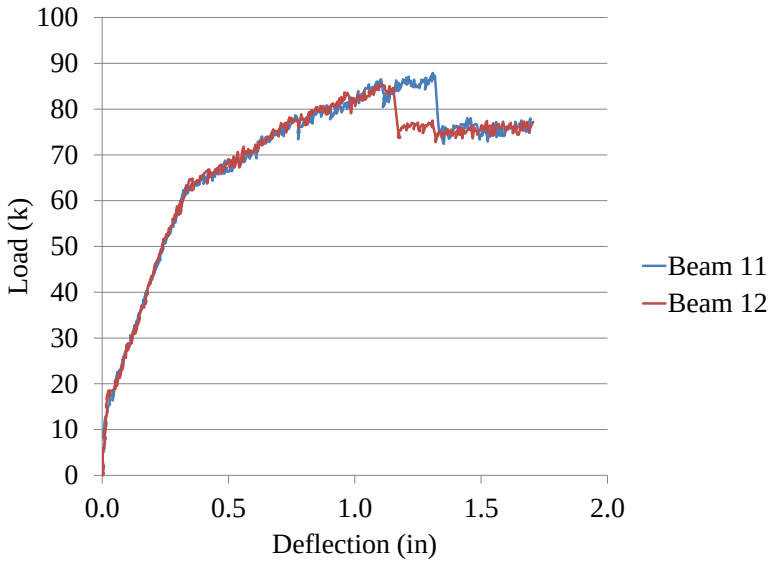

Figure 4.90. Load-Deflection: Beams 11 and 12

4.10.3. Ductility Improvement. In order to show the increase in ductility, a load-deflection curve was created for the 2 stage beams from the second phase beam test. This curve is seen in Figure 4.91. A control beam, Beam 2, and conventionally installed FRP beam, Beam 3, are included in the graph for comparison when the total width of all FRP strips was equal. In this study, the displacement ductility of a FRP strengthened beam is defined as the ratio between the initial yield displacement of steel rebar and the deflection when all FRP strips fractured. An improvement in ductility can be seen for each of the 2 stage beams when compared to conventionally installed beam. The percentage of increase in deflection ductility ranges from 10-30% for the 2 stage beams. The deflection ductility was calculated from the final failure deflection of Beam 3 to the final failure of each individual beam.

The 3 stage beams from the second phase beam test were also compared for improvement in ductility. The load-deflection curve for a control beam, conventionally installed FRP beam, and the 3 stage beams are seen in Figure 4.92. The beams in this set, Beams 9-12, also increased in deflection ductility for each of the beams tested. This set showed increases of 10-35%.

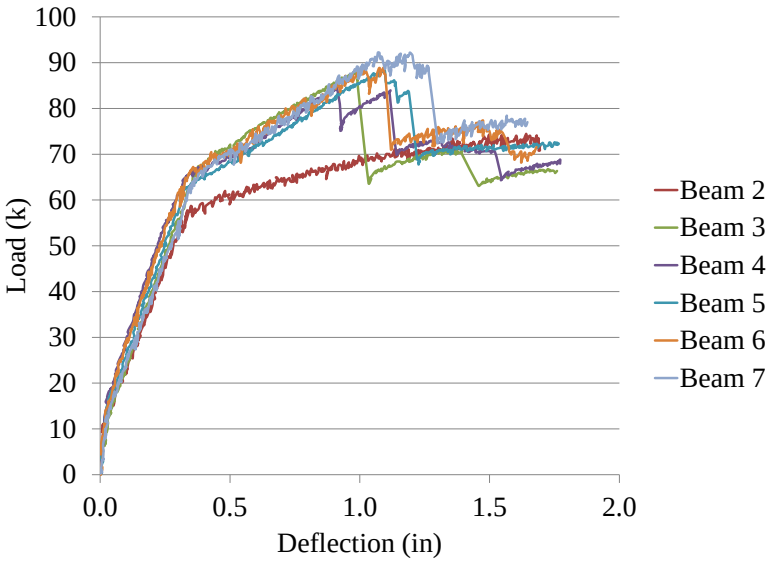

Figure 4.91. Load-Deflection: 2 Stage Comparisons

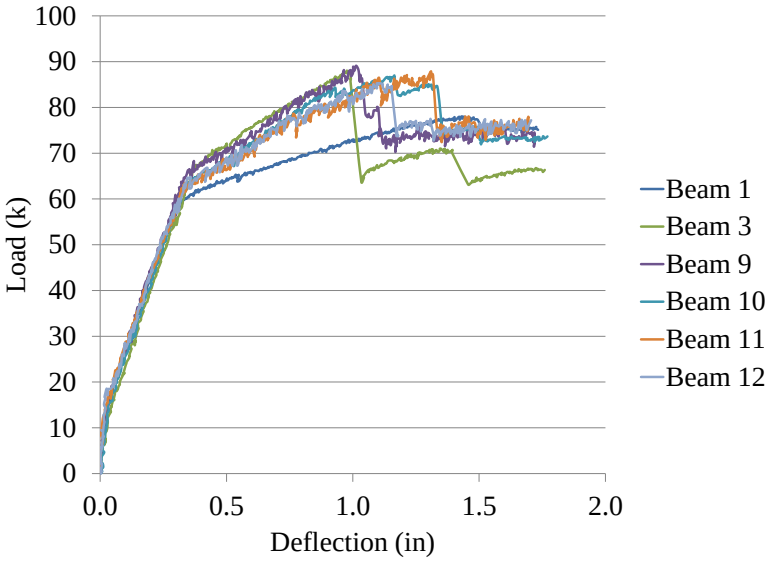

Figure 4.92. Load-Deflection: 3 Stage Comparisons

5. CONCLUSIONS

The main technical disadvantage of fiber reinforced polymers (FRP) is their brittle behavior with little warning of impending failures. This study proposes and develops a new FRP system that exhibits a significantly more ductile behavior than conventional systems. The new FRP system includes separate sheets of FRP that are applied at various staged levels and thus engaged at different loads, achieving the high strength over a large range of deformation. Two FRP installation methods were explored in this study: 1) externally preloading technique and 2) intermittently debonding technique. The former is to install FRP layers when a RC beam is subjected to various preloading levels within the design load of the beam while the latter is to create local arches by embedding intermittent foams between the beam and FRP layers. In order to evaluate the effectiveness of the new FRP system, 25 thin steel sheets were tension tested to determine their stress-strain curves with various implementations of FRP sheets under preloading and 14 RC beams were tested to determine their load-deflection curves with FRP sheets directly applied in stage.

5.1. MAIN FINDINGS AND RECOMMENDATIONS

Based on the experimental study in this thesis, the following main conclusions can be drawn:

1. Since preloading is limited by the design load of beams, the strain difference between installations of various FRP layers is insignificant in elastic range. As a result, the level of pseudo ductility that can be achieved with an externally preloading installation technique is small. Although implementable with loading bridges with trucks in field condition, the preloading technique is practically insignificant in civil engineering applications.
2. The intermittently debonding technique cannot be effectively implemented with plastic wires that are used to create periodical arches in FRP layers. This is because, once fully cured, the hardened primer filled around the plastic wires and prevented the FRP layers from flattening out against the surface of beams.

3. The intermittently debonding technique has been successfully implemented by periodically embedding flexible foams and creating local arches in FRP layers. Under external loads, the FRP layers are flattened out so that various FRP layers are engaged at different strain levels (due to nonlinear geometry effects). As a result, the fracture strain of the FRP strengthened beam system is significantly higher than that of a conventionally FRP strengthened beam. The maximum increase of deflection ductility of all beams tested in this study is approximately 35% by comparing Beam 10 with Beam 3 in the second phase.

5.2. FUTURE WORK

Although the new FRP system installed with the intermittently debonding technique is promising for improved ductile behavior, several issues must be resolved before it can be applied to civil engineering structures. The first issue is the variability in FRP application process. It was difficult to manually create local arches in the FRP layers. The amount of space that was physically bonded to the concrete may not be constant over the length of the arched section. This could be improved by automating the installation of FRP layers. The automation in FRP installation also reduces the FRP installation time in applications. An alternative solution to accelerating the foam labeling and placement process is to have the material used to create local arches woven into the FRP sheets during production. This would allow that sheet to be quickly rolled out and applied as well as aid in the consistency of the project.

BIBLIOGRAPHY

ACI 440.2R-02, Guide for the Design and Construction of Externally Bonded FRP Systems for Strengthening Concrete Structures, American Concrete Institute, 2002.

ASTM A370-10, Standard Test Methods and Definitions for Mechanical Testing of Steel Products, American Society for Testing and Materials, 2010.

ASTM D3039-08, Standard Test Methods for Tensile Properties of Polymer Matrix Composite Materials, American Society for Testing and Materials, 2008.

Bakis, C. E., Nanni, A., Terosky, J. A., and Koehler, S. W., Self-Monitoring, Pseudo-Ductile, Hybrid FRP Reinforcement Rods for Concrete Applications, Composites Science and Technology, p. 815-823, 2001.

Bunsell, A. R., and Harris, B., Hybrid Carbon and Glass Fibre Composites, Composites, p. 157-164, 1974.

Ceroni, F., Experimental Performances of RC Beams Strengthened with FRP Materials, Construction and Building Materials, p. 1547-1559, 2010.

Cromwell, J. R., Harries, K. A., and Shahrooz, B. M., Environmental Durability of Externally Bonded FRP Materials Intended for Repair of Concrete Structures, Construction and Building Materials, p. 2528-2539, 2011.

Diab, H., Wu, Z., and Iwashita, K., Short and Long Term Bond Performance of Prestressed FRP Sheet Anchorages, Engineering Structures, p. 1241-1249, 2009.

El-Hacha, R., Wright, R. G., and Green, M. F., Prestressed Carbon Fiber Reinforced Polymer Sheets for Strengthening Concrete Beams at Room and Low Temperatures, ASCE Journal of Composites for Construction, p. 3-13, 2004.

El-Hacha, R., Wright, R. G., and Green, M. F., Prestressed Fibre-Reinforced Polymer Laminates for Strengthening Structures, Progress in Structural Engineering and Materials, p. 111-121, 2001.

Grace, N., Ragheb, W., and Abdel-Sayed, G., Development and Application of Innovative Triaxially Braided Ductile FRP Fabric for Strengthening Concrete Beams, Composite Structures, p.521-530, 2004.

Hosny, A., Shaheen, H., Abdelrahman, A., and Elafandy, T., Performance of Reinforced Concrete Beams Strengthened by Hybrid FRP Laminates, Cement and Concrete Composites, p. 906-913, 2006.

Kachlakev, D., and McCurry, D. D., Behavior of Full-Scale Reinforced Concrete Beams Retrofitted for Shear and Flexural with FRP Laminates, Composites Part B: Engineering, p. 445-452, 2000.

Kretsis, G., A Review of the Tensile, Compressive, Flexural, and Shear Properties of Hybrid Fibre-Reinforced Plastics, Composites, p. 13-23, 1987.

Meier, U., Strengthening of Structures using Carbon Fibre/Epoxy Composites, Construction and Building Materials, p. 341-351, 1995.

Nanni, A., North American Design Guidelines for Concrete Reinforcement and Strengthening using FRP: Principles, Applications and Unresolved Issues, Construction and Building Materials, p. 439-446, 2003.

Pan, J., and Leung, C., Debonding along the FRP-Concrete Interface under Combined Pulling/Peeling Effects, Engineering Fracture Mechanics, p. 132-150, 2007.

Wu, Z., Hu, C., Wu, Y., and Zheng, J., Application of Improved Hybrid Bonded FRP Technique to FRP Debonding Prevention, Construction and Building Materials, p. 2898-2905, 2011.

VITA

Laura Marie Rathe attended Kickapoo High School in Springfield, Missouri, where she graduated valedictorian in May 2005. She began her undergraduate studies at Missouri State University in August of 2005. She later transferred to the Missouri University of Science and Technology in January 2007. She was involved in Chi Epsilon, Chi Omega, Society of Women Engineers, and Omega Sigma. She served as treasurer and assistant new member educator for Chi Omega as well as secretary of Omega Sigma. Laura graduated magna cum laude with a Bachelor of Science in Architectural Engineering in May 2009 from the Missouri University of Science and Technology. She received certification as an Engineering Intern in July 2009 in the state of Missouri. She began her graduate studies at Missouri University of Science and Technology in January 2010. She served as a Graduate Research Assistant under Dr. Genda Chen. Laura graduated with her Master of Science in Civil Engineering in May 2012.